# Insights into the molecular mechanisms of mitochondrial outer membrane tethering and fusion

Emily A Engelhart

A dissertation

submitted in partial fulfillment of the

requirements for the degree of

Doctor of Philosophy

University of Washington

2019

Reading Committee:

Suzanne Hoppins, Chair

Alexey Merz

Justin Kollman

Program Authorized to Offer Degree:

Biochemistry

University of Washington

**Abstract**

Insights into the molecular mechanisms of mitochondrial outer membrane tethering and fusion

Emily A Engelhart

Chair of the Supervisory Committee:

Suzanne Hoppins

Department of Biochemistry

Mitochondrial dynamics are crucial for cellular health as perturbations in these processes which include mitochondrial fusion, division, transport and mitophagy are associated with numerous diseases, cancer and neurodegeneration. The mechanisms of mitochondrial outer membrane tethering and fusion are poorly understood. It is known that Mitofusin proteins are required on both membranes of the fusion pair and that they are responsible for mitochondrial tethering, but the mechanism of tethering and the steps required to progress to lipid mixing are unknown. As members of the Dynamin related protein family, we predict that Mitofusin-mediated membrane fusion will be driven by the catalytic cycle, which will be coupled to self-assembly and conformational changes. To gain insight into the molecular steps of mitochondrial outer membrane tethering and fusion, I worked on three distinct but related projects: (1) purification and characterization of recombinant Mitofusin protein from *Escherichia coli*, (2) identification and characterization of a mutant variant of the Mitofusins that uncouples mitochondrial tethering

and fusion, and (3) fractionation of mammalian cytosol to identify new factors that stimulate mitochondrial fusion. The purification of recombinant mouse Mitofusin protein from *E. coli* was extremely difficult and highly variable in both the quality and quantity of the final purified protein. The vast majority of protein purifications resulted in the formation of soluble aggregates as assessed by sucrose gradient ultracentrifugation and negative stain electron microscopy. This recombinant Mitofusin protein did potentially possess nucleotide binding activity and appeared to have some structural features by negative stain electron microscopy and limited trypsin digestion. Despite this encouraging data, purified recombinant Mitofusin protein lacked GTP hydrolysis activity and proteoliposomes with recombinant Mitofusin lacked tethering and fusion activity. Although functional recombinant Mitofusin protein was not obtained, this work lays the groundwork for future attempts at obtaining purified protein.

To gain insights into functional features of the GTPase domain, we performed a screen of disease-associated mutant variants and identified a mutant variant of Mfn1 that caused mitochondrial hyperfusion and perinuclear collapse of the network. The substitution was Mfn1 Phe-202 to leucine, which is located in a conserved central beta-sheet. Despite the high degree of organelle connectivity observed in cells, our in vitro mitochondrial fusion assay revealed that $Mfn1^{F202L}$ lacked mitochondrial fusion activity. Further biochemical analysis indicated that this mutant variant uncouples mitochondrial tethering from fusion due to impaired higher-order assembly. This mutant variant of the Mitofusins has provided insight into the molecular steps of mitochondrial outer membrane fusion placing nucleotide dependent self-assembly after the initial tethering event.

To find additional factors that stimulate mitochondrial fusion, we performed cytosol fractionation by ion exchange chromatography and tested for pro-fusion activity in our cell-free

assay. We identified a discrete fraction of cytosolic factors that tightly bound to cation exchange resin that significantly stimulated mitochondrial fusion in vitro. Incubation of the stimulatory fraction with either RNase, protease or heat reduced the stimulatory activity suggesting that the stimulatory factor might have both RNA and polypeptide components. This work indicates that classical biochemical fractionation can identify novel pro-fusion proteins. Together, these three independent projects have given us insights into the molecular mechanisms of mitochondrial outer membrane tethering and fusion.

# Table of Contents

# List of Figures

# List of Tables

# Acknowledgements

I would like to thank my thesis advisor, Suzanne Hoppins for her support and mentorship over the past 6 years. She has helped me develop into an independent and thoughtful scientist. I would like to thank all the members of the Hoppins lab for their encouragement, thoughtful suggestions and advice during my time in the lab. I would like to thank my thesis committee members Rich Gardner, Alexey Merz, Leo Pallanck and Justin Kollman for their numerous project ideas and support. I would like to thank my Mom for all her support and visits during my time in graduate school. We were able to stay connected through riding bike and got to participate in various bike events together. Finally, I would like to thank my husband Alex, without you I would have never made it through graduate school.

# Dedication

To my friends and family. I could not have done this without your support.

# Chapter 1: General Introduction

## 1.1 Mitochondrial dynamics

Mitochondria are dynamic organelles that undergo frequent fusion and division events and that move throughout the cell using microtubule-based transport (Hollenbeck & Saxton, 2005; Lewis & Lewis, 1914; Ligon & Steward, 2000). Mitochondrial fusion and division events are roughly balanced in most cell types, resulting in a reticular network of mitochondria (Yang et al., 2015). Mitochondrial network structure is influenced by numerous cellular cues. Mitochondrial hyperfusion is observed at the onset of stress conditions like starvation and inhibition of protein synthesis (Tondera et al., 2009) and also occurs at the G1-S transition (Mitra et al., 2009). The hyperfused mitochondrial network supports increased ATP production, due at least in part to cristae remodeling which may help the cell cope with a short-term stress (Tondera et al., 2009). Equally important, mitochondrial fission is needed to produce small mitochondria for mitophagy, movement of mitochondria along microtubules, equal distribution of mitochondria during mitosis and to assist in apoptosis. Mitochondrial fusion is thought of as protective as it supports complementation of damaged mtDNA, lipids, proteins, mRNAs and metabolites (Legros et al., 2004; Yang et al., 2015). Moreover, perturbations in mitochondrial dynamics have been observed in numerous diseases, cancers and neurodegeneration. Therefore, the disruption of mitochondrial dynamics is extremely deleterious, and the proper structure and dynamics of the mitochondrial network are crucial for cellular health.

### 1.1.1 Members of the Dynamin related protein family mediate mitochondrial dynamics

To overcome the energetic barriers required to divide or merge lipid bilayers, protein machines are required. The proteins involved in mitochondrial dynamics are members of the dynamin related protein (DRP) family which are large GTPase proteins that self-assemble (Figure 1.1). This self-assembly is regulated in cells and stimulates GTPase hydrolysis resulting in membrane remodeling events (Heymann & Hinshaw, 2009). DRP membrane fission proteins form large helical structures around lipid tubules and conformational changes are predicted to cause constriction events leading to Dynamin disassembly. In contrast, DRP membrane fusion proteins have been observed as much smaller oligomers. For example, the homotypic endoplasmic reticulum fusogen Atlastin forms dimers when monomers on opposing membranes interact to support fusion (Bian et al., 2011; Byrnes & Sondermann, 2011). Recent evidence suggests that in yeast, Fzo1-mediated mitochondrial outer membrane fusion involves the formation of a ring-like structure composed of discrete smaller assemblies (Brandt et al., 2016). The lipid environment also stimulates the self-assembly of mitochondrial inner membrane fusion proteins, Opa1/Mgm1, which form higher order assemblies that are dependent on cardiolipin (Ban et al., 2017; DeVay et al., 2009).

### 1.1.2 Mitochondrial division

Mitochondrial division is well characterized and is mediated by the cytosolic dynamin-related protein 1 (Drp1) (Smirnova et al., 1998). Cytosolic Drp1 is recruited to sites of division independently by one of four integral mitochondrial outer membrane adaptor proteins (Fis1, Mff, MiD49 and MiD51) through interactions with Drp1's insert B domain (Loson et al., 2013; Strack & Cribbs, 2012). Mff is considered the primary adaptor protein, whereas Fis1 & MiD49/51 may engage Drp1 for mitochondrial division during mitophagy or cellular stress, respectively. In

addition, the endoplasmic reticulum and actin/myosin generate pre-constriction sites of high membrane curvature that promote localization of the Drp1 adaptors (Hatch et al., 2014, Murley et al., 2013). The activity and recruitment of Drp1 to sites of division is also regulated through post-translation modifications including phosphorylation, acetylation and ubiquitination (Otera et al., 2013). How the cell determines sites of mitochondrial division is unknown, but many sites of division are associated with mtDNA (Murley et al., 2013). This may allow for selective distribution of mtDNA to one or both mitochondria after a division event.

The mechanism of mitochondrial division is best understood in yeast and most attributes of Dnm1 are likely conserved in mammalian cells. Dnm1 is recruited to the mitochondrial outer membrane as obligate dimers. The dimer species possesses low basal GTPase activity that is stimulated 25-fold upon assembly (Ingerman et al., 2005). The assembled state corresponds to rings and helices which are predicted to wrap around the mitochondria. Current models predict that when the GTPase domains on adjacent rungs of the helix interact, GTPase activity is stimulated. GTP hydrolysis results in a conformational change in Dnm1 causing constriction and/or disassembly of the helix. This mechanism tightly couples assembly on the mitochondria to the catalytic cycle and membrane scission (Mears et al., 2011).

### 1.1.3 Mitochondrial outer membrane fusion

In mammals, Mitofusin proteins (Mfn1 and Mfn2) promote fusion of the mitochondrial outer membrane (Santel & Fuller, 2001). Human Mfn1 and Mfn2 have 60% sequence identity and 77% similarity (Santel & Fuller, 2001) but are not fully functionally redundant (Chen et al., 2003; Eura et al., 2003). Deletion of either Mitofusin in mice leads to embryonic lethality and deletion of both Mfn1 and Mfn2 results in earlier embryonic death, indicating a role in

development (Chen et al., 2003). Both Mitofusins to are required to maintain mitochondrial form and function as deletion of either Mitofusin results in a fragmented mitochondrial network although the Mitofusins can independently mediate mitochondrial fusion at low levels (Chen et al., 2005; Chen et al., 2003; Hoppins et al., 2011). In addition, the fusion activity of Mfn1 and Mfn2 are regulated by unique protein binding partners (de Brito & Scorrano, 2009; Hoppins et al., 2011; Kumar et al., 2016; Zhang et al., 2010) and post-translational modifications (Chen & Dorn, 2013; Ferreira et al., 2019; Glauser et al., 2011; Leboucher et al., 2012; Lee et al., 2014; Pyakurel et al., 2015; Rakovic et al., 2011; Sarraf et al., 2013; Shutt et al., 2012; Tanaka et al., 2010).

The Mitofusins are targeted to the mitochondrial outer membrane by a hairpin transmembrane domain which results in the majority of the protein in the cytosol (Santel & Fuller, 2001). This topology has recently been challenged for Mfn2 as a new finding suggests that Mfn2 carboxyl terminus (C-terminus) may be located in the inner membrane space (Mattie et al., 2018). This result is challenging to reconcile with as recent atomic structures of a minimal Mfn1 GTPase domain construct ($Mfn1_{IM}$) revealed that the C-terminus of Mfn1 is a component of a 4 helical bundle with 3 helices from the amino terminus (N-terminus) (Cao et al., 2017; Qi et al., 2016; Liming Yan et al., 2018). A $Mfn1_{IM}$ construct lacking the C-terminus results in complete insolubility of the protein, which strongly implies that the C-terminus does indeed fold back to form a 4 helical bundle, even in the context of full length protein (Qi et al., 2016).

The Mitofusins also each contain two heptad repeat (HR) domains which are classically thought to be involved in protein-protein interactions. HR1 has been proposed to be involved in destabilizing the lipid bilayer by functioning as an amphipathic helix when examined in vitro using isolated HR1 peptide (Daste et al., 2018). However, it is unclear whether the HR1 domain

in the context of full length Mitofusin would be accessible to the membrane. The C-terminal HR2 domain has been implicated in tethering due to the formation of an anti-parallel dimer when the domain was crystallized in isolation (Koshiba et al., 2004). Recent work using small molecules or peptides mimicking the protein structure of either HR1 or HR2 support this model of tethering (Franco et al., 2016; Rocha et al., 2018). The authors hypothesized that molecules designed to mimic HR1 would promote the displacement of the HR2 helix from the 4 helical bundle and would therefore enhance mitochondrial fusion in cells, perhaps by allowing the HR2 to interact with another HR2 domain on a nearby mitochondria. In contrast, molecules that are designed to mimic HR2 would prevent HR2 domains from interacting and would inhibit mitochondrial fusion in cells. Indeed, the authors observed an increase in mitochondrial fusion with molecules mimicking HR1 and an inhibition of mitochondrial fusion with molecules mimicking HR2 although future work will be required to rule out any off-target effects. These data are consistent with a role for HR2 in membrane tethering; however, the C-terminal domain is not sufficient for mitochondrial fusion as a construct missing the entirety of the GTPase domain only tethers mitochondria together (Koshiba et al., 2004).

An alternative model of tethering has been recently proposed; atomic structures of $Mfn1_{IM}$ revealed a new dimer interface at the GTPase domain, which is a characteristic assembly interface for other DRPs (Cao et al., 2017; Jimah & Hinshaw, 2019; Liming Yan et al., 2018) (Figure 1.2 B&C). This intermolecular interaction of two GTPase domains (G-G) is thought to stimulate GTP hydrolysis and act similarly to the function of GTPase Activating Proteins (GAPs) (Jimah & Hinshaw, 2019). $Mfn1_{IM}$ is capable of binding and hydrolyzing GTP, dimerizing at the G-G interface and tethering liposomes, but not membrane fusion (Cao et al., 2017). Together, this suggests that the G-G interface could establish a physical tether, but also

that the second predicted helical bundle and transmembrane domain play important roles in membrane fusion.

Three different crystal structures have been obtained for the $Mfn1_{IM}$ construct based on its nucleotide state: (1) monomeric when crystallized in the absence of nucleotide or the presence of GDP, GTPγS or GMPPCP, (2) dimeric when crystallized in the presence of GDP $AlF_4$ with the helical bundles point away from each other and (3) dimeric when crystallized in the presence of GDP $BeF_3$ with the helical bundles pointing in the same direction (Figure 1.2) (Cao et al., 2017; Qi et al., 2016; Liming Yan et al., 2018). This is the first direct evidence that the Mitofusins make large nucleotide dependent conformational changes.

The Mitofusins have highest sequence homology and are predicted to be most structurally similar to bacterial dynamin-like proteins (BDLP) (Bramkamp, 2012; J. Liu et al., 2018). A BDLP from *Nostoc punctiforme* was purified and crystalized in a closed clamp conformation in the presence of GDP (Low & Löwe, 2006) (Figure 1.3 B). Structural alignment of $Mfn1_{IM}$ and BDLP crystal structures bound to GDP overlay exceptionally well (~4Å RMSD) (Liming Yan et al., 2018). BDLP also adopted an open elongated conformation in the presence of liposomes when incubated with a non-hydrolysable analog of GTP, GMPPNP (Figure 1.3 A) which had a similar relative orientation of the GTPase domain to helical bundles as $Mfn1_{IM}$ in the presence of GDP $BeF_3$ (compare Figure 1.3 A to Figure 1.2 C) (Low et al., 2009; Yan et al., 2018). Together, these very different structures suggest a potential mechanism for mitochondrial outer membrane fusion. Models predict that the extended conformation will exists as the pre-fusion state and will perform membrane tethering, perhaps through the intermolecular G-G interface. The closed state is predicted to be a post-fusion state, where the large conformational change triggered by GTP hydrolysis are harnessed to drive membranes together. This model of Mitofusin-mediated fusion

needs to be tested experimentally and how these events are regulated, coordinated and coupled are also not well understood.

### 1.1.4 Mitochondrial inner membrane fusion

The dynamin-related GTPase, Optic atrophy 1 (Opa1), is required for mitochondrial inner membrane fusion (Olichon et al., 2003, 2002; Song et al., 2007). In cells, mitochondrial outer membrane fusion is usually spatially and temporally coupled to inner membrane fusion (Cipolat et al., 2004; X. Liu et al., 2009), but can occur independently as mitochondrial outer membrane fusion can occur in the absence of Opa1 (Hoppins et al., 2011; Malka et al., 2005; Meeusen et al., 2004; Song et al., 2009). Multiple isoforms of Opa1 are found in different tissues due to alternative splicing and proteolytic processing by the inner membrane peptidases Oma1 and Yme1, which generate two topologically distinct isoforms of Opa1 (Ehses et al., 2009; Z. Song et al., 2007). Membrane anchored Opa1-L is cleaved to generate a short soluble form, Opa1-S. While some studies suggest that both Opa1-L and Opa1-S are required for inner membrane fusion (Head et al., 2009; Song et al., 2007), recent in vitro data indicate that Opa1-L and cardiolipin are sufficient to mediate membrane fusion (Anand et al., 2014; Ban et al., 2017). Opa1 is primarily regulated through proteolytic cleavage by inner membrane proteases, Yme1 and Oma1 which have increased activity when the mitochondria have low ATP or membrane potential (Head et al., 2009; Z. Song et al., 2007). These conditions would result in more proteolytic processing of Opa1-L to Opa1-S which was shown to inhibit fusion and was proposed to function as a mechanism to sequester damaged mitochondria from the network for turnover (Baricault et al., 2007; Ehses et al., 2009; Head et al., 2009; Ishihara et al., 2006; Mishra & Chan, 2014; Song et al., 2007). Opa1 is also important for maintaining the

organization and structure of the mitochondrial inner membrane and cristae (Frezza et al., 2006; Olichon et al., 2003).

## 1.2 Mitochondrial transport

Mitochondria move in both the anterograde and retrograde direction along microtubules using kinesin and dynein motor complexes, respectively. These motor complexes are attached to the mitochondria through Miro1/2 and TRAK1/2 (Fransson et al., 2006). Miro is a resident mitochondrial outer membrane protein containing a single pass transmembrane domain, two GTPase domains and two $Ca^{2+}$ binding EF hand motifs. There is limited function data on Miro's GTPase domains, but they likely play a regulatory role (Babic et al., 2015). The EF hand motifs sense and bind $Ca^{2+}$ which has been hypothesized to be a regulatory mechanism to halt mitochondria at sites of high $Ca^{2+}$ (MacAskill et al., 2009; X. Wang & Schwarz, 2009). TRAK acts as an adaptor protein between Miro and the motor proteins, physically interacting with Miro, Kinesin and Dynein and is required for directional mitochondrial movement (van Spronsen et al., 2013). Both Miro and TRAK interact with the Mitofusins when overexpressed, possibly coupling mitochondrial transport and mitochondrial fusion through the co-localization of the two protein complexes (Misko et al., 2010; Nemani et al., 2018).

## 1.3 Mitophagy

Mitophagy is the selective degradation of mitochondria using the autophagy machinery (Lemasters, 2005). This cellular process removes malfunctioning mitochondria to protect the cell from accumulating mtDNA mutations, minimize reactive oxygen species and eliminate

misfunctioning electron transport chains. The removal of mitochondria from the network is important for the cellular health as mutations in the mitophagy pathway leads to neurological diseases such as Parkinson's Disease. Mitophagy occurs during cell stress or when mitochondria become damaged and therefore the mitochondria have a low membrane potential (Narendra et al., 2008). Many levels of regulation go into removing dysfunctional mitochondria. Generally, upon loss of membrane potential mitochondria fragment into small discrete organelles. This occurs due to three independent processes: (1) Opa1-L is proteolytically cleaved to Opa1-S which is fusion incompetent on its own inhibiting mitochondrial inner membrane fusion, (2) Drp1 is dephosphorylated and recruited to the mitochondria resulting in mitochondrial division (Cereghetti et al., 2008; Chang & Blackstone, 2007; Cribbs & Strack, 2007) and (3) the Mitofusins are ubiquitinated by Parkin and targeted for degradation therefore inhibiting mitochondrial outer membrane fusion (Tanaka et al., 2010). This allows for PINK1, a serine/threonine kinase, to accumulate on the surface of the mitochondria because of stalled mitochondrial protein import which requires membrane potential (Jin et al., 2010; Lazarou et al., 2015). PINK1 phosphorylates ubiquitin molecules on the mitochondrial surface and this acts as a signal to recruit Parkin which then is phosphorylated by PINK1 (Kane et al., 2014; Kazlauskaite et al., 2014; Kondapalli et al., 2012; Koyano et al., 2014; Shiba-Fukushima et al., 2012). Phosphorylation of Parkin relieves autoinhibition and Parkin ubiquitinates mitochondrial outer membrane proteins. These hyper-ubiquitinated mitochondria acts as a signal to recruit the autophagy machinery and leads to the removal of the mitochondria (Stolz et al., 2014).

## 1.4 Mitochondrial dynamics in disease

Mitochondrial dynamics play important roles in the health of cells. All four DRP proteins (Drp1, Opa1, Mfn1 and Mfn2) are required for embryonic development in mice, underscoring the importance of mitochondrial dynamics in development (Chen et al., 2003; Davies et al., 2007; Ishihara et al., 2009; Wakabayashi et al., 2009). In addition, mutations in Opa1 and Mfn2 lead to neurodegenerative diseases Dominant Optic Atrophy and Charot-Marie Tooth Syndrome Type 2A, respectively (Alexander et al., 2000; Züchner et al., 2004). Mutations in Drp1 cause a range of diseases characterized broadly by developmental delays and neurological dysfunction (Chang et al., 2010; Chao et al., 2016; Fahrner et al., 2016; Sheffer et al., 2016; Vanstone et al., 2016; Waterham et al., 2007; Whitley et al., 2018; Zaha et al., 2016). Mutations in other proteins involved in mitochondria dynamics also lead to disease including the Drp1 receptors Mff (Koch et al., 2016; Nasca et al., 2018; Shamseldin et al., 2012) and MiD49 (Bartsakoulia et al., 2018) and the Opa1 protease Yme1 (B. Hartmann et al., 2016). Furthermore, mitochondrial fusion is required for the differentiation of cardiomyocytes and proper development of the heart in mice (Kasahara et al., 2013), protects against neurodegeneration in the cerebellum (Chen et al., 2007), promotes neuronal maturation and differentiation (Fang et al., 2016) and is required for the maintenance of haematopoietic stem cells (Luchsinger et al., 2016). Therefore, understanding the mechanism of mitochondrial fusion and division is required to understand their role in health and disease.

## 1.5 Figures

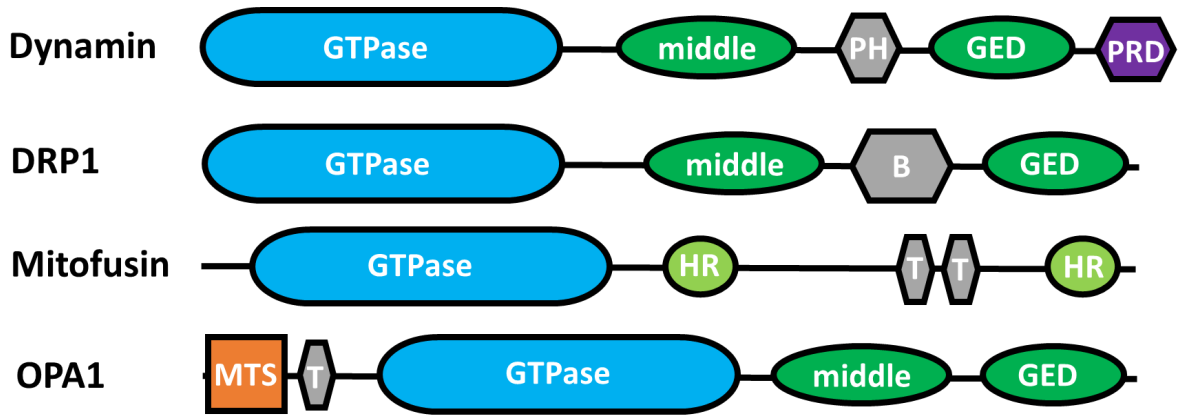


**Figure 1.1 Domain structure of Dynamin Related Proteins**

PH = pleckstrin homology domain; GED = guanosine effector domain; PRD = proline rich domain; HR = heptad repeat; T = transmembrane; MTS = mitochondrial targeting sequence

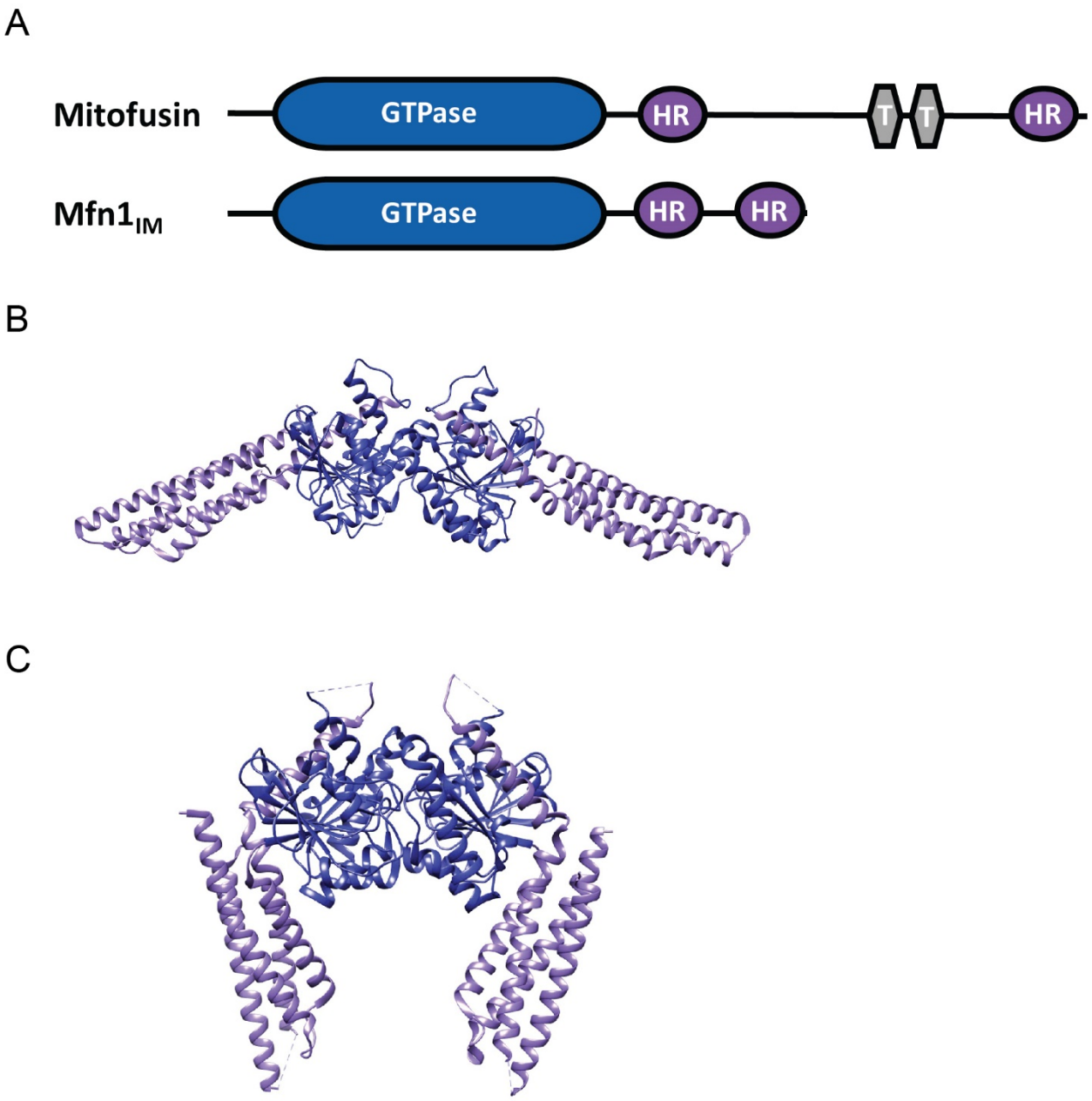


**Figure 1.2 Domain structure of Mitofusin and $Mfn1_{IM}$ and crystal structures**

**(A)** Domain structure of Mitofusin 1 and Mfn1IM **(B)** Crystal structure of $Mfn1_{IM}$ in the presence of GDP $AlF_4$ (PDB 5GOM) **(C)** Crystal structure of $Mfn1_{IM}$ in the presence of GDP $BeF_3$ (PDB 5YEW)

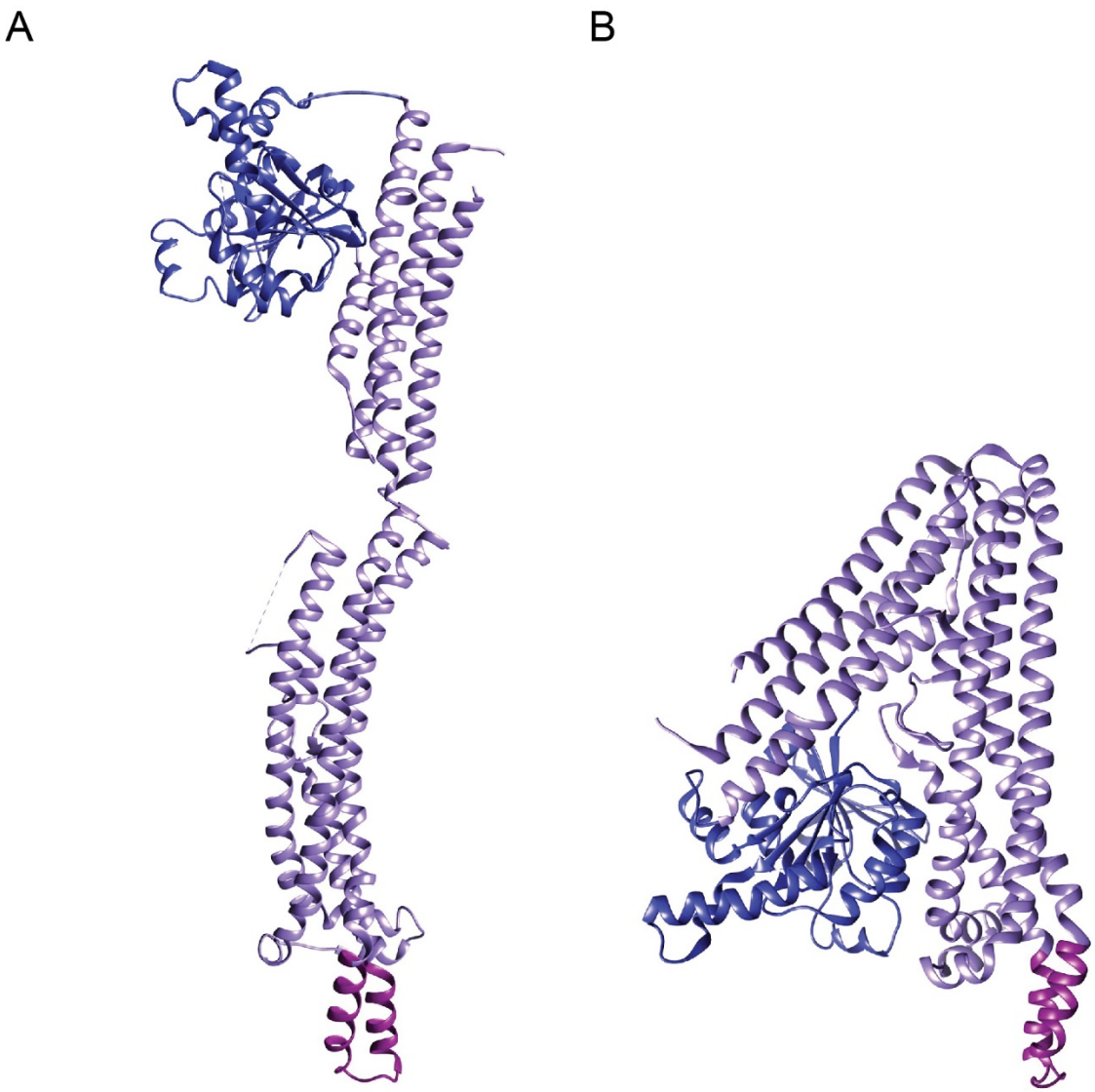


**Figure 1.3 BDLP from *Nostoc punctiforme* in two different conformations**

**(A)** BDLP in an open conformation in the presence of liposomes and GMPPNP (PDB 2W6D)
**(B)** BDLP in a closed conformation in the presence of GDP (PDB 2J68)

# Chapter 2: Purification and Characterization of Recombinant Mfn1 & Mfn2

## 2.1 Abstract

The purification of full length recombinant Mitofusin protein containing the transmembrane domain region would allow for numerous biochemical and structural analyses including making comparisons in enzymatic activities between Mfn1 and Mfn2 and the development of proteoliposome tethering and fusion assays. Recombinant Mitofusin protein was expressed in *E. coli* and purified using nickel affinity chromatography. Obtaining soluble Mitofusin protein was extremely difficult and not reproducible. The protein tended to form large soluble aggregates at higher protein concentrations. The recombinant Mitofusin protein obtained potentially possessed nucleotide binding activity but lacked GTPase activity. No significant nucleotide dependent conformational changes in the protein structure were captured by BN-PAGE, chemical crosslinking or trypsin digestion. Sucrose gradient ultracentrifugation showed that Mitofusin protein oligomerizes in the presence of GTP or GDP $BeF_3$, but not $Mg^{2+}$, GDP, GTPγS or $BeF_3$. Mitofusin protein efficiently inserted into liposomes mimicking the lipid composition of the mitochondrial outer membrane in an outward facing direction. Unfortunately, the Mitofusin containing proteoliposomes lacked tethering and fusion activity. If this project were to be pursued in the future, I would recommend moving from *E. coli* to a different host expression system like mammalian HEK-293 cells.

## 2.2 Introduction

Members of the dynamin related protein (DRP) family are large GTPase proteins that remodel membranes. Many of the family members have been recombinantly purified and biochemically characterized including Dynamin, Dnm1/Drp1, Mgm1/Opa1, Atlastin and various bacterial dynamin like proteins (Ban et al., 2017; Byrnes & Sondermann, 2011; Cao et al., 2017; DeVay et al., 2009; Ford et al., 2011; Liu et al., 2018; Low & Löwe, 2006; Low et al., 2009; Qi et al., 2016; Varlakhanova et al., 2018; L. Yan et al., 2015; Yan et al., 2018). All of these proteins contain a similar domain architecture: a globular amino-terminal GTPase domain, elongated alpha helical bundle(s) and a lipid interaction domain (Figure 2.1). The GTPase domain binds nucleotide with a higher affinity (micromolar range) than small GTPase proteins like Ras (picomolar range) (Jimah & Hinshaw, 2019). Therefore, DRPs do not require guanosine exchange factors (GEFs) and an intermolecular interaction between GTPase domains (G-G) is generally thought to stimulate GTP hydrolysis acting like a guanosine activating proteins (GAPs). GTP hydrolysis is required for membrane remodeling activity, but the exact role that nucleotide binding and hydrolysis play in self-assembly, conformational changes and membrane remodeling is still unclear. There are seemingly contradictory findings about whether GTP hydrolysis provides the energy to remodel membranes or whether GTP hydrolysis promotes the disassembly of the protein complex after a membrane remodeling event (O'Donnell et al., 2017; Sundborger et al., 2014; Winsor et al., 2018). Regardless, there are 3 conserved properties that all DRP family members possess: higher-order oligomerization, self-assembly stimulated GTP hydrolysis activity and GTP hydrolysis dependent membrane remodeling. In the following section I detail the biochemical properties of various DRP family members that have been

purified and biochemically characterized as we believe that the Mitofusin will share some of these properties.

**Dynamin**

Dynamin, the founding member of the DRP family, performs the membrane scission event in clathrin mediated endocytosis (Figure 2.1 A). Dynamin self-assembles into rings and helices in solution which are clearly visible by negative stain electron microscopy (Figure 2.2 left) (J. A. Mears & Hinshaw, 2008). Dynamin's has low basal GTPase activity but was stimulated ~100 fold when assembled onto a lipid scaffold (Song et al., 2004).

**Dynamin related protein 1 (Drp1)**

Drp1 is structurally and functionally similar to Dynamin and is involved in division of the mitochondria (Figure 2.1 B) (Smirnova et al., 1998). Drp1 makes larger rings and helices in solution than Dynamin fitting closer to the diameter of mitochondria (Figure 2.2 right) (Ingerman et al., 2005). Drp1 GTPase activity is stimulated when assembled onto a lipid scaffold but the presence of cardiolipin further increased its GTP hydrolysis activity (Francy et al., 2015; Francy et al., 2017).

**Atlastin**

Atlastin (ATL) mediates the homotypic fusion of the endoplasmic reticulum (Orso et al., 2009). ATL contains a helical bundle, hairpin transmembrane domain and a short C-terminal amphipathic helix which is required for lipid mixing (Bian et al., 2011; Byrnes & Sondermann, 2011; Moss et al., 2011; Pendin et al., 2011). In reconstituted proteoliposomes, purified ATL supports tethering and fusion activity (Orso et al., 2009). The protein is monomeric and interacts

across two membranes through interactions between GTPase domains to form a dimer which is proposed to be a tethered assembly (Hu & Rapoport, 2016). Crystal structures and extensive biochemical characterization of ATL reveal that after the initial G-G domain interaction, a large conformational crossover of the helical bundles occurs which drives membrane fusion (Byrnes et al., 2013; Morin-Leisk et al., 2011; Winsor et al., 2017) (Figure 2.1 G&H).

**Mgm1/Opa1**

Mgm1/Opa1 is required for the fusion of the mitochondrial inner membrane and cristae maintenance (Cipolat et al., 2004; Meeusen et al., 2006). Mgm1/Opa1 proteins are anchored to the mitochondrial inner membrane facing the inner membrane space. The long membrane bound Mgm1-L/Opa1-L is proteolytically processed to generate a short soluble isoform (Mgm1-S/Opa1-S) (Anand et al., 2014; Z. Song et al., 2007). Mgm1, the yeast ortholog of Opa1 was first recombinantly purified and it was determined that Mgm1-L has no enzymatic activity but stimulates the enzymatic activity of Mgm1-S (DeVay et al., 2009). In cells, both Opa1-S and Opa1-L are required for mitochondrial inner membrane fusion, but recent work as shown that in vitro Opa1-L proteoliposomes containing high cardiolipin levels are capable of robust fusion in the absence of Opa1-S (Ban et al., 2017). Both Mgm1 and Opa1 form higher order assemblies that are dependent on cardiolipin (Ban et al., 2017; DeVay et al., 2009).

**Bacterial Dynamin Like Protein (BDLP)**

BDLP is the DRP family member that is most structurally similar and has the highest sequence homology to the Mitofusins. In fact, the recent high-resolution structure of the $Mfn1_{IM}$ minimal GTPase domain construct overlays extremely well to the GTPase domain of BDLP from *N. punctiforme* (~4Å RMSD) (Yan et al., 2018). BDLP was crystallized in a closed clamp

conformation (Figure 2.1 C), but when incubated with lipids and non-hydrolysable analog of GTP, GMPPNP, the protein was found in an open elongated conformation (Low & Löwe, 2006; Low et al., 2009) (Figure 2.1 D). It has been proposed that the Mitofusins may also make these large conformational changes from an open pre-fusion state to a closed post-fusion state.

**Mfn1$_{IM}$**

Recent crystal structures and biochemical characterization of a minimal GTPase domain construct of Mfn1 (Mfn1$_{IM}$) have provided significant insight into the mechanism of Mitofusin mediated membrane fusion (Cao et al., 2017; Qi et al., 2016; Yan et al., 2018). The protein has been captured in three different states: (1) a monomeric state without nucleotide or in the presence of GDP, GTPγS or GMPPNP (2) a dimeric state with the helical bundles pointed in the opposite direction in the presence of GDP $AlF_4$ (Figure 2.1 E) and (3) a dimeric state with the helical bundles in the same direction in the presence of GDP $BeF_3$ (Figure 2.1 F). Mfn1$_{IM}$ also dimerizes in the presence of GTP observed by analytical ultracentrifugation and FRET analysis (Qi et al., 2016; Yan et al., 2018). This suggests a mechanism in which dimerization at the G-G interface requires GTP hydrolysis and would act as tethering step. Further large conformational changes in the protein are predicted to move the membranes closer together to facilitate membrane fusion.

## 2.3 Results

### 2.3.1 Development of recombinant protein purification protocol

We decided to develop a recombinant protein purification method for mouse Mfn1 and Mfn2 in *Escherichia coli* (*E. coli*) as many other mammalian DRP family members have been successfully purified from *E. coli*. Mouse Mitofusin was chosen because the main cell culture model used in our lab are mouse embryonic fibroblasts; therefore, any biochemical information obtained could be directly compared to results from in vivo experiments. Many different variables contribute to the successful purification of a recombinant protein including the identification and position of an affinity tag, *E. coli* strain, growth media, isopropyl β-D-1-thiogalactopyranoide (IPTG) induction concentration, and the buffer composition at lysis and subsequent purification steps. Initial attempts to purify Mfn1 with an amino-terminal (N-terminal) 6X Histidine ($His_6$) affinity tag with high IPTG concentrations produced very little to no soluble protein. The Mitofusins contain a small hairpin transmembrane domain which is not very hydrophobic and replacement with a short flexible linker did not appear to alter the initial protein production or solubility of the protein. Therefore, full length mouse Mitofusin protein containing the transmembrane domain was pursued. A variety of strategies were tested before significant soluble Mitofusin protein was obtained as described below and summarized in Table 2.1.

#### 2.3.1.1 Affinity tag

A variety of affinity tags and solubility factors were tested to improve the expression and solubility as a minimal N-terminal $His_6$ tag produced little to no soluble protein. A C-terminal

superfolder GFP (sfGFP) tag produced no detectable protein. N-terminal maltose binding protein (MBP) and N-terminal small ubiquitin-like modifier (SUMO) tags produced large amounts of protein, but most of the protein was insoluble. These data indicate that Mitofusin protein can be expressed in *E. coli* but that it may require additional support to be soluble. Therefore, we used an N-terminal $His_6$-Trigger Factor solubility tag. Trigger factor is an endogenously expressed *E. coli* chaperon protein that helps nascent polypeptides fold. $His_6$-Trigger Factor N-terminal fusion significantly improved the solubility of the Mitofusin protein shifting the majority of the protein out of the insoluble fraction. During further protocol development we found that an N-terminal $His_6$-SUMO-Trigger Factor fusion further improved expression and solubility. Therefore, we moved forward with this affinity tag for further optimization.

#### 2.3.1.2 *E. coli* strain

Many different *E. coli* expression strains are available for recombinant protein production. A commonly utilized strain of *E. coli,* BL21 RIPL contains additional tRNA synthetase genes shown to improve recombinant protein expression levels of mammalian proteins in *E. coli*. Therefore, BL21 RIPL cells were used for the initial screening of the affinity tag. We observed that a significant percentage of recombinant Mitofusin protein in BL21 RIPL cells was still insoluble; therefore, we tested a strain of *E. coli* known to help improve solubility. SoluBL21 *E. coli* is a randomly mutagenized strain which was developed to produce more soluble protein in cases were little soluble protein was obtained with standard BL21 *E. coli*. SoluBL21 *E. coli* significantly improved the solubility without effecting the overall expression level of $His_6$-SUMO-Trigger Factor tagged Mitofusin protein as compared to BL21 RIPL cells and was therefore used for the purification of recombinant Mitofusin protein described below.

#### 2.3.1.3 Removal of the affinity tag

The N-terminal tag could impact the enzymatic activities of the recombinant Mitofusin, especially because of its large size of approximately 75 kilodaltons (kDa) and therefore, we engineered a protease cleavage site between the Trigger fusion and the start of the Mitofusin protein. Unfortunately, the cleavage and removal of the $His_6$-SUMO-Trigger Factor tag was inefficient by either Tobacco Etch Virus (TEV) or 3C (PreScission) protease with no additional amino acids in between the Mitofusin and the SUMO-Trigger Factor tag. Therefore, two different linkers were inserted between the affinity tag and the Mitofusin. We hypothesized that additional amino acids between the TEV protease site and the Mitofusin might increase the accessibility of the protease to the cleavage site. We tested two different linker sequences, 10x asparagine (N10) and flexible 8x glycine (G8) linker. We found that both linkers greatly improved the cleavage of the $His_6$-SUMO-Trigger Factor tag and choose N10 linker as it showed slightly higher and more reproducible tag cleavage. Even with the addition of the N10 linker, the cleavage of the $His_6$-SUMO-Trigger Factor tag from Mfn2 was significantly lower than for Mfn1. Mfn2 has a 21 amino acid extension on the N-terminus in comparison to Mfn1. Therefore, we tested a construct where these 21 amino acids were removed from the N-terminus (starting at the second methionine). This greatly increased the efficiency of $His_6$-SUMO-Trigger Factor tag cleavage and removal. The final constructs used were as follows: $His_6$-SUMO-Trigger Factor-TEV-N10-Mfn1 and $His_6$-SUMO-Trigger Factor-TEV-N10-Short Mfn2.

#### 2.3.1.4 *E. coli* growth medium

Three different *E. coli* growth medias were tested: LB, 2XYT and TB. Cells grown in TB increased had increased protein insolubility. Cells grown in LB media produced moderate levels

of protein but did not alter the solubility of the protein. Cells grown in 2XYT produced the most soluble protein per liter of culture and was therefore used for the rest of the protocol development described below.

#### 2.3.1.5 IPTG induction concentration and temperature

We used the IPTG induction system to induce recombinant Mitofusin protein production. This system utilizes IPTG as a mimic for allolactose which binds to the lac operon and drives expression of metabolic genes. The Mitofusin gene was placed under the control of the lac operator and expression of the Mitofusin was controlled by the addition of IPTG. Varying the concentration of IPTG can affect both the amount and rate at which recombinant protein is produced. Initially a high IPTG concentration (400 μM) was tested which produced large amounts of the recombinant protein but most protein was insoluble at lysis and any purified protein had a higher propensity to aggregate during the purification. Given the relatively low solubility we considered that moderate expression could improve the protein folding and solubility. Therefore, different concentrations of IPTG were tested and the ratio of soluble to insoluble protein was compared. The induction was subsequently lower to 100 μM, 75 μM and finally 60 μM all of which helped reduce the overall amount of recombinant protein produced and improve the solubility. Lower IPTG concentrations were also tested (10 μM, 25 μM and 50 μM) but these failed to robustly induce protein expression. It was also determined that moderating the rate of protein expression by growth at cold temperatures improved the solubility of Mitofusin proteins. The final induction conditions utilized were 60 μM IPTG overnight (~16 hrs) at 16°C.

#### 2.3.1.6 Development of buffer conditions

The DRPs have been extremely difficult to purify as they have the propensity to form large oligomeric structures. We started with buffer composition similar to that used to purify the yeast inner membrane fusion protein Mgm1: 25 mM HEPES [pH 7.0], 25 mM PIPES [pH 7.0], 500 mM NaCl, 0.1% Triton X-100, 2 mM 2-mercaptoethanol (DeVay et al., 2009). Mgm1 was the only recombinantly purified mitochondrial fusion protein reported at the start of this project and has a similar modest hydrophobic transmembrane domain as the Mitofusins. Over the course of buffer development, it was determined that increasing the buffer pH to 7.4, addition of 10% glycerol which helps to minimizes hydrophobic contacts and increasing the Triton X-100 detergent concentration during lysis to 1.0% improved the solubility and stability of the protein. To facilitate in the insertion of Mitofusins into liposomes a detergent exchange was performed during the on-column wash step to 0.1% N-octanoyl-N-methylglucamine (Mega8) which was also done for the Mgm1 protein purification. The final buffers used are as follows: Lysis buffer: 50 mM HEPES-KOH [pH 7.4], 500 mM KCl, 10% glycerol, 1% Triton X-100, 75 mM imidazole [pH 8.0], 0.5 mM phenylmethanesulfonylfluoride (PMSF), 0.5x protease inhibitor cocktail, 4 mM dithiothreitol (DTT); Wash buffer: 50 mM HEPES-KOH [pH 7.4], 500 mM NaCl, 90 mM imidazole [pH 8.0], 10% glycerol, 0.1% Mega8, 4 mM DTT, 0.5 mM PMSF; Elution buffer: 50 mM HEPES-KOH [pH 7.4], 500 mM KCl, 500 mM imidazole [pH 8.0], 10% glycerol, 0.1% Mega8, 4 mM DTT, 0.5 mM PMSF; Desalting buffer: 50 mM HEPES-KOH [pH 7.4], 500 mM KCl, 10% glycerol, 0.1% Mega8, 1 mM tris(2-carboxyethyl)phosphine (TCEP). Final protein concentration for each preparation was highly variable and ranged from 100 µg/mL to 1500 µg/mL per 2 to 4 liters of culture *E. coli*. Typically, lower protein concentrations correlated with a higher quality of protein based on solubility assessed by sucrose gradient ultracentrifugation.

#### 2.3.1.7 Final protein purification method

The final constructs ($His_6$-SUMO-Trigger-TEV-N10-Mfn1/Short 2) were expressed in *E. coli* SoluBL21 cells cultured in 2XYT medium. Cells were initially grown at 37°C to an $OD_{600}$ of ~ 0.6 and were then chilled on ice to approximately 16°C before protein expression was induced by the addition of 60 μM IPTG. Two to four liters of cells were grown overnight (16-20 hours) at 16°C, pelleted, washed in PBS buffer, snap frozen in liquid nitrogen and store at -80°C. Cells were resuspended in 50 mL lysis buffer and lysed by passing through a microfluidizer 3 to 4 times. The lysate was subjected to centrifugation at 14,000 RPM for 45 minutes. The supernatant was applied to a 1 mL HisTrap HP column equilibrated with wash buffer attached to AKTAprime plus at a flowrate of 0.5 mL/min, non-specific interactors were then removed by washing with 30 column volumes of wash buffer at a flowrate of 1 mL/min and subsequently, bound proteins were removed with elution buffer at a flowrate of 0.7 mL/min. Mfn1/2 containing elution fractions (generally 1-1.5 mL) were mixed with $His_6$-fused TEV protease at a 1:20 ratio (TEV:Mitofusin) and this was immediately desalted using a spin column against desalting buffer and incubated at 4°C overnight to facilitate cleavage and removal of the $His_6$-SUMO-Trigger Factor tag. The next morning, the protein was applied twice to 50 μL Ni-NTA beads equilibrated with desalting buffer for 30 minutes to adsorb uncleaved protein, cleaved affinity tag and TEV protease. Glycerol was added to the unbound fraction to a final concentration of 20% before the protein was aliquoted into thin-walled PCR tubes, snap frozen in liquid nitrogen and stored at -80°C. Protein concentration was determined by Bradford assay. Figure 2.3 shows a representative SDS-PAGE gel of a Mitofusin protein preparation.

## 2.3.2 Characterization of purified recombinant Mitofusin protein

DRPs are characterized as large GTPase proteins that bind and hydrolyze nucleotide and self-assemble into higher order structures. Therefore, we sought to quantify Mitofusin protein nucleotide binding and hydrolysis and assess the oligomeric state under different nucleotide conditions. GTPase activity was measured with the malachite green colorimetric assay. Nucleotide binding was measured by intrinsic tryptophan fluorescence and MANT-nucleotide binding assays. Higher order assembly was assessed by negative stain electron microscopy, BN-PAGE and sucrose gradient ultracentrifugation. We also predict that the Mitofusins make large conformational changes, which were assessed by limited protease protection.

### 2.3.2.1 GTPase activity

GTPase activity was measured using a colorimetric malachite green assay that detects inorganic phosphate liberated by GTP hydrolysis. Very low levels of phosphate release were observed for both Mfn1 and Mfn2, but when mutant proteins predicted to lack enzymatic activity were purified, we observed no decrease in phosphate release, suggesting that we were detecting non-specific activity. Various buffers, salt concentrations, detergents, addition of lipids, mixing Mfn1 and Mfn2 together and protein concentrations were tested, but no significant GTPase activity was ever detected. This suggests that my preparations of Mfn1 and Mfn2 lacked GTP hydrolysis activity, at least in solution.

#### 2.3.2.2 Nucleotide binding

Two different assays were used to measure the nucleotide binding by Mfn1 or Mfn2. Firstly, an intrinsic tryptophan fluorescence assay measured changes in the local environment of 8 tryptophan residues; in particular 4 are located in the GTPase domain, which are likely to change upon nucleotide binding. This assay has been successfully used to measure nucleotide binding of the homotypic ER fusogen Atlastin, which also contains 4 tryptophan residues exclusively in the GTPase domain (Winsor et al., 2018). Intrinsic tryptophan fluorescence was measured by exciting the protein's tryptophan residues at a wavelength of 280 nm and measuring the emission at 360 nm. The tryptophan fluorescence intensity decreased for Mfn1 upon addition of either GTP, GDP or GTPγS (Figure 2.4 A). A variety of different GTPase domain mutant variants were tested and all showed similar changes in fluorescence upon the addition of GTP or GDP (Figure 2.4 B&C). Although $Mfn1^{K88A}$, $Mfn1^{S89N}$, $Mfn1^{D178A}$ and $Mfn2^{K109A}$ are all predicted to lack GTP hydrolysis it is unclear whether these mutant variants lack nucleotide binding, therefore we lacked a proper negative control for this assay. Recent analysis of the high-resolution structure of the $Mfn1_{IM}$ minimal GTPase domain construct showed that there is a tryptophan residue positioned in the nucleotide binding pocket that substantially moves upon nucleotide binding acting as a tryptophan switch (Cao et al., 2017). In retrospect this is possibly why we observe a decrease in tryptophan fluorescence even with mutant variants that lack GTP hydrolysis as a binding event would cause this tryptophan to move and other GTP hydrolysis dependent structural changes would not be required which is the case for Atlastin. Isothermal titration calorimetry analysis of the tryptophan switch mutant variant ($Mfn1^{W239A}$) indicated that it lacked both nucleotide binding and hydrolysis and therefore could be used as a negative

control in the future (Cao et al., 2017). These results suggest that both Mfn1 and Mfn2 including multiple mutants in the GTPase domain were capable of binding nucleotide.

Secondly, two different MANT-nucleotides were used to measure nucleotide binding, MANT-GTP and MANT-GMPPNP. The relative fluorescence of fluorescent labeled MANT-nucleotides increases when bound to protein. No change in either MANT-GTP or MANT-GMPPNP fluorescence was observed for either Mfn1 or Mfn2. The tryptophan fluorescence and MANT binding assays produced contradictory results. The high-resolution $Mfn1_{IM}$ structure revealed that Mfn1 possesses a very shallow nucleotide binding pocket on the surface of the protein. It's conceivable that this shallow pocket would not change the environment of the MANT-moiety enough to significantly increase its fluorescence upon nucleotide binding. These results suggest that recombinant Mitofusin protein is possibly binding nucleotide and that GTPase domain mutations have little to no effect on nucleotide binding.

#### 2.3.2.3 Sucrose gradient ultracentrifugation

The oligomeric state of the Mitofusins was assessed with sucrose gradient velocity ultracentrifugation. Mitofusin protein pre-incubated with or without various nucleotides was layered on top of a linear sucrose gradient. Following ultracentrifugation, fractions were taken and subjected to SDS-PAGE, then Coomassie stained, silver stained or subjected to western blot analysis based on the amount of input protein. The size characteristics of recombinant Mitofusin protein varied greatly from preparation to preparation. Most protein preparations resulted in the vast majority of the protein in the pellet (>669kDa), indicative of the formation of soluble aggregates (Figure 2.5 B). In a small number of protein preparations, the majority of the protein was in the gradient, although the protein did not form a discrete peak but was distributed through

many fractions (fractions 3-9) corresponding to molecular weights between 140-669kDa without nucleotide (Figure 2.5 A). When the same Mfn1 protein preparation was incubated with either GTP or a transition state mimic GDP $BeF_3$, the majority of the protein shifted to the pellet fraction (Figure 2.6). This shift did not occur with GDP, GTPγS or $BeF_3$ salt only control (Figure 2.6). This suggests that either GTP hydrolysis or the state that immediately follows GTP hydrolysis promote higher order complexes assembly. Therefore, we purified several GTPase domain mutants predicted to lack GTP hydrolysis activity: $Mfn1^{K88A}$, $Mfn1^{T109A}$, $Mfn1^{D178A}$ and $Mfn1^{W239A}$. All of these mutant variants also resulted in the majority of the protein in the pellet fraction of the sucrose gradient in the absence of nucleotide (Figure 2.5 C&D). This likely means that there are multiple factors contributing to the soluble aggregation of recombinant Mitofusin protein. It is possible that the protein is not folded correctly, causing the formation of soluble aggregates. Another possibility is that the protein is assembling into large oligomeric structures which has been observed for other DRP proteins at higher protein concentrations (Bohuszewicz & Low, 2018).

#### 2.3.2.4 Negative stain electron microscopy

An additional way to assess higher order assembly is negative stain electron microscopy which allows for the visualization of Mitofusin protein complexes. Mfn1 formed elongated structures of approximately 15-25 nM containing a globular head domain that may contain 2-4 molecules of Mfn1 (Figure 2.7 A). The protein appeared to be extremely flexible and heterogenous as the majority of particles looked different from each other (Figure 2.7 B). Based on distance measurements of BDLP, Mfn1 fully extended would be approximately 17 nM and in a closed conformation would be 10 nM (PDB 2W6D and 2J68, respectively). Incubating the

protein with either GTP or GTPγS did not obviously change the size or shape/conformation of the protein. Protein aggregation was also evident as it was common to observe large clusters of protein ranging from 100-200 nM in size (Figure 2.7 C). Protein preparations that resulted in the majority of protein residing in the pellet fraction of sucrose gradients had increased number and size of these protein aggregation clusters. Therefore, negative stain electron microscopy could be used as a screening tool for the quality of the protein preparation moving forward.

#### 2.3.2.5 Blue native polyacrylamide gel electrophoresis

Blue native polyacrylamide gel electrophoresis (BN-PAGE) is a technique utilized to determine the native molecular weight of a protein complex. Purified Mitofusin protein was separated by BN-PAGE in the presence or absence of nucleotide. Under both conditions most of the protein ran around the 1,048 and 1,236 kDa markers in a broad smeary band (Figure 2.8 A). This is consistent with the large complexes/aggregates observed by negative stain electron microscopy and the fact that most protein preparations tested by sucrose gradient ultracentrifugation resulted in most of the protein in the pellet fraction. When protein was run on a sucrose gradient (Figure 2.8 B) and then subsequently run on a blue native gel, lower sucrose gradient fractions ran further into the gel than higher sucrose gradient fractions (Figure 2.8 C). These data together suggest that purified Mitofusin protein forms large oligomeric complexes that are prone to aggregate.

#### 2.3.2.6 Protease protection

The Mitofusins are predicted to make large conformational changes upon nucleotide binding and hydrolysis. We reasoned that we might be able to detect these large conformational

changes by performing a limited protease protection assay. This assay uses limiting amounts of protease to generate protease resistant fragments which may change based on the conformation of the protein. Purified Mitofusin protein was incubated with or without nucleotide before being subjected to limited trypsin digestion. Incubation with protease resulted in the appearance of several protected bands, but the pattern was the same in the presence and absence of nucleotide although the protein appeared to be more suspectable to protease in the presence of GTP, GTPγS and GMPPNP (Figure 2.9). This suggests that either the protein does not undergo large conformational changes during nucleotide binding/hydrolysis, that these changes cannot be assessed by protease protection or that the protein is not binding nucleotide.

To probe the identity of these protected bands we utilized a carboxy terminal (C-terminal) FLAG tagged Mfn1. This allowed us to probe purified Mfn1 by silver stain to show the overall digestion pattern, anti-FLAG antibody which binds to the C-terminus and anti-Mfn1 antibody which binds to the middle (residues 350-580) of Mfn1 before and after trypsin digestion (Figure 2.10 B). Mfn1-FLAG recombinant protein purified from *E. coli* was incubated with 3 different concentrations of trypsin protease. Three major unique bands appear, one on the anti-FLAG blot and two on the anti-Mfn1 blot (Figure 2.10 A). A 30 kDa band appeared on the anti-FLAG blot which would represent a protected C-terminal fragment. Two protected bands on the anti-Mfn1 blot appeared at 85 and 50 kDa which could represent a protected fragment that is missing the C-terminus and one that is missing significant portion of the C-terminus including the transmembrane domain, respectively. These results suggest that the protein is likely folded as unique protected bands appeared although addition of nucleotide doesn't appear to significantly alter the digestion pattern.

### 2.3.3 Insertion and characterization of proteoliposomes

The Mitofusins reside in the mitochondrial outer membrane therefore; we reasoned that the Mitofusins might have enzymatic activities in a lipid environment. In addition, many DRP family members enzymatic activities are stimulated by lipids. Ultimately our goal was to characterize these proteins as membrane fusion proteins with fully reconstituted proteoliposome tethering and fusion assays.

#### 2.3.3.1 Insertion of Mitofusins into liposomes

Both Mfn1 and Mfn2 inserted efficiently into detergent solubilized liposomes with lipid composition mimicking the mitochondria outer membrane using a rapid dilution method (described here and was the mostly commonly used method) or by removal of detergent using Bio-Beads (only described in the methods). Two different lipid compositions were used, either a pre-mixed soybean polar lipid extract (45.7%, PC, 22.1% PE, 18.4% PI, 6.9% PA, 6.9% unknown) or a defined mitochondrial outer membrane composition (47% PC, 22% PE, 20% PI, 3% PA, 2% PS, 6% CL). Liposomes were generated with lipid compositions described above with the addition of fluorescently labeled lipids if indicated for visualization after liposome floatation or if needed for downstream assays (i.e. fluorescence microscopy or liposome fusion). Liposomes were also extruded through a polycarbonate filter to either 100 nM or 1000 nM before solubilization to obtain uniform size and to generate unilamellar vesicles. These preformed liposomes were incubated with Mega8 and then Mitofusin protein was added. Detergent was rapidly diluted below the critical micelle concentration (CMC) and salted washed proteoliposomes were separated by centrifugation through a gradient of OptiPrep density

medium. Mitofusin containing proteoliposomes floated to the 6-20% interface and were collected from this interface for biochemical characterizations. (Figure 2.11 A&B).

#### 2.3.3.2 Proteoliposome validation

With this approach, proteins can insert into liposomes either facing in or facing out. The correct topology for the Mitofusins is to face out, the orientation observed in cells where both the amino and carboxy termini are facing the cytosol. To determine the orientation of the proteins in the proteoliposomes, protease protection assays were performed where proteins facing outward will be suspectable to proteolytic cleavage whereas proteins facing inwards will be protected. No proteolytic degradation of Mfn1 occurred if trypsin was pre-inactivated by soybean trypsin inhibitor. Incubation of proteoliposomes with trypsin protease resulted in complete proteolytic degradation of Mfn1, which confirmed that the vast majority of the protein was in the correct orientation (Figure 2.11 C). As a positive control, the proteoliposomes were solubilized with detergent and this also resulted in complete proteolytic degradation of the protein. Together these results confirm that the inserted Mitofusin protein is in the correct orientation.

In addition, different lipid compositions were tested as other DRPs enzymatic activity can be modulated by lipid composition. The concentration of PA and CL was varied in the defined mitochondrial outer membrane composition (see above). Previous work suggests that the conversion of CL to PA by mitoPLD increases Mitofusin activity (Choi et al., 2006). Of note, increasing the PA concentration from the standard 3% to 15% or 33% in the defined mitochondrial outer membrane composition resulted in the proteoliposomes to float as a flocculent band (Figure 2.12). These results suggest that recombinant Mitofusin protein was sensitive to the lipid environment. In the future, using liposomes with high percentage of PA

could be valuable as the flocculation of proteoliposomes is suggestive of Mitofusin dependent tethering.

#### 2.3.3.3 Proteoliposome GTPase activity

For other DRPs, the GTPase activity is stimulated in the presence of lipids (Ban et al., 2017; DeVay et al., 2009; Francy et al., 2015, 2017; Song et al., 2004). Therefore, we set out to measure enzymatic activity of membrane inserted Mitofusin protein using the malachite green colorimetric assay. The GTPase activity was measured using various protein to lipid ratios and lipid compositions; unfortunately, no GTPase activity over background was detected. This suggests that this recombinant Mitofusin protein also lacks GTPase activity in a lipid environment or that its activity is too low to measure.

#### 2.3.3.4 Proteoliposome nucleotide binding

Nucleotide binding of Mitofusin-containing liposomes was tested using intrinsic tryptophan fluorescence assay. The change in tryptophan fluorescence before and after addition of nucleotide was measured. Unfortunately, the fluorescent signal was too low to be confident in the results. This result it not surprising given the small amount of protein in each reaction.

#### 2.3.3.5 Proteoliposome protease protection

Large nucleotide dependent protein conformational changes of Mitofusin-containing liposomes were assessed again by protease protection. Proteoliposomes containing Mitofusin protein were incubated either with or without nucleotide before being subjected to either trypsin or chymotrypsin protease digestion. Incubation with protease resulting in the appearance of

several protected bands, but the pattern was the same in the presence and absence of nucleotide (Figure 2.13 A&B). This suggests that the protein does not undergo large conformational changes upon nucleotide binding and/or hydrolysis, that these changes cannot be assessed by protease protection or that the protein is not binding nucleotide.

#### 2.3.3.6 Proteoliposome protein assembly

Detergent solubilized Mitofusin proteoliposomes were run on a BN-PAGE in the presence or absence of nucleotide. Under both conditions most of the protein ran around the 1,048 and 1,236 kDa markers in a broad smeary band (Figure 2.14). These results looked very similar to blue native gels of purified protein in the absence of lipids (compare to Figure 2.8).

#### 2.3.3.7 Proteoliposome chemical crosslinking

An additional way to monitor high-order protein assembly is by chemical crosslinking. Proteoliposomes containing Mfn1 were incubated either with or without nucleotide before being subjected to bis(sulfosuccinimidyl)suberate ($BS_3$) crosslinker (Figure 2.15). Mfn1 without crosslinker runs as a predicted monomer whereas incubating with increasing concentrations of crosslinker results smeary bands that correspond to tetramers and larger oligomers (> 460kDa). Pre-incubation with either GTPγS or GMPPNP did not significantly alter the banding pattern. These results support the sucrose gradient, BN-PAGE and negative stain electron microscopy data that recombinant Mitofusin protein forms very large oligomeric complexes.

#### 2.3.3.8 Proteoliposome tethering assays

The Mitofusins have been proposed to tether two mitochondria together before membrane fusion. Therefore, we developed two different assays to measure proteoliposome tethering. Firstly, proteoliposomes were incubated with and without nucleotide and then imaged by fluorescent microscopy, looking for proteoliposomes that were in close proximity. There were no conditions where we observed significant proteoliposome tethering by fluorescence microscopy. Secondly, proteoliposome tethering was probed by measuring the turbidity of the reaction with and without the addition of nucleotide. The turbidity of a sample can be measured by optical light at 405 nM in a plate reader. As a solution becomes more turbid or as proteoliposomes tether together more light is diffracted leading to an increase in optical density of the solution. Results were highly variable with most experiments resulting in no significant increase in the turbidity of the reaction with the addition of nucleotide. On a few occasions with lipid compositions containing either 15% or 33% PA, addition of GTPγS resulted in small increase (~0.04-0.08 $OD_{405}$) in turbidity of the reaction, but this result was not highly reproducible (Figure 2.16). Therefore, it appears that recombinant purified Mitofusin-containing proteoliposomes were incapable of performing membrane tethering.

#### 2.3.3.9 Proteoliposome fusion assays

Two different assays were developed to measure Mitofusin-dependent proteoliposome fusion. Firstly, proteoliposome fusion was measured by the dequenching of NBD fluorescence. For NBD dequenching, two proteoliposomes populations were generated, one population that contained both rhodamine and NBD lipids and one unlabeled population. The rhodamine moiety and NBD moiety at equal molar ratios are sufficiently close to each other to promote

fluorescence quenching of the NBD moiety. Upon proteoliposome fusion the two-fold dilution of the rhodamine and NBD lipids is significant enough to unquench the NBD fluorescence. Various protein to lipid ratios and lipid compositions were tested, but unfortunately no dequenching of NBD fluorescence was observed. Additionally, visualization of differentially labeled proteoliposome populations by fluorescence microscopy failed to result in colocalization of the two fluorophores in the same vesicle under any nucleotide condition. In concordance with the lack of GTP hydrolysis and proteoliposome tethering, it appears that under the conditions studied here, Mitofusin proteoliposomes are unable to perform membrane fusion.

## 2.4 Discussion

The purification of recombinant full length Mitofusin protein was extremely difficult. The vast majority of protein preparations resulted in the formation of soluble aggregates even at final protein concentrations of less than 0.5mg/mL. In addition, most biochemical assays failed to show that the recombinant protein had predicted enzymatic activities including GTP hydrolysis, nucleotide binding, making large conformational changes and tethering or fusing proteoliposomes. Several experiments indicate that the recombinant Mitofusin protein was folded: it was protected from proteolytic digestion through the appearance of several protected bands, appeared to have some structural order by negative stain electron microscopy, appeared to bind nucleotide by a decrease in tryptophan fluorescence and appeared to form larger oligomeric complexes in the presence of nucleotide by sucrose gradient ultracentrifugation.

The protein purification method evolved over the 2 years I worked on this project. The biggest factors that contributed to the solubility and stability of recombinant Mitofusin protein were expression of the protein in SoluBL21 *E. coli* cells using low (60 μM) IPTG induction conditions, lysing the *E. coli* cells in 1% Triton X-100 detergent and the addition of 10% glycerol and 500 mM KCl to all buffers. Both Mfn1 and Mfn2 were expressed and purified using a large N-terminal solubility/affinity tag ($His_6$-SUMO-Trigger Factor-N10-Mfn) for all of the experiments described above. Using the final purification conditions described in the methods, I was able to obtain Mitofusin protein using only a minimal N-terminal $His_6$ affinity tag. Unfortunately, this construct still suffered from the same problem as the larger affinity tag where a significant amount of the protein (approximately 30%) formed soluble aggregates (Figure 2.17). I propose that when the protein becomes too concentrated at any step during the

purification, irreversible soluble aggregates form. In the future, I would continue using the smaller $His_6$ affinity tag as it eliminates an overnight incubation step with TEV protease and subsequent steps to remove the protease and cleaved tag. This allows for the protein to be aliquoted and frozen approximately 18 hours sooner which reduces the amount of time the protein has to aggregate. I would also attempt to keep the protein at lower protein concentrations during the duration of the purification (< 0.5 mg/mL). It was common for the protein to elute off the column at concentrations greater than 1.0 mg/mL. Possible solutions to combat this high protein concentration would be to use a smaller culture size, greater column size or immediately dilute the protein as it comes off the column.

One possible explanation as to why recombinant Mitofusin protein from *E. coli* lacked any enzymatic activity is that the protein requires post-translational modifications that would be absent in *E. coli*. The Mitofusin proteins have been shown to be phosphorylated, acetylated and ubiquitinated which regulate the protein's activity or degradation. In yeast, Fzo1 requires a cascade of ubiquitination events for membrane fusion. Therefore, use of a mammalian expression system could provide these necessary post-translational modifications. The lab in currently working to develop a doxycycline inducible HEK-293 cell line. This cell line allows for the proper targeting of the Mitofusin to the mitochondria and to induce Mitofusin expression rapidly (significant expression after 4 hours). This is extremely useful as overexpression of the Mitofusin proteins leads to aggregation of the mitochondria which might also impair the Mitofusin enzymatic activity and could lead to Mitofusin protein aggregation. We will likely be able to tune the system to provide high quality protein by changing either the amount of doxycycline and/or induction time. Because the Mitofusin protein is properly targeted to the mitochondria, isolation of the mitochondria could be used as a purification and enrichment step.

The DRP family of proteins have been challenging to purify because the proteins self-assemble into large structures. In order to achieve high resolution crystal structures of Dynamin and Drp1, amino acid substitutions in the alpha helical stalk domain blocking self-assembly were required (Ford et al., 2011; Fröhlich et al., 2013). In addition, Dynamin can self-assemble into rings and helices in the absence of nucleotide by reducing the ionic strength of the buffer (Hinshaw & Schmid, 1995). It is possible that recombinant Mitofusin protein was experiencing something similar with the formation of these soluble aggregates. We observed that Mitofusin mutant variants that lack nucleotide binding and/or hydrolysis were still capable of forming soluble aggregates. These results are inconsistent from Dynamin as sucrose gradient ultracentrifugation was performed at high ionic strength which should minimize oligomerization. Therefore, another possibility is that a portion of the protein is not properly folded and consequently at higher protein concentrations this leads to aggregation. This problem is difficult to address and may be fixed by moving to a different expression system.

In conclusion, the expression and purification of recombinant Mitofusin protein in *E. coli* was largely unsuccessful. If this project were to be attempted again, I would consider moving to a different host expression system. If *E. coli* were to be used again, I would start with the expression and purification methods described below but use an N-terminal $His_6$ affinity tag instead of $His_6$-SUMO-Trigger Factor-N10 affinity tag.

## 2.5 Material and Methods

### 2.5.1 Full length Mitofusin protein purification

Mutations were made by Gibson assembly and confirmed by sequencing. $His_6$-SUMO-Trigger-N10-Mfn1/2 constructs were expressed in *Escherichia coli* SoluBL21 cells. Cells were cultured in 2xYT medium with 150 μg/mL ampicillin at 37°C to an $OD_{600}$ of ~ 0.6, cultures were chilled on ice to approximately 16°C and protein expression was induced by the addition of 60 μM isopropyl-1-thio-β-d-galactopyranoside (IPTG). Induced cultures were grown overnight at 16°C. Two liters of cells were harvested by centrifugation at 6,000 x *g* for 10 minutes. Cell pellets expressing Mfn1/2 were resuspended in 5 mL phosphate buffered saline, pelleted by centrifugation at 4,000 x *g* for 20 minutes, frozen in liquid nitrogen and stored at -80°C. Cells were thawed in a room temperature water bath and resuspended in 50 mL 50 mM HEPES-KOH [pH 7.4], 500 mM KCl, 10% glycerol, 1% Triton X-100, 75 mM imidazole, 0.5 mM phenylmethanesulfonylfluoride (PMSF), 0.5x protease inhibitor cocktail (Thermo Scientific), 4 mM dithiothreitol (DTT). Cells were lysed using a microfluidizer at approximately 10,000 Psi and passed through 3 to 4 times (Avestin). The lysate was subjected to centrifugation at 14,000 RPM for 45 minutes. The supernatant was applied to 1 mL HisTrap HP column (GE Healthcare) attached to AKTAprime plus (GE Healthcare) equilibrated with Wash Buffer (50 mM HEPES-KOH [pH 7.4], 500 mM NaCl, 90 mM imidazole [pH 8.0], 10% glycerol, 0.1% N-octanoyl-N-methylglucamine (Mega8), 4 mM DTT, 0.5 mM PMSF) at a flowrate of 0.5 mL/min. HisTrap HP column bound to protein were washed with 30 column volumes of wash buffer at a flowrate of 1 mL/min and proteins were eluted with elution buffer (50 mM HEPES-KOH [pH 7.4], 500 mM KCl, 500 mM imidazole [pH 8.0], 10% glycerol, 0.1% Mega8, 4 mM DTT, 0.5 mM

PMSF) at a flowrate of 0.7 mL/min. Mfn1/2 containing elutions were mixed with 1:20 ratio of $His_6$-fused Tobacco Etch Virus (TEV) protease to remove the amino-terminal $His_6$-SUMO-Trigger Factor tag. This was immediately desalted using Zeba™ Spin Desalting Columns 10 MWCO (Thermo Fisher Scientific) against desalting buffer (50 mM HEPES-KOH [pH 7.4], 500 mM KCl, 10% glycerol, 0.1% Mega8, 1 mM tris(2-carboxyethyl)phosphine (TCEP)) and incubated at 4°C overnight. The protein was applied twice to 50 µL Ni-NTA beads for 30 minutes each time (Thermo Fisher Scientific) equilibrated with desalting buffer. Glycerol was added to 20% before the protein was aliquoted and stored at -80°C. Protein purification was performed at 4°C. Protein concentration was determined by Bradford assay (Bio-Rad Laboratories).

### 2.5.2 Tobacco Etch Virus (TEV) protein purification

$His_6$-MBP-TEV construct was transformed into *Escherichia coli* BL21 RIPL cells. Cells were cultured in LB medium with 150 µg/mL ampicillin and 25 µg/mL chloramphenicol at 37°C to an $OD_{600}$ of ~ 0.6 and protein expression was induced by the addition of 1 mM isopropyl-1-thio-β-d-galactopyranoside (IPTG). Induced cultures were grown at 30°C for 4 hours. 1.5 liters of cells were harvested by centrifugation at 6,000 x *g* for 10 minutes. Cell pellets expressing TEV were resuspended in 5 mL phosphate buffered saline, pelleted by centrifugation at 4,000 x *g* for 20 minutes, frozen in liquid nitrogen and stored at -80°C. Cells were thawed in a room temperature water bath and resuspended in 50 mL 20 mM HEPES-KOH [pH 7.5], 1000 mM KCl, 10% glycerol, 0.1% Triton X-100, 0.5 mM phenylmethanesulfonylfluoride (PMSF), 0.5x protease inhibitor cocktail (Thermo Scientific). Cells were lysed using a microfluidizer at approximately 10,000 Psi and passed through 5 times (Avestin). The lysate was subjected to centrifugation at

14,000 x g for 35 minutes. The cleared supernatant was nutated with 5 mL Ni-NTA beads for 1 hour (Thermo Fisher Scientific) equilibrated with lysis buffer. Ni-NTA beads bound to protein were washed with 10 column volumes of lysis buffer, followed by 5 column volumes of wash buffer (20 mM HEPES-KOH [pH 7.5], 1000 mM KCl, 10% glycerol, 0.1% Triton X-100, 20 mM Imidazole [pH 8.0], 0.5 mM phenylmethanesulfonylfluoride (PMSF)). Bound proteins were eluted with elution buffer (20 mM HEPES-KOH [pH 7.5], 1000 mM KCl, 10% glycerol, 0.1% Triton X-100, 250 mM Imidazole [pH 8.0], 0.5 mM phenylmethanesulfonylfluoride (PMSF). 5 mLs of elution fractions containing highest protein concentrations were subsequently loaded onto a Superdex200 16/60 column (GE Healthcare) equilibrated with gel filtration buffer ((20 mM HEPES-KOH [pH 7.5], 500 mM KCl, 10% glycerol, 0.1% Triton X-100). Glycerol was added to 50% to TEV containing fractions before the protein was aliquoted and stored at -80°C. Protein purification was performed at 4°C. Protein concentration was determined by Bradford assay (Bio-Rad Laboratories).

### 2.5.3 PreScission protein purification

GST-PreScission construct was transformed into *Escherichia coli* BL21 RIPL cells. Cells were cultured in 2XYT medium with 150 μg/mL ampicillin at 37°C to an $OD_{600}$ of ~ 0.6 and protein expression was induced by the addition of 200 μM isopropyl-1-thio-β-d-galactopyranoside (IPTG). Induced cultures were grown at 30°C overnight. One liter of cells was harvested by centrifugation at 6,000 x *g* for 10 minutes. Cell pellets expressing PreScission were resuspended in 5 mL phosphate buffered saline, pelleted by centrifugation at 4,000 x *g* for 20 minutes, frozen in liquid nitrogen and stored at -80°C. Cells were thawed in a room temperature water bath and resuspended in 50 mL lysis buffer (50 mM Tris [pH 7.6], 100 mM NaCl, 1 mM

phenylmethanesulfonylfluoride (PMSF)). Cells were lysed using a microfluidizer at approximately 10,000 Psi and passed through 3 to 4 times (Avestin). The lysate was subjected to centrifugation at 12,500 x g for 40 minutes. The cleared supernatant was nutated with 12 mL Glutathione agarose resin for 1 hour (Pierce) equilibrated with lysis buffer. Ni-NTA beads bound to protein were washed with 3 column volumes of lysis buffer. Bound proteins were eluted with 10 mL elution buffer (50 mM Tris [pH 7.6], 100 mM NaCl, 20 mM Glutathione). PreScission protease containing elutions were concentrated to 11.5 mg/mL using an Amicon Ultra Centrifugal Filter (MWCO 30) (Millipore) with a buffer exchange during the concentration into storage buffer (50 mM Tris [pH 7.6], 150 mM NaCl, 5 mM DTT, 20% glycerol). Protein was aliquoted and stored at -20°C. Protein purification was performed at 4°C. Protein concentration was determined by Bradford assay (Bio-Rad Laboratories).

### 2.5.4 Liposome preparation

Either chloroform solutions of soybean polar lipid extract or a defined mitochondrial outer membrane lipid composition (47% PC, 22% PE, 20% PI, 3% PA, 2% PS, 6% CL) were dried by nitrogen air stream and then additionally dried for 1 hour in a desiccator under vacuum. Fluorescently labeled lipids were added when indicated. Lipids were rehydrated overnight in 25 mM HEPES-KOH [pH 7.4], 100 mM KCl. Hydrated lipids were vortexed continuously for 5 minutes and extruded through a polycarbonate membrane (0.1 μM or 1 μM) at least 11 times.

### 2.5.5 Liposome protein insertion

Mega8 Insertion Protocol

100 µL extruded liposomes in 25 mM HEPES [pH 7.4], 100 mM KCl buffer were incubated with 10 µL of 10% w/v Mega8 in $H_2O$ for 1 hour at room temperature. Mitofusin protein was added and incubated with solubilized lipids for 15 minutes at room temperature before addition of 435 µL of detergent free buffer (25 mM HEPES [pH 7.4], 100 mM KCl) and incubated at room temperature for 15 minutes. Proteoliposomes were washed at a final concentration of 500 mM KCl and incubated at room temperature for 15 minutes. 685 µL of salt washed proteoliposomes were mixed with 1.165 mL 53% OptiPrep medium (Sigma) and placed at the bottom of an ultracentrifuge tube (Beckman Coulter 3P ultra clear superspeed tube). A step gradient was created by layering 1.5 mL 20% OptiPrep (Sigma), 1 mL 6% OptiPrep and 750 uL 0% OptiPrep medium in 25mM HEPES [pH 7.4], 100mM KCl buffer. Gradients were spun at 46,000 RPM for 2.5 hours at 4°C. Mitofusin-containing proteoliposomes were usually found at the 6-20% interface and were collected for biochemical characterization.

Triton X-100 Insertion Protocol

50 µL extruded lipids in 25 mM HEPES [pH 7.4], 100 mM KCl buffer were incubated with 1 µL of 10% Triton X-100 (Sigma) for 1 hour at room temperature. Mitofusin protein was added and incubated with solubilized lipids for 15 minutes at room temperature before addition of 875 µL of detergent free buffer (25 mM HEPES [pH 7.4], 100 mM KCl). 100 mg of Bio-Beads SM-2 Resin (Bio-Rad) were added and nutated at 4°C for 1 hour. Proteasome liposomes were washed with 117 µL 4M KCl (final concentration of 500 mM KCl) and incubated at room temperature for 15 minutes. 685 µL of salt washed proteoliposomes were mixed with 1.165 mL 53% OptiPrep medium (Sigma) and placed at the bottom of an ultracentrifuge tube. A step gradient was created by layering 1.5 mL 20% OptiPrep, 1 mL 6% OptiPrep and 750 uL 0% OptiPrep medium in 25 mM HEPES [pH 7.4], 100 mM KCl. Gradients were spun at 46,000 RPM for 2.5

hours at 4°C. Mitofusin containing proteoliposomes were usually found at the 6-20% interface and were collected for biochemical characterization.

### 2.5.6 GTPase assay

Frozen protein was thawed on ice and diluted to 1 μM in 50 mM HEPES-KOH [pH 7.4], 100 mM KCl, 5 mM MgCl2, 1 mM TCEP, 0.1% Mega8 or freshly prepared proteoliposomes in 50 mM HEPES [pH 7.4], 2.5 mM $MgCl_2$ buffer. Variable concentrations of GTP were added and reactions were incubated at 37°C for indicated time. Reactions were stopped by mixing 10 μL of the reaction with 40 μL of 200 mM EDTA. Concentrations of free inorganic phosphate were measured using malachite green reagent. Malachite green reagent was added, and reactions were incubated at room temperature for 15 minutes. The optical density at 650 nM was measured and a potassium phosphate standard curve was used to determine the amount of GTP hydrolyzed.

### 2.5.7 Negative stain electron microscopy

Protein was incubated on a glow-discharged carbon coated grid for 30 seconds, washed with water 3 times and stained with 3% uranyl acetate for 30 seconds. Stained grids were imaged using a FEI Morgagni 100 kV TEM Microscope equipped with a Gatan Orius camera.

### 2.5.8 BN PAGE

Protein was thawed on ice, mixed with 5 mM $MgCl_2$ and 2 mM indicated nucleotide and incubated at 37°C for 30 minutes or freshly prepared proteoliposomes in 50 mM HEPES [pH 7.4], 2.5 mM $MgCl_2$ buffer. Digitonin was added to a final concentration of 1% and sample loading buffer was added to a final concentration of 1X (5% Coomassie Brilliant Blue, 100 mM Bis-Tris, 500 mM (E)-amino-caproic acid [pH 7.0]) and mixed occasionally for 10 minutes on

ice. Samples were run on a Novex™ NativePAGE™ 3 - 12% Bis-Tris Protein Gels (Invitrogen) at 4°C. Gels were run at 100 volts for 60 minutes with dark cathode buffer (15 mM Bis-Tris, 50 mM Tricine, 0.02% Serva Coomassie G-250). Dark cathode buffer was replaced with light cathode buffer (15 mM Bis-Tris, 50 mM Tricine) and the gel was run at 500 volts until the dye front ran off the gel. After electrophoresis was complete, gels were either Coomassie stained or transferred to PVDF membrane (Bio-Rad Laboratories) at 30 volts for 16 hours in transfer buffer (25 mM Tris, 192 mM glycine, 20% methanol). Membranes were blocked in 3% BSA for 45 minutes and were probed with anti-Mfn1 antibody overnight at 4°C. Membranes were incubated with DyLight secondary antibody (Invitrogen) at room temperature for 1 hour. Membranes were imaged on LI-COR Imaging System (LI-COR Biosciences). NativeMark Unstained Protein Standard (Life Technologies) was used to estimate molecular weights of Mitofusin protein complexes.

### 2.5.9 MANT nucleotide binding

The baseline fluorescence of 10 µM MANT-GTP in 50 mM HEPES [pH 7.4], 100 mM KCl, 5 mM $MgCl_2$, 0.1% Mega8, 1 mM TCEP was measured for 5 minutes at $360nm_{ex}/440nm_{em}$ at 37°C before addition of variable concentrations of protein and fluorescence intensity was again measured at $360nm_{ex}/440nm_{em}$ for 10 minutes at 37°C. Gemini XPS plate reader (Molecular Devices) was used to perform fluorescent measurements. Fluorescent intensity before and after addition of protein was used to calculate nucleotide binding.

### 2.5.10 Intrinsic tryptophan fluorescence

Variable concentrations of protein were incubated at 37C in 50 mM HEPES [pH 7.4], 100 mM KCl, 5 mM $MgCl_2$, 0.1% Mega8, 1 mM TCEP or freshly prepared proteoliposomes in 50 mM

HEPES [pH 7.4], 2.5 mM $MgCl_2$ buffer and baseline tryptophan fluorescence was measured at $297nm_{ex}/360nm_{em}$ at 1-minute intervals for 10 minutes. 2 mM of the indicated nucleotide was added and fluorescence was measured again. Fluorescent intensity before and after addition of nucleotide was used to calculate nucleotide binding.

### 2.5.11 Sucrose gradient velocity ultracentrifugation

5-25% linear gradients of sucrose were generated by layering 2.5 mL of 5% sucrose buffer (50 mM HEPES [pH 7.4], 500 mM KCl, 0.1% Mega8, 5 mM $MgCl_2$, 1 mM TCEP, 5% glycerol, 5% sucrose) on top of 2.5 mL 25% sucrose buffer (50 mM HEPES [pH 7.4], 500 mM KCl, 0.1% Mega8, 5 mM $MgCl_2$, 1 mM TCEP, 5% glycerol, 25% sucrose) in an ultracentrifuge tube. The tube was parafilmed and laid horizontally for 2 hours at room temperature then vertically for 1 hour at 4°C. 20 ug purified protein or protein standards (HMW calibration kit, GE Healthcare) was pipetted on top of the gradient. If nucleotide was included in the experiment, it was added at a final concentration of 2 mM GDP, 2 mM GTP, 1.25 mM GTPγS, 2.5 mM $BeSO_4$ or 25 mM NaF. Gradients were spun at 100,000 x g for 16 hours at 4°C. 500 µL fractions were collected and a final concentration of 12.5% tricyclic acid was added to the samples. Samples were incubated on ice for at least 15 minutes and then spun at 21,000 x g for 15 minutes. The supernatant was removed, and pellets were washed in 500 uL of cold acetone and spun at 21,000 x g for 15 minutes. The supernatant was removed, and pellets were allowed to dry briefly before being resuspended in 25 µL 1X gel loading buffer. The bottom of the ultracentrifuge tube was also resuspended in 25 µL 1X gel loading buffer and is denoted as pellet or fraction 11. Samples were run on an SDS-PAGE gel and either Coomassie stained or transferred onto nitrocellulose at 100V for 50 minutes in 1X transfer buffer. Membranes were blocked in 4% Milk for at least 45 minutes and were probed with anti-Mfn1 or anti-Mfn2 (Sigma) antibody for 4 hours at room

temperature or overnight at 4°C. Membranes were incubated with DyLight secondary antibody (Invitrogen) at room temperature for 1 hour. Membranes were imaged on LI-COR Imaging System (LI-COR Biosciences).

### 2.5.12 Protease protection

Purified protein or freshly prepared proteoliposomes were incubated with indicated nucleotide and 2.5 mM $MgCl_2$ at 37°C for 10-30 minutes. Subsequentially various concentrations of trypsin or chymotrypsin were added and incubated at 37°C for 5-30 minutes. Reactions were quenched by adding gel loading buffer to a final concentration of 1X. Samples were run on an 12.5% SDS-PAGE gel and silver stained.

### 2.5.13 Fluorescence microscopy for visualizing proteoliposome tethering and/or fusion

Proteoliposomes were generated with either Texas Red DHPE (Invitrogen) or Oregon Green 488 DHPE (Invitrogen) lipids; early experiments used NBD PE (Avanti Polar Lipids) or Rhodamine PE (Avanti Polar Lipids) lipids. Proteoliposomes were mixed in equal molar ratio in 50 mM HEPES [pH 7.4], 1 mM TCEP, 2.5 mM $MgCl_2$ buffer with or without indicated nucleotide at 37°C. 6 μL were pipetted onto a glass slide and covered with coverslip and sealed with nail polish. Images were collected with a Nikon Ti-E widefield microscope with a 100X NA 1.4 oil objective (Nikon), a solid-state light source (Spectra X, Lumencor), and a sCMOS camera (Zyla 5.5 Megapixel).

### 2.5.14 Turbidity tethering assay

Proteoliposomes were incubated in 96 well plate (final reaction volumes tested between 50 and 200 μL) in 50 mM HEPES [pH 7.4], 2.5 mM $MgCl_2$ buffer with 1-2 mM indicated nucleotide

and optical density at $OD_{405nm}$ was measured once per minutes for 45 minutes. Optical density at time zero was used as a baseline.

### 2.5.15 NBD dequenching assay

Donor (NBD + Rhodamine) and acceptor (unlabeled) proteoliposomes were mixed in equal molar ratio with 2 mM GTP and 2.5 mM $MgCl_2$ in a 96 well plate (final reaction volume of 50-100 µL). Fluorescence was measured at $460_{ex}$nm/$538_{em}$nm every 30 seconds at 37°C. Fluorescence at time zero was used as a baseline.

### 2.5.16 Proteoliposome protein crosslinking

Freshly prepared proteoliposomes were pre-incubated with 1 mM indicated nucleotide and 2.5 mM $MgCl_2$ for at least 5 minutes on ice. Variable concentrations of bis(sulfosuccinimidyl)suberate ($BS_3$) crosslinker (Thermo Scientific) was added for indicated amounts of time on ice. Reactions were quenched by adding 50 mM Tris [pH 7.4] for 15 minutes at room temperature. Triton X-100 was added to a final concentration of 1%. Gel loading sample buffer was added to a final concentration of 1X. Samples were run on a NuPAGE™ 3-8% Tris-Acetate gel (Invitrogen) at 150 volts for 75 minutes with Tris-Acetate SDS Running Buffer (50 mM Tricine, 50 mM Tris Base, 0.1% SDS [pH 8.24]). After electrophoresis was complete, gels were transferred to PVDF membrane (Bio-Rad Laboratories) at 104 volts for 1 hour in transfer buffer (25 mM Tris, 192 mM glycine, 20% methanol). Membranes were blocked in 4% Milk for 45 minutes and were probed with anti-Mfn1 or anti-Mfn2 (Sigma) antibody for 4 hours at room temperature or overnight at 4°C. Membranes were incubated with DyLight secondary antibody (Invitrogen) at room temperature for 1 hour. Membranes were imaged on LI-COR Imaging

System (LI-COR Biosciences). HiMark Pre-stained Protein Standard (Life Technologies) was used to estimate molecular weights.

### 2.5.17 Proteoliposome orientation assay

Freshly prepared proteoliposomes were treated with either 4 µg soybean inhibitor, 2 µg trypsin pre-incubated with 4 µg soybean inhibitor, 2 µg trypsin then 4 µg soybean inhibitor, or pre-incubated with final concentration of 1% Triton X-100 then 2 µg trypsin. All reactions were incubated at 37°C for 30 minutes before a gel loading sample buffer was added to a final concentration of 1X. Samples were run on an 8% SDS-PAGE gel and silver stained.

## 2.6 Acknowledgements

I would like to thank all the members of Hoppins lab for their support during this difficult project and the Seattle Organelle Biology Interest Group for their helpful suggestions.

## 2.7 Figures

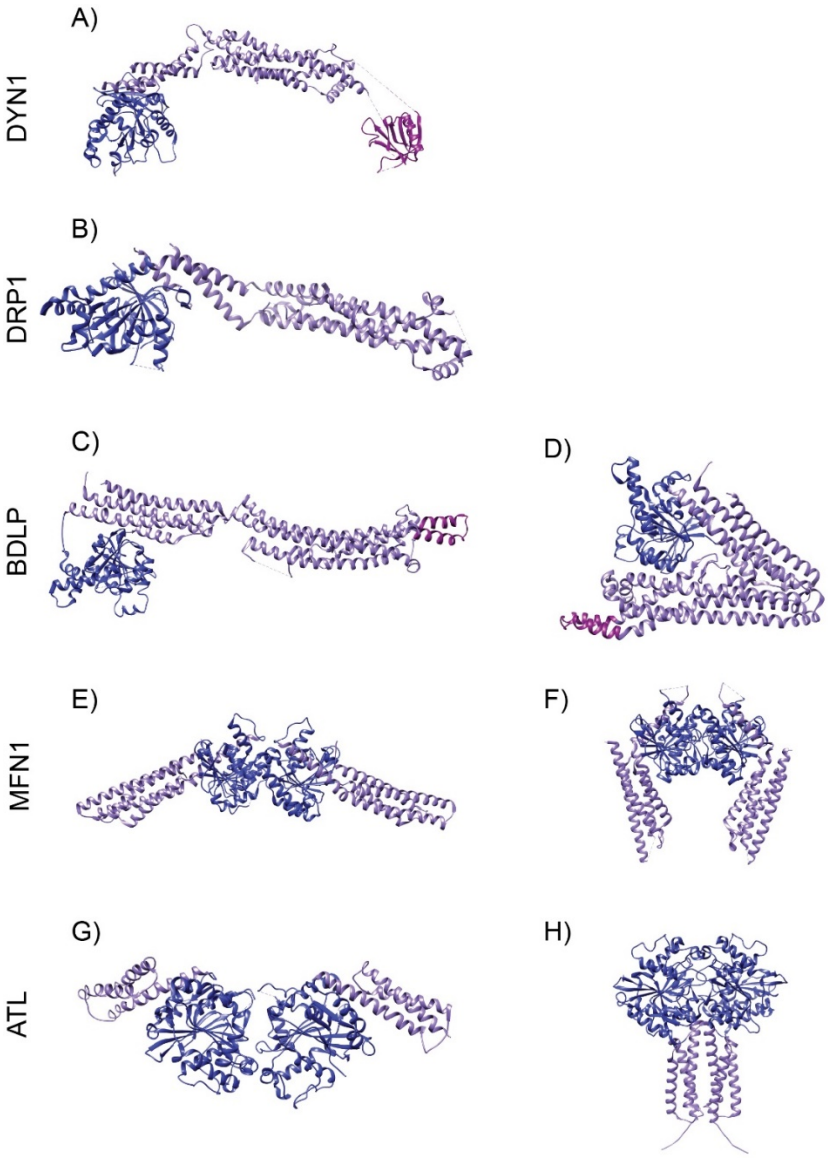


**Figure 2.1 Crystal structures of DRPs**

Globular GTPase is colored in blue, alpha helical bundles are colored in purple and lipid interaction domain (if present in the structure) is colored in magenta. **(A)** DYN1 (PDB 3ZVR), **(B)** DRP1 (PDB 4BEJ), **(C&D)** BDLP (PDB 2J68, 2W6D), **(E&F)** MFN1 (PDB 5GOM, 5YEW), **(G&H)** ATL (PDB 3QOF, 4IDQ).

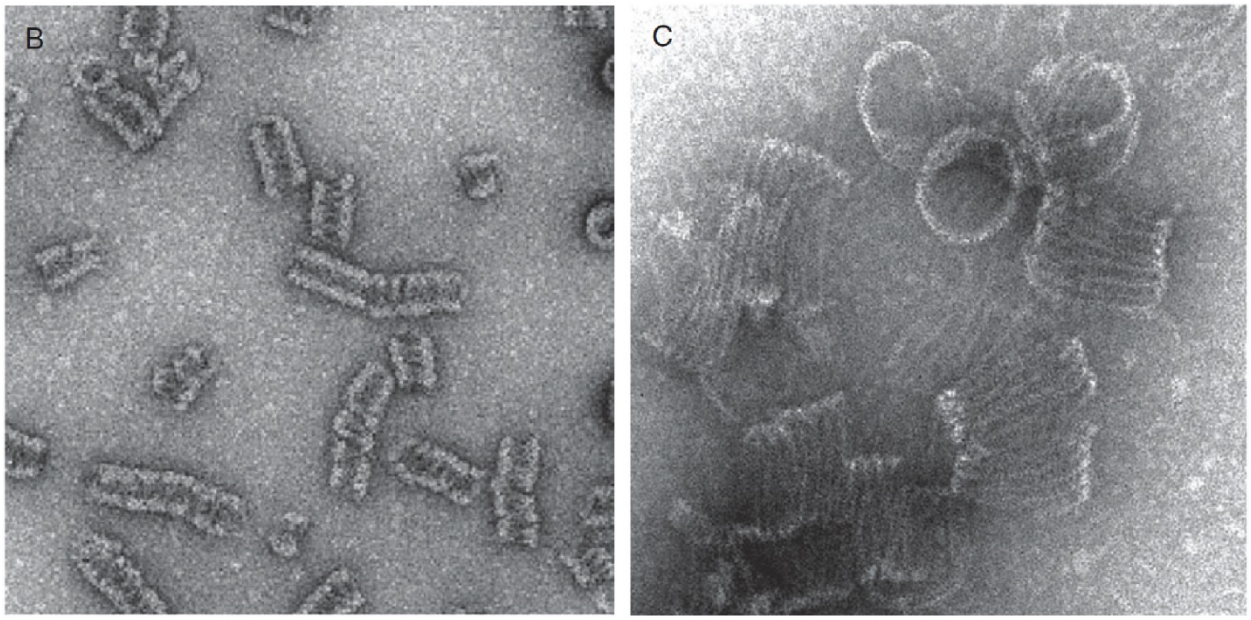


**Figure 2.2 Dynamin and Dnm1 form higher order structures in solution visualized by negative stain electron microscopy**

Adapted from Mears and Hinshaw (2008).

| | Tag | E. coli strain | Detergent | Buffer/pH | Solubility | Binding to beads | Elution from beads | Protease processing |
|---|---|---|---|---|---|---|---|---|
| Mfn1 | His6 | RIPL | up to 4% Triton X-100 | Tris pH 8.0 | inclusion bodies | no data | no data | no data |
| | His6-MBP-N10-TEV | RIPL | 1% Triton X-100 | HEPES/PIPES pH 7.0 | less than half soluble | no data | no data | no data |
| | His6-Trigger-TEV | RIPL | 1% Triton X-100 | HEPES/PIPES pH 7.0 | more than half soluble | (less than) half | (most) all | 90% |
| | | RIPL | None | HEPES/PIPES pH 7.0 | more than half soluble | no data | no data | no data |
| | | RIPL | 1% Triton X-100 | HEPES/PIPES pH 7.0 | more than half soluble | half | all | 90% |
| | | SoluBL21 | 1% Triton X-100 | HEPES/PIPES pH 7.0 | almost all soluble | half | all | 90% |
| | | SoluBL21 | 1% triton | Tris pH 8.0 | almost all soluble | half | all | most |
| | | SoluBL21 | None | Tris pH 8.0 | almost all soluble | half | all | most |
| | | SoluBL21 | 1% Mega8 | Tris pH 8.0 | almost all soluble | half | all | most |
| | His6-SUMO-Trigger-Asn10-TEV | SoluBL21 | 1% Mega8 | Tris pH 8.0 | almost all soluble | half | most | all |
| | | SoluBL21 | 1% Mega8 | HEPES pH 7.4 | almost all soluble | half | most | all |
| | His6-SUMO-Trigger-Strep-TEV | SoluBL21 | 1% Mega8 | Tris pH 8.0 | almost all soluble | half | most | half |
| | His6-SUMO | RIPL | 1% triton | Tris pH 8.0 | most insoluble | no data | no data | no data |
| | | SoluBL21 | 1% triton | Tris pH 8.0 | no expression | no data | no data | no data |
| | | | | | | | | |
| Mfn2 | His6 | RIPL | up to 4% Triton X-100 | Tris pH 8.0 | inclusion bodies | no data | no data | no data |
| | His6-MBP-N10-TEV | RIPL | None | Tris pH 7.6 | less than half soluble | no data | no data | no data |
| | | RIPL | 1% Triton X-100 | Tris pH 7.6 | less than half soluble | less than half | most | barely |
| | | RIPL | 2% Triton X-100 | Tris pH 7.6 | less than half soluble | less than half | most | no data |
| | His6-Trigger-TEV | RIPL | 1% Triton X-100 | HEPES/PIPES pH 7.0 | more than half soluble | half | all | not detectable |
| | | RIPL | 0.1% Triton X-100 | HEPES/PIPES pH 7.0 | half | half | all | not detectable |
| | | RIPL | 1% Triton X-100 | Tris pH 8.0/8.5 | almost all soluble | half | all | not detectable |
| | | SoluBL21 | 1% MEGA8 | Tris pH 8.0 | almost all soluble | half | all | not detectable |
| | | SoluBL21 | 1% Triton X-100 | HEPES/PIPES pH 7.0 | almost all soluble | half | all | not detectable |
| | | SoluBL21 | 1% Triton X-100 | Tris pH 8.0/8.5 | almost all soluble | half | all | not detectable |
| | | SoluBL21 | 1% MEGA8 | Tris pH 8.0 | almost all soluble | half | all | not detectable |
| | | SoluBL21 | 1% n-octyl-beta-glucoside | Tris pH 8.0 | most insoluble | half | all | not detectable |
| | His6-Trigger-PreScission | RIPL | None | HEPES/PIPES pH 7.0 | half | less than half | most | not detectable |
| | | SoluBL21 | 1% Triton X-100 | Tris pH 8.0 | almost all soluble | half | most | barely |
| | His6-SUMO-Trigger-PreScission | RIPL | 0.1% Triton X-100 | HEPES/PIPES pH 7.0 | more than half soluble | less than half | most | not detectable |
| | | SoluBL21 | 1% Triton X-100 | Tris pH 8.0 | almost all soluble | half | most | barely |
| | His6-SUMO-Trigger-TEV | RIPL | 0.1% Triton X-100 | Tris pH 7.6 | half | half | all | no data |
| | | SoluBL21 | 1% Mega8 | Tris pH 8.0 | almost all soluble | half | most | barely |
| | His6-SUMO-Trigger-Asn10-TEV | SoluBL21 | 1% Mega8 | Tris pH 8.0 | almost all soluble | half | most | most |
| | His6-SUMO-Trigger-G8-TEV | SoluBL21 | 1% Mega8 | Tris pH 8.0 | almost all soluble | half | most | most |
| | His6-sfGFP | RIPL | 1% Triton X-100 | Tris pH 8.0 | no expression | no data | no data | no data |
| | | SoluBL21 | 1% Triton X-100 | Tris pH 8.0 | no expression | no data | no data | no data |
| | His6-SUMO | RIPL | 1% triton | Tris pH 8.0 | most insoluble | no data | no data | no data |
| | | SoluBL21 | 1% triton | Tris pH 8.0 | no expression | no data | no data | no data |
| | | | | | | | | |
| Mfn2 2nd Met | His6-SUMO-Trigger-Asn10-TEV | SoluBL22 | 1% Mega8 | Tris pH 8.0 | almost all soluble | half | most | all |
| | | SoluBL21 | 1% Mega8 | HEPES pH 7.4 | almost all soluble | half | most | all |

**Table 2.1 Summary table of recombinant Mitofusin purification method development**

The table includes different affinity tags, *E. coli* strains, detergent, linkers and buffers used.

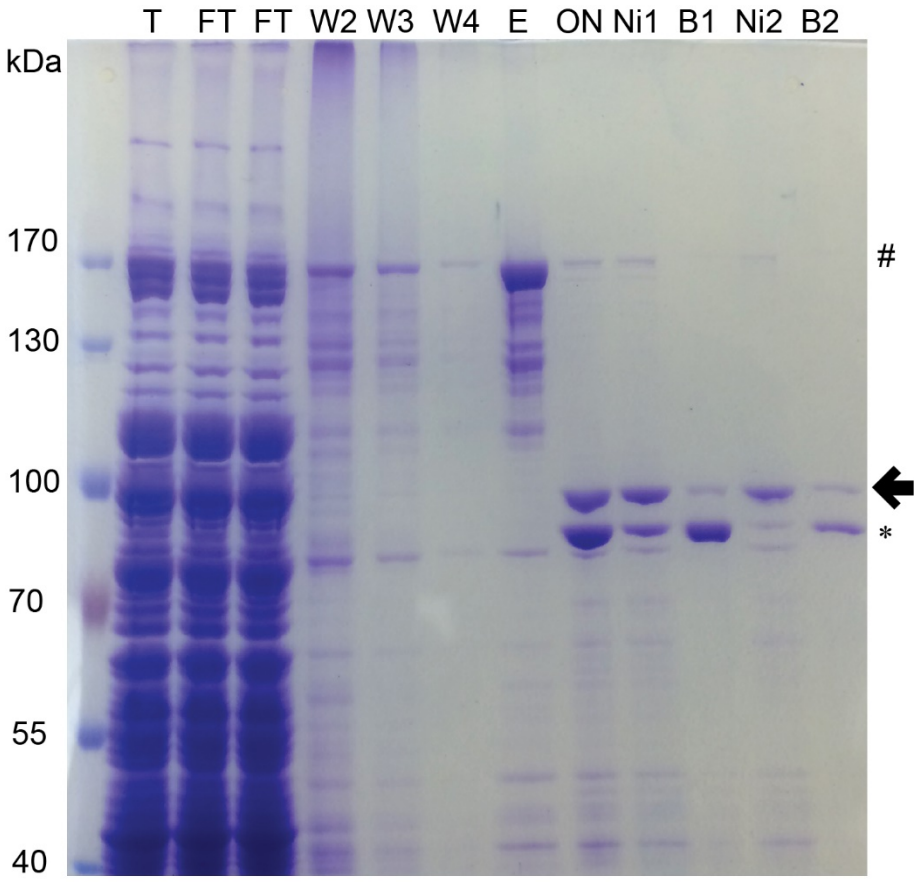


**Figure 2.3 Recombinant protein purification of His6-SUMO-Trigger Factor-N10-Mfn1**

Representative Coomassie stained 8% SDS-PAGE gel of recombinant Mfn1 purification. T = total, FT = flow through, W = wash, E = elution, ON = overnight digestion, Ni = supernatant after binding to nickel beads, B = protein bound to nickel beads. # indicates full length protein, arrow indicates cleaved Mfn1, * indicates cleaved tag. Ni2 represents the final purified protein.

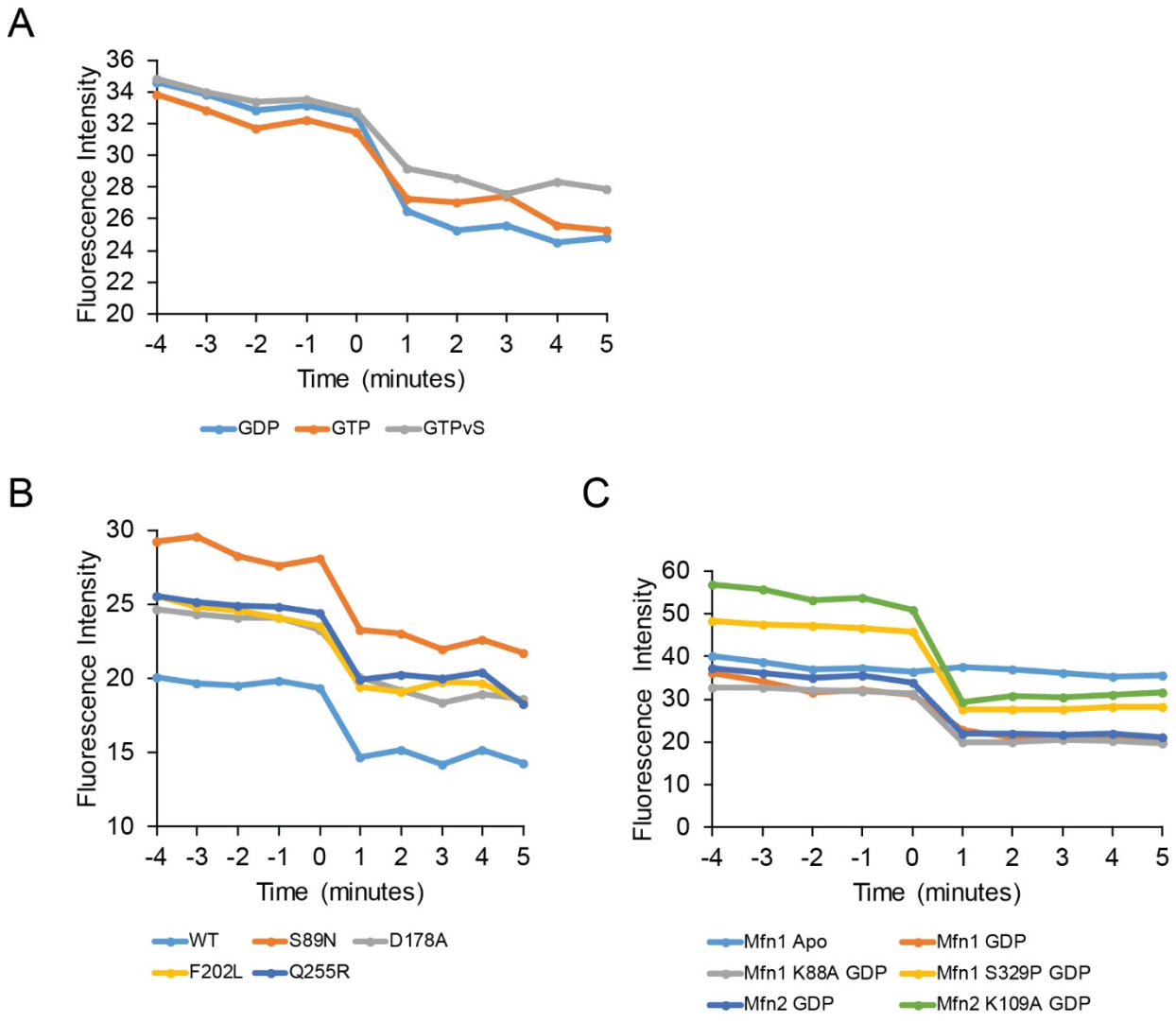


**Figure 2.4 Tryptophan fluorescence of recombinant Mitofusin shows nucleotide binding**

Recombinant Mitofusin proteins were incubated at 37°C prior to addition of nucleotide to achieve a baseline signal. Indicated nucleotide was added between time 0 and 1 and the change in fluorescence was monitored. **(A)** Wild-type Mfn1 with indicated nucleotides. **(B)** Mfn1 mutant variants with the addition of GTP. **(C)** Various Mitofusin proteins with or without the addition of GDP.

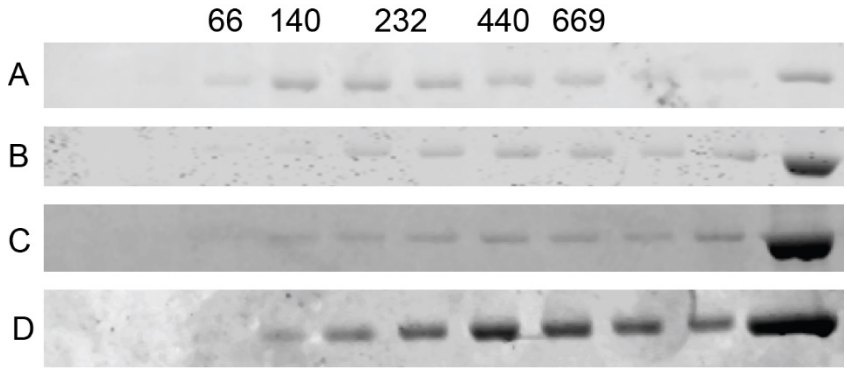


**Figure 2.5 Sucrose gradient ultracentrifugation show variability in solubility of recombinant Mfn1 protein**

**(A)** An example where wild-type Mfn1 protein remains mostly soluble. **(B)** An example where wild-type Mfn1 protein is mostly insoluble. **(C)** $Mfn1^{K88A}$ protein predicted to lack GTP hydrolysis is mostly insoluble. **(D)** $Mfn1^{W239A}$ protein predicted to lack GTP binding and hydrolysis is mostly insoluble. Recombinant Mitofusin protein was loaded onto a 5-25% sucrose gradient (50 mM HEPES [pH 7.4], 500 mM KCl, 5 mM $MgCl_2$, 0.1% Mega8, 5% Glycerol, 1 mM TCEP), spun at 100,000xg for 16 hours and fractions were subsequentially taken and TCA precipitated. Fractions were run on an SDS-PAGE gel and Coomassie stained.

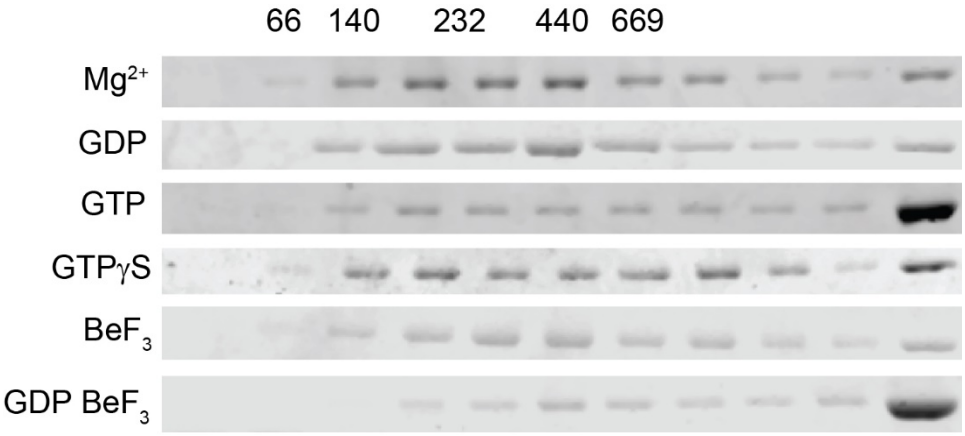


**Figure 2.6 Sucrose gradient ultracentrifugation reveals nucleotide dependent assembly of Mfn1**

Recombinant Mitofusin protein was incubated with indicated nucleotide for 15 minutes on ice before loading onto a 5-25% sucrose gradient (50 mM HEPES [pH 7.4], 500 mM KCl, 5 mM $MgCl_2$, 0.1% Mega8, 5% Glycerol, 1 mM TCEP), spun at 100,000xg for 16 hours and fractions were subsequentially taken and TCA precipitated. Fractions were run on an SDS-PAGE gel and Coomassie stained.

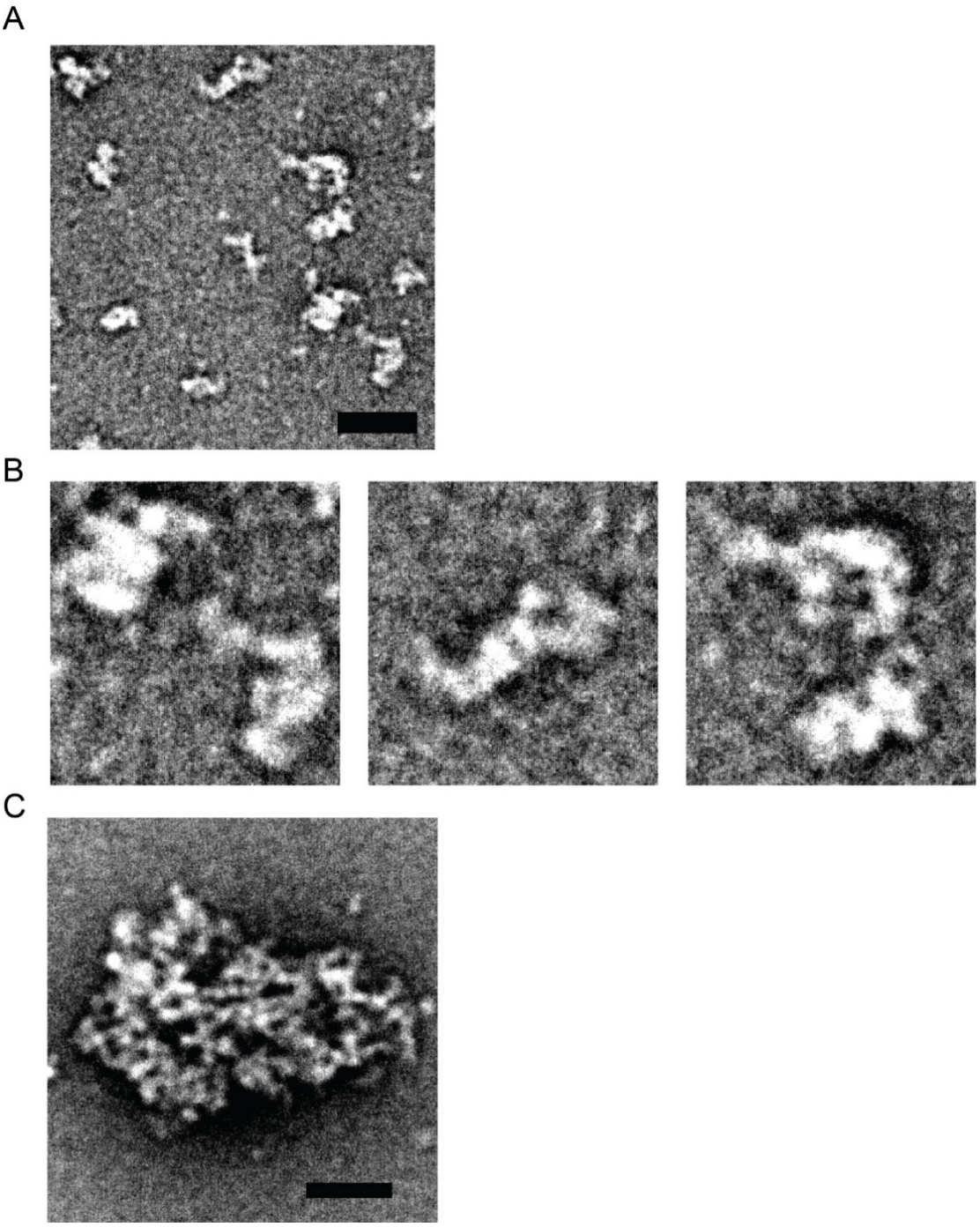


**Figure 2.7 Negative stain electron microscopy of recombinant Mfn1 protein**

**(A)** Representative image of a protein purification that results in soluble protein. **(B)** Heterogeneity in shape observed in Mfn1 particles. **(C)** Representative image of a protein purification that resulted in aggregated protein. Scale bars 50 nm. Protein was incubated on a

glow-discharged carbon coated grid for 30 seconds, washed with water 3 times and stained with 3% uranyl acetate for 30 seconds.

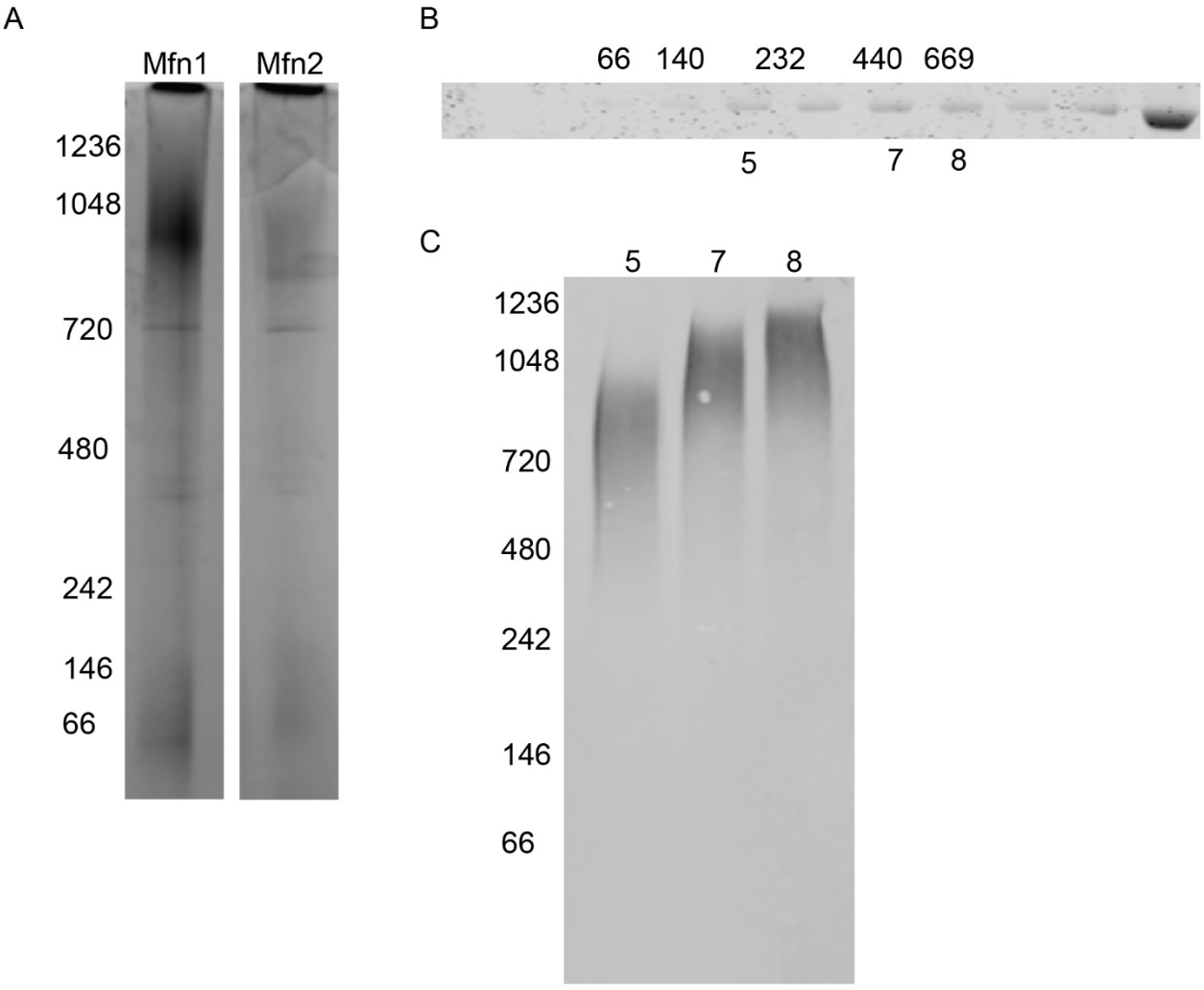


**Figure 2.8 BN-PAGE reveals that recombinant Mfn1 and Mfn2 protein forms large oligomeric complexes**

**(A)** BN-PAGE of recombinant Mfn1 and Mfn2 visualized by Coomassie staining. **(B)** Sucrose gradient ultracentrifugation of recombinant Mfn1 protein visualized by SDS-PAGE and Coomassie stained; indicated fractions were subsequently run on a BN-PAGE. **(C)** Corresponding fractions from sucrose gradient in (B) were run on a BN-PAGE and visualized by western blot analysis.

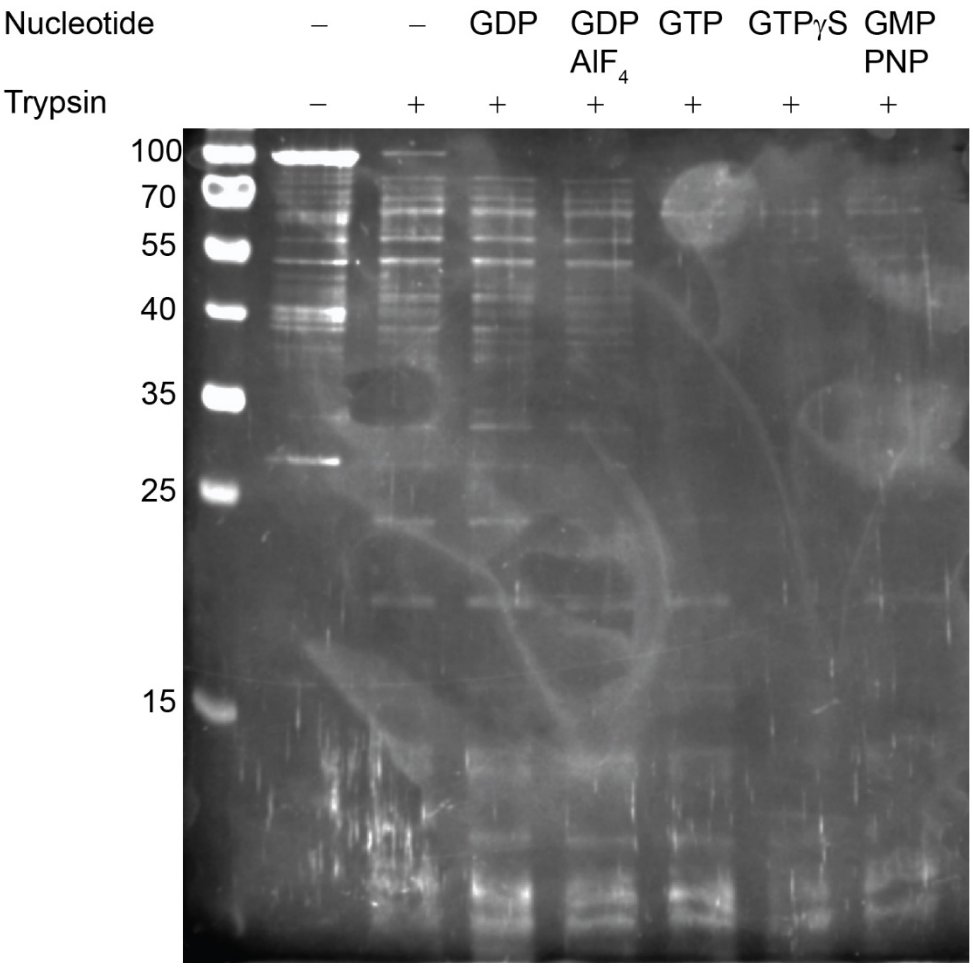


**Figure 2.9 Trypsin digestion of Mitofusin with various nucleotides**

Recombinant Mitofusin 1 was incubated with indicated nucleotide at 37°C before trypsin protease was added if indicated. Samples were run on an SDS-PAGE gel and silver stained.

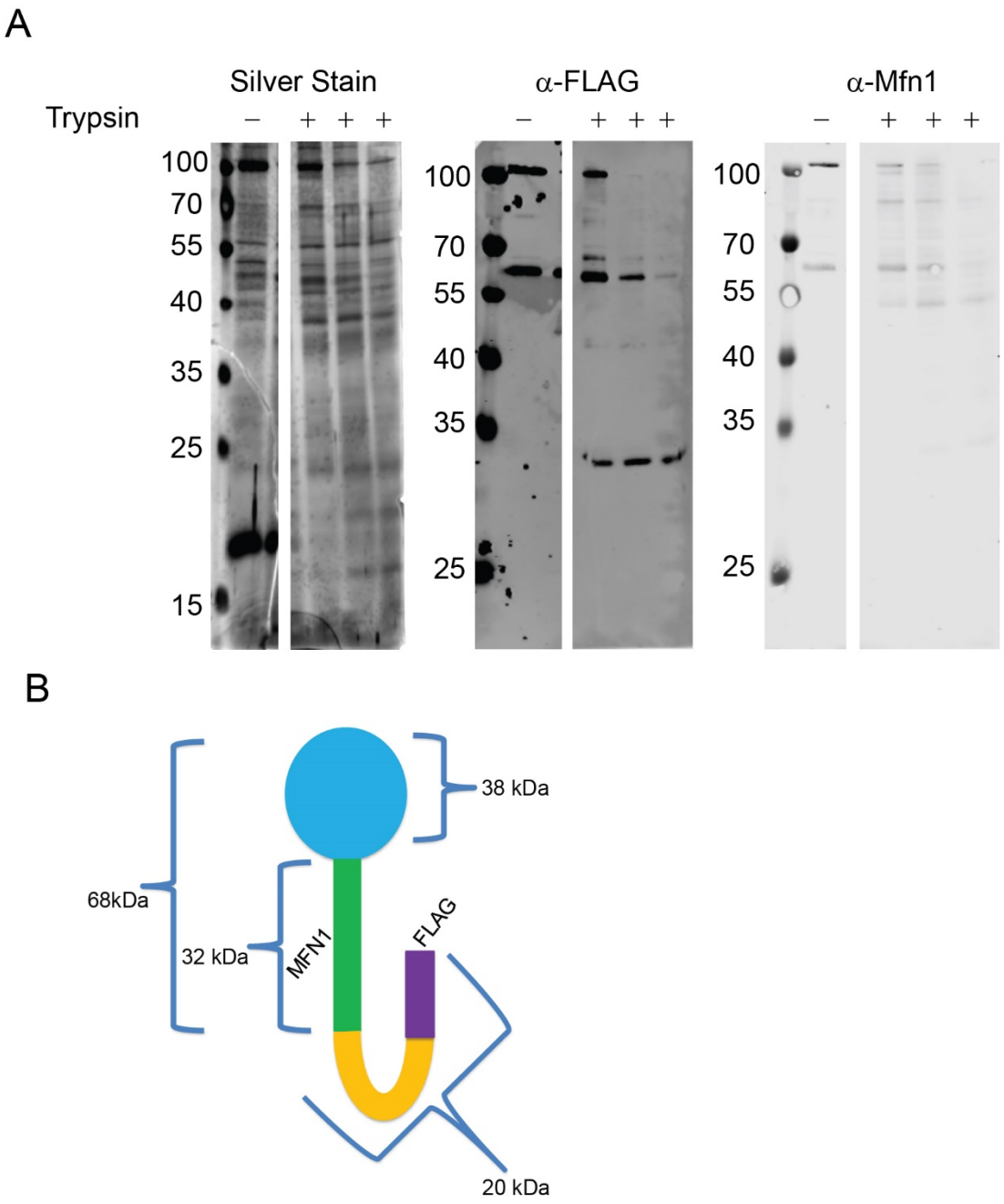


**Figure 2.10 Trypsin digestion of Mfn1-FLAG without nucleotide**

**(A)** Recombinant Mitofusin 1 was incubated with trypsin if indicated. Samples were run subjected to SDS-PAGE and either silver stained or immunoblotted with α-FLAG or α-Mfn1. **(B)** Schematic of potential Mitofusin fragments and epitope locations of antibodies.

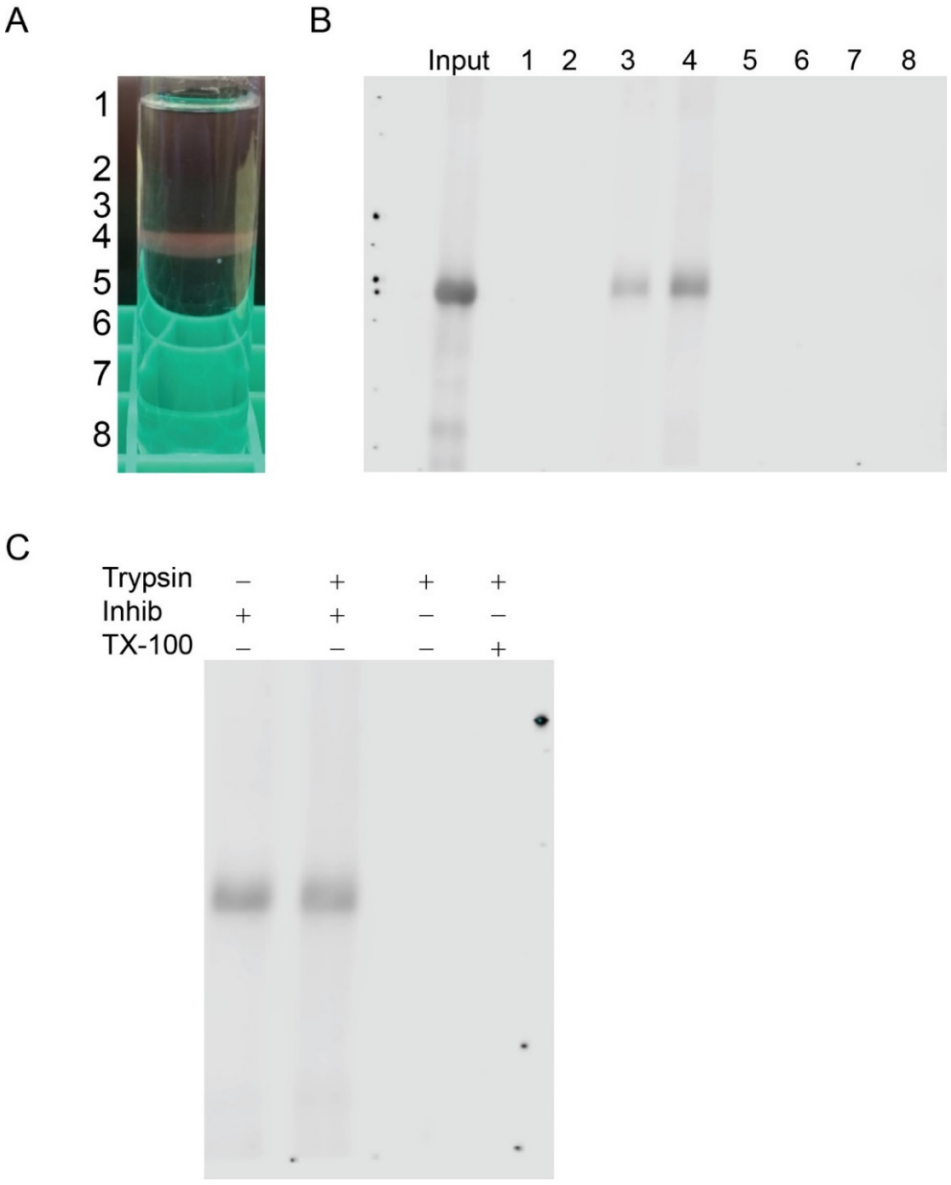


**Figure 2.11 Mfn1 inserts into proteoliposomes and is oriented facing outward**

**(A**) Picture of Mfn1 proteoliposome float using soybean polar extract spiked with PE-Rhodamine; proteoliposome are found in fraction 4. **(B)** Western blot of TCA precipitated fractions of the corresponding proteoliposome float fractions in A. **(C)** Western blot of trypsin orientation assay of fraction 4 from A & B. Inhib stands for soybean trypsin inhibitor, TX-100 stands for Triton X-100.

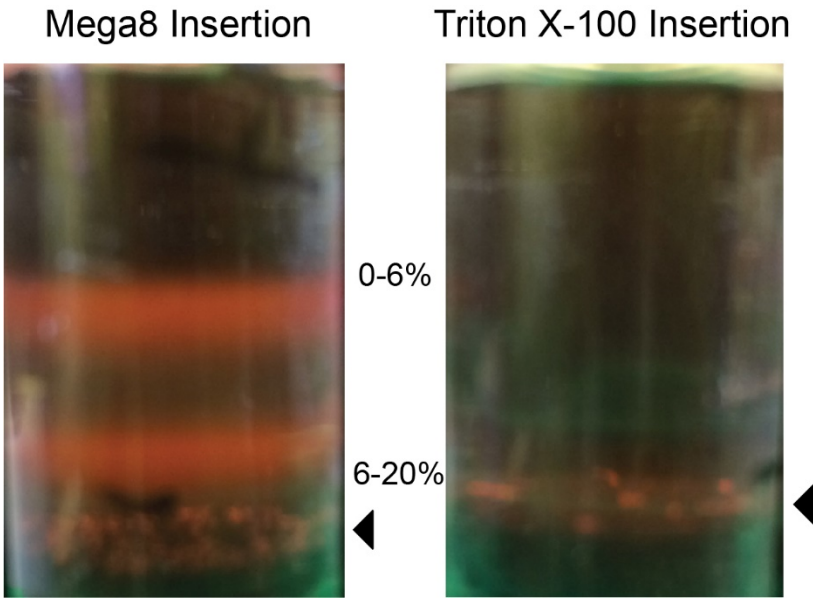


**Figure 2.12 Mfn1 causes proteoliposome flocculation when inserted into liposome containing MOM with 15% PA**

Pictures of Mfn1 proteoliposome floats using defined mitochondrial outer membrane composition at 15% PA with PE-Rhodamine and PE-NBD using either the Mega8 or Triton X-100 insertion protocol; liposomes contain Mitofusin were found at the layer indicated with the arrowhead.

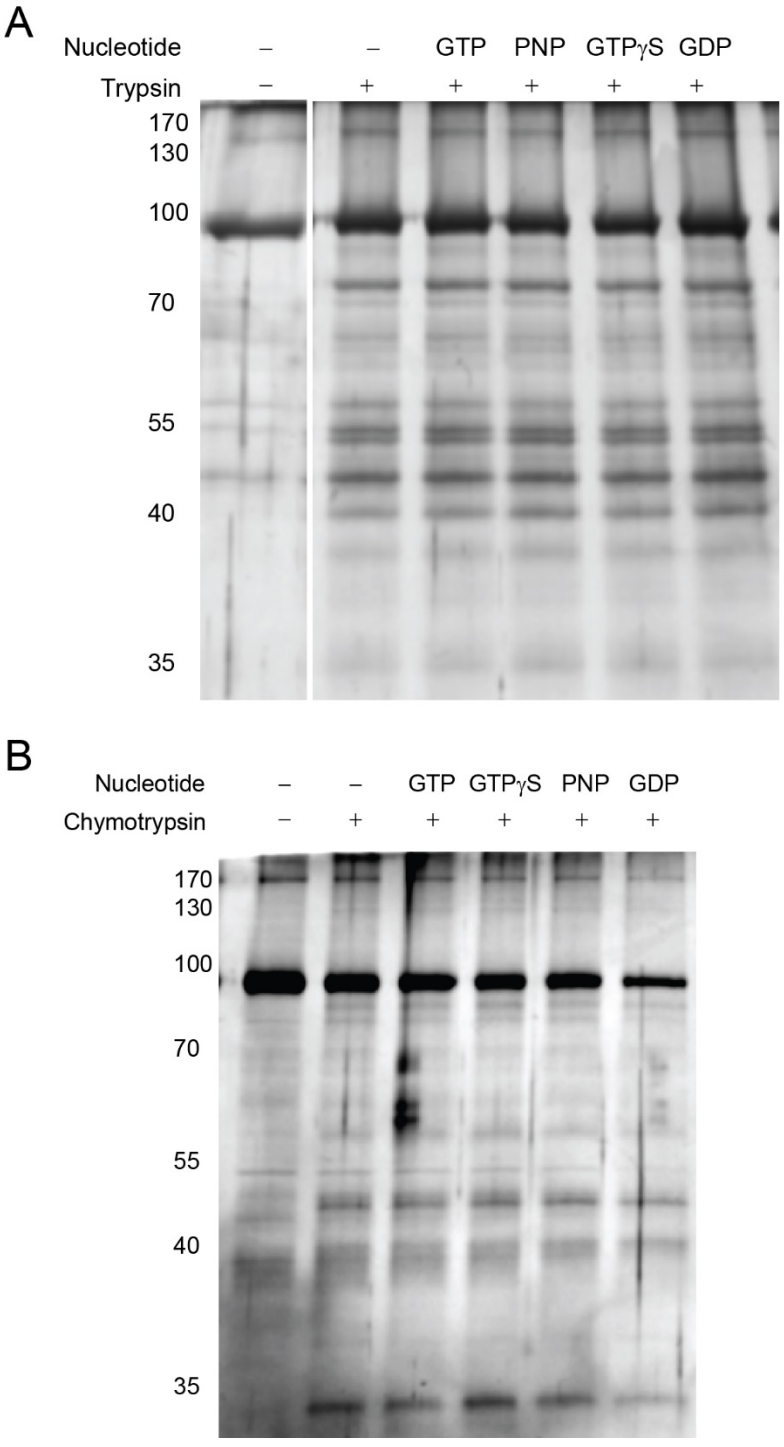


**Figure 2.13 Mfn1 proteoliposome limited protease protection reveals no nucleotide dependent conformational changes**

**(A)** Trypsin limited digestion with indicated nucleotide; PNP stands for GMPPNP. **(B)** Chymotrypsin limited digestion with indicated nucleotide. Samples were run on an SDS-PAGE gel and silver stained.

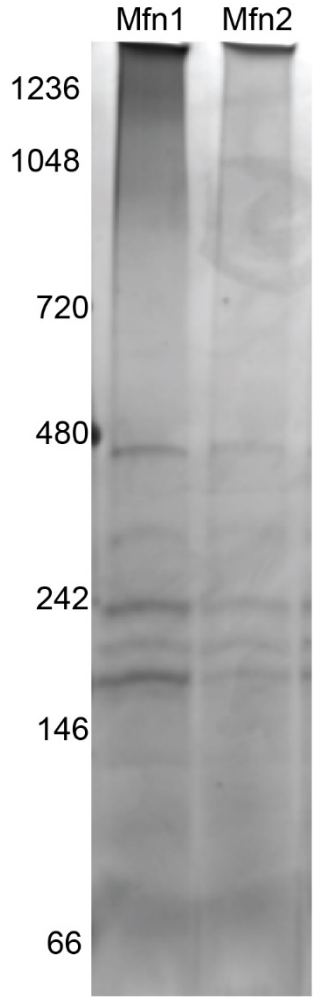


**Figure 2.14 BN-PAGE of Mitofusin proteoliposomes reveals large oligomeric species**

Freshly prepared Mitofusin proteoliposomes were detergent solubilized and subjected to BN-PAGE and Coomassie stained.

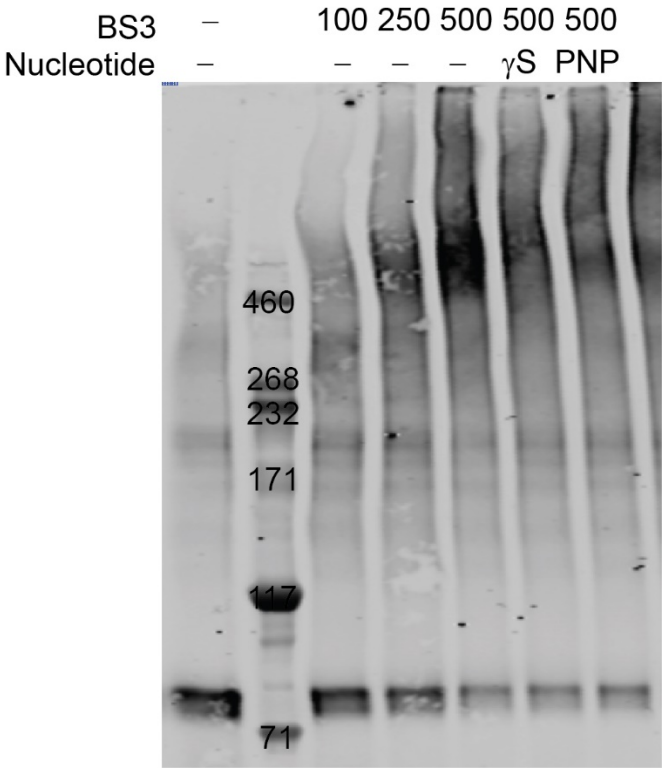


**Figure 2.15 Proteoliposomes BS3 crosslinking reveals higher order oligomers**

Freshly prepared Mfn1 proteoliposomes were incubated with or without indicated nucleotide before incubation with BS3 crosslinker, samples were run on a 3-8% tris-acetate gel and analyzed by western blot.

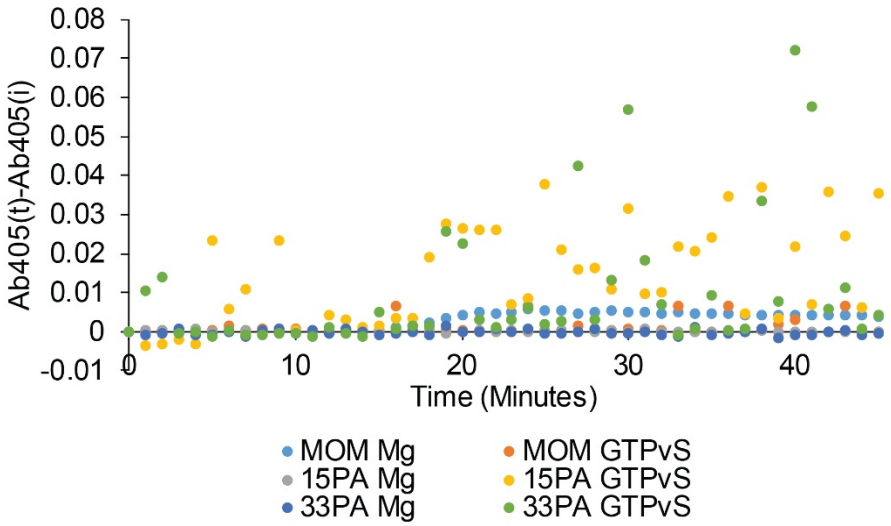


**Figure 2.16 Mfn1 proteoliposomes show tethering activity dependent on high concentration of PA lipids**

Freshly prepared Mfn1 proteoliposomes were incubated at 37°C with or without GTPγS. $OD_{405nm}$ was read every minute for 45 minutes and plotted as the difference between initial $OD_{405nm}$ and $OD_{405nm}$ at time = t.

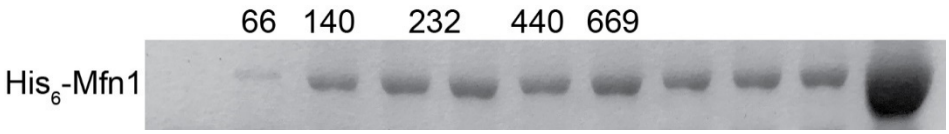


**Figure 2.17 Sucrose gradient ultracentrifugation of $His_6$-Mfn1 remains partially soluble**

Recombinant $His_6$-Mfn1 protein was loaded onto a 5-25% sucrose gradient (50 mM HEPES [pH 7.4], 500 mM KCl, 5 mM $MgCl_2$, 0.1% Mega8, 5% Glycerol, 1 mM TCEP), spun at 100,000xg for 16 hours and fractions were subsequentially taken and TCA precipitated. Fractions were run on an SDS-PAGE gel and Coomassie stained. Image quantification using ImageJ shows that approximately 70% of the protein remains soluble.

# Chapter 3: A catalytic domain variant of Mitofusin requiring a wildtype paralog for function uncouples mitochondrial outer-membrane tethering and fusion[11]

## 3.1 Abstract

Mitofusins (Mfn) are dynamin-related GTPases that mediate mitochondrial outer membrane fusion, a process that is required for mitochondrial and cellular health. In Mfn1 and Mfn2 paralogs, a conserved phenylalanine (Phe-202) located in the GTPase domain on a conserved beta strand and is part of an aromatic network in the core of this domain. To gain insight into the poorly understood mechanism of Mfn-mediated membrane fusion, here we characterize a Mitofusin mutant variant etiologically linked to Charcot Marie Tooth Syndrome. From analysis of mitochondrial structure in cells and mitochondrial fusion in vitro, we found that conversion of Phe-202 to leucine in either Mfn1 or Mfn2 diminishes the fusion activity of heterotypic complexes with both Mfn1 and Mfn2 and abolishes fusion activity of homotypic complexes. Using co-immunoprecipitation and native gel analysis, we further dissect the steps of mitochondrial fusion and demonstrate that the mutant variant has normal tethering activity, but impaired higher-order nucleotide-dependent assembly. The defective coupling of tethering to membrane fusion observed here suggests that nucleotide-dependent self-assembly of Mitofusin is required after tethering to promote membrane fusion.

[1] This chapter is closely adapted from the published paper (Engelhart & Hoppins, 2019).

## 3.2 Introduction

Mitochondria play many important roles in critical cellular pathways including metabolism, cellular signaling, and cell death. Mitochondria are highly dynamic organelles that form an interconnected network through ongoing fusion, division, and movement (Labbé et al., 2014). These activities are required to maintain both the structure and function of the mitochondrial network. This is crucial for the health of cells, as aberrant mitochondrial structures have been observed in many pathological states and neurodegenerative disorders (Chan, 2012; Dorn, 2019; Itoh et al., 2013; Labbé et al., 2014; Nasrallah & Horvath, 2014; Pareyson et al., 2015; Pernas & Scorrano, 2016). Both mitochondrial fusion and division are mediated by large GTPase proteins of the Dynamin Related Protein (DRP) family. In vertebrates, mitochondrial outer membrane fusion is mediated by two paralogous membrane fusion DRPs, Mitofusin 1 and Mitofusin 2 (Mfn1 and Mfn2, respectively) (Santel & Fuller, 2001). Mitochondrial outer membrane fusion is temporally coupled to mitochondrial inner membrane fusion, which is facilitated by Optic Atrophy 1 (Opa1) (Ban et al., 2017; Cipolat et al., 2004; Mishra & Chan, 2014; Song et al., 2009). As paralogs, Mfn1 and Mfn2 share high sequence identity and similarity (Santel & Fuller, 2001), but are functionally and mechanistically distinct (Chen et al., 2003; Hoppins et al., 2011; Ishihara et al., 2004). For example, heterozygous point mutations only in Mfn2 lead to the peripheral neuropathy, Charot-Marie Tooth Syndrome Type 2A (CMT2A), which causes progressive loss of function and sensation in the extremities (Stuppia et al., 2015; Züchner et al., 2004). In addition, in contrast to a reticular and connected network in wildtype cells, Mfn1-null or Mfn2-null mouse embryonic fibroblasts (MEFs) both have fragmented mitochondrial networks, suggesting that Mfn1 and Mfn2 work together to create a

connected mitochondrial network (H. Chen et al., 2003). Indeed, Mfn1 and Mfn2 have been shown to form functionally distinct homotypic and heterotypic complexes (Detmer & Chan, 2007; Hoppins et al., 2011). Together, these reports illustrate that the heterotypic Mfn1-Mfn2 complexes are the most fusion competent, while the fusion activity of either Mfn1 or Mfn2 homotypic complexes is relatively low.

To date, all DRP family members studied share a characteristic structure, including a globular GTPase domain (G domain) with extended alpha helical bundle(s) and a membrane interacting domain. DRPs mediate membrane remodeling events by using GTP binding and hydrolysis to promote self-assembly and conformational changes. For example, to divide mitochondria, Dynamin related protein 1 (Drp1) forms a macromolecular ring around the organelle, which then constricts and disassembles with nucleotide hydrolysis (Antonny et al., 2016; Friedman & Nunnari, 2014; Smirnova et al., 1998). In contrast, the molecular mechanisms of Mitofusin-mediated mitochondrial outer membrane fusion are poorly understood. A Mitofusin is required on both membranes of the fusion pair and together are likely to mediate tethering by interacting in trans (Hoppins et al., 2011; Koshiba et al., 2004; Meeusen et al., 2004). The tethered state is predicted to advance to lipid mixing by the progression through the GTP catalytic cycle to stimulate self-assembly, GTP hydrolysis and conformational changes, which together drive membrane fusion (Daumke & Roux, 2017).

Similar to the division DRPs, an interface between the GTPase domains of two molecules is required for GTP hydrolysis for the fusion DRPs (Bian et al., 2011; Byrnes & Sondermann, 2011; Cao et al., 2017). For Atlastin, which mediates homotypic fusion of the endoplasmic reticulum, this interface is formed in trans between fusion partners, and GTP hydrolysis drives conformational changes that lead to membrane fusion (Hu & Rapoport, 2016). A similar

tethering mechanism has been proposed for the Mitofusins (Cao et al., 2017; Qi et al., 2016; Liming Yan et al., 2018), although another proposed model for mitochondrial tethering requires the C-terminal heptad repeat domain (Koshiba et al., 2004). Recent evidence suggests that in yeast, Fzo1-mediated homotypic mitochondrial fusion involves the formation of a ring-like structure in trans, where multiple rounds of GTP hydrolysis are required to progress from an early tethering event to membrane fusion (Brandt et al., 2016). In vertebrates, it remains unclear if higher order assembly of Mfn1 and Mfn2 is required for tethering and/or fusion.

Here we present characterization of a mutant variant of the Mitofusins that is etiologically linked to the neurodegenerative disorder CMT2A (Kijima et al., 2005). While a mitochondrial fusion defect is not apparent in cells, we observe reduced fusion efficiency in our reconstituted mitochondrial in vitro fusion assay. We show that this variant is non-functional in homotypic complexes, but supports fusion in the context of heterotypic fusion complexes with a wildtype copy of the opposite Mfn, in cis or trans. By assessing Mfn-dependent mitochondrial tethering and nucleotide dependent assembly, we demonstrate that the mutant variant cannot effectively couple mitochondrial tethering to membrane fusion. This suggests a mechanism of mitochondrial outer membrane fusion where nucleotide dependent assembly of Mfn is required following tethering to drive membrane fusion.

## 3.3 Results

### 3.3.1 Mfn1$^{F202L}$ is a unique GTPase domain mutant variant

To gain insight into the molecular mechanism of mitochondrial outer membrane tethering and fusion, we performed a functional screen of mutant variants of Mfn1 at highly conserved positions in the GTPase domain. Mfn1-null MEFs have a fragmented mitochondrial network characterized by short rod-shaped mitochondria due to low rates of mitochondrial fusion (Chen et al., 2005; Chen et al., 2003). We generated 12 mutant variants of Mfn1, selecting positions that were both conserved (in Mfn1, Mfn2 and MARF, the *Drosophila* Mitofusin) and that were associated with CMT2A in Mfn2 (Table S3.1). These variants were stably expressed with a C-terminal eGFP tag in Mfn1-null MEFs by viral transduction. The GFP signal co-localized with MitoTracker Red, indicating correct expression and targeting to the mitochondrial outer membrane. In cells with eGFP signal, the structure of the mitochondrial network was assessed as a proxy for fusion activity of the Mitofusin variant expressed. As expected, expression of Mfn1$^{WT}$-eGFP restored a reticular mitochondrial network, which is defined as having a connected network of mitochondria tubules distributed throughout the cytoplasm (Fig. 3.1A). Of the 12 mutant variants tested, 9 variants did not significantly alter the fragmented mitochondrial network in Mfn1-null cells, consistent with loss of function (Table S3.1, Fig. 3.1A Mfn1$^{H144R}$). There were two variants of Mfn1 whose expression restored a reticular mitochondrial network, indicating fusion activity when expressed with endogenous Mfn2 (Table S3.1, Fig. 3.1A Mfn1$^{F263Y}$).

The remaining variant, F202L, altered both the distribution and connectivity of the mitochondria in Mfn1-null cells. Expression of $Mfn1^{F202L}$-eGFP was associated with a highly connected network (Fig. 3.1A). In some of these cells, the mitochondrial distribution was also affected, with most of the mitochondria coalesced in the perinuclear region. This residue is located in the highly conserved beta 4G sheet in the core of the GTPase domain and the conversion of phenylalanine to leucine in the corresponding Mfn2 residue is associated with CMT2A (Fig. 3.1B and C). Given the striking changes in mitochondrial structure and distribution in cells, we chose to further characterize the molecular features of this variant in Mfn1 (F202L) and Mfn2 (F223L).

Since the phenylalanine residue is located in the GTPase domain, we sought to determine if the enzymatic properties of $Mfn1^{F202L}$ were altered. We utilized the Mfn1 minimal GTPase domain construct ($Mfn1_{IM}C$) recently used to obtain a high-resolution crystal structure (Cao et al., 2017). We determined that the $V_{max}$ of $Mfn1^{F202L}$ was only slightly lower than $Mfn1^{WT}$ (Fig. S3.1A). Indeed, full kinetic analysis of $Mfn1^{WT}$ and $Mfn1^{F202L}$ demonstrate that the mutant enzyme is similar to wildtype (Fig. S3.1B). Together, these data suggest that the basal catalytic activity of $Mfn1^{F202L}$ is only mildly impacted compared to wildtype. These changes in enzyme kinetics are relatively modest, making it unlikely that they account for the dramatic mitochondrial morphology changes observed in cells, although we cannot rule out this possibility.

To determine if $Mfn1^{F202L}$ is altering or changing the structure of the GTPase domain, we solved the structure of $Mfn1_{IM}{}^{F202L}$ bound to GDP by X-ray crystallography. The structure of $Mfn1_{IM}{}^{F202L}$ is very similar to $Mfn1_{IM}{}^{WT}$ (PDB 5GOE) with an RMSD of 0.413Å and the central β-sheet where Phe-202 is located is retained with the Phe-202/Leu-202 residue in the same

rotamer (Fig. S3.11 B & D). However, two differences between wildtype and Mfn1$^{F202L}$ were apparent. Firstly, the Mfn1$_{IM}^{F202L}$ crystal structure had additional density in the nucleotide binding pocket which we believe to be a $Mg^{2+}$ ion. This is unique as all other structures of Mfn1$_{IM}$ bound to GDP have lacked the $Mg^{2+}$ ion. It is difficult to know whether the presence of the $Mg^{2+}$ ion in the nucleotide pocket is significant as Mfn1$_{IM}^{F202L}$ was crystallized under different conditions which may have allowed for stabilization of the $Mg^{2+}$ ion. The second major difference observed was that the Mfn1$_{IM}^{F202L}$ crystal structure had less well-resolved loops in the GTPase domain (Fig S3.11 A & C). These unresolved loops may be the result of destabilization of the protein core by the phenylalanine to leucine substitution. The Phe-202 is a component of an aromatic network, and the stability offered by these stacking interactions could be disrupted by the leucine substitution (Fig. S9). However, this could also be due to the unique crystallization conditions. Overall, the Mfn1$_{IM}^{F202L}$ crystal structure did not provide insight to the functional deficits that this substitution causes to evoke the striking mitochondrial phenotype in cells.

### 3.3.2 Mfn1$^{F202L}$ and Mfn2$^{F223L}$ restored a connected mitochondrial network in cells lacking Mfn1 or Mfn2

We first wanted to assess the function of Mfn1$^{F202L}$ and the equivalent mutant variant in Mfn2, Mfn2$^{F223L}$ in the presence of the opposite wildtype paralog utilizing established cell lines lacking Mfn1 (Mfn1-null) or Mfn2 (Mfn2-null), respectively (H. Chen et al., 2003). To do this, we generated stable cell lines expressing Mfn1 or Mfn2 with a C-terminal 3xFLAG tag using retroviral transduction in the genetic null background. To ensure that non-physiological expression levels did not alter protein function, we then expanded and screened clonal

populations and selected those with near wildtype protein levels for further characterization (Fig. S3.2).

The expression of Mfn1$^{WT}$-FLAG in Mfn1-null MEFs restored a connected mitochondrial network, whereas transduction with an empty vector did not alter the fragmented mitochondrial structure (Fig. 3.2A and B). Consistent with the results from our screen, cells expressing Mfn1$^{F202L}$-FLAG possessed mitochondria that were highly connected and often coalesced in the perinuclear space. To resolve the mitochondrial structure in cells expressing Mfn1$^{F202L}$-FLAG, we treated cells with nocodazole to depolymerize microtubules, which has been previously shown to redistribute highly connected mitochondria in cells overexpressing a dominant negative Drp1 variant to reveal the degree of connectivity (Smirnova et al., 1998). Abolishing the microtubule network did not significantly alter the mitochondrial structure in wildtype or Mfn1$^{WT}$-FLAG rescue cells (Fig. 3.2C). Mfn1-null transduced with empty vector maintained a fragmented network, although some short, rod shaped mitochondria were observed after treatment with nocodazole. In contrast, the mitochondria in Mfn1$^{F202L}$-FLAG expressing cells were redistributed throughout the cytoplasm following nocodazole treatment, revealing a mitochondrial network that was highly connected in each clonal population (Fig. 3.2C). Mitochondrial connectivity was further assessed utilizing a mitochondrial matrix targeted photoactivatable GFP (mt-paGFP). Following activation of paGFP within a one micron square, the localization and intensity of paGFP was monitored to assess mitochondrial connectivity, movement and fusion. Over the course of 50 minutes, we observed that in wildtype cells mt-paGFP reduced in intensity and spread out of the ROI, consistent with diffusion within a connected network and fusion events (Fig. S3.3A). In contrast, in Mfn1-null empty vector control cells individual mitochondria with mt-paGFP move from the ROI, but there was limited

change in signal intensity and no increased co-localization with red signal, consistent with a disconnected network and few fusion events (Fig. S3.3B). The clonal populations of Mfn1-null cells expressing Mfn1$^{F202L}$ exhibited similar characteristics to wildtype controls with both decreased intensity of paGFP and movement out of the ROI (Fig. S3.3C). Finally, we have quantified the number of individual mitochondria and the mean network size utilizing MiNA, which are also consistent with the conclusion that Mfn1-null cells expressing Mfn1$^{F202L}$ are highly connected (Fig. S3.3D) (Valente et al., 2017). Together, these results suggest that Mfn1$^{F202L}$ and endogenous Mfn2 can support mitochondrial fusion, which results in a connected mitochondrial network in these cells.

While Mfn1 and Mfn2 share high similarity, several lines of evidence indicate that they are functionally distinct. Therefore, we set out to characterize the equivalent mutant variant in Mfn2, Mfn2$^{F223L}$, which is associated with CMT2A disease. As described above, we generated stable clonal populations with Mfn2-FLAG expressed in Mfn2-null cells at levels comparable to endogenous protein (Fig. S3.2B).

As in Mfn1-null cells, expression of Mfn2$^{WT}$-FLAG in Mfn2-null MEFs restored a reticular mitochondrial network, whereas transduction with an empty vector did not alter the fragmented mitochondrial structure (Fig. 3.2D and E). Analysis of Mfn2$^{F223L}$-FLAG clonal populations revealed that cells expressing this variant possessed a reticular mitochondrial network, similar to that observed in cells expressing Mfn2$^{WT}$-FLAG. However, the perinuclear clustering of mitochondria was not observed, suggesting that this altered distribution is unique to mutant Mfn1. These data suggest that Mfn2$^{F223L}$ can also support mitochondrial fusion in cells, when expressed with a wildtype Mfn1 partner.

### 3.3.3 Mfn1$^{F202L}$ requires a wildtype paralog for fusion activity

Mitochondrial fusion is most efficient when both Mfn1 and Mfn2 are expressed, indicating that the heterotypic fusion complexes are functionally distinct from homotypic complexes. Therefore, we sought to systematically characterize the function of each variant in the presence and absence of either Mfn1 or Mfn2 utilizing wildtype, Mfn1-null, Mfn2-null and Mfn1/2-null MEFs. To visualize cells expressing Mfn1$^{F202L}$ or Mfn2$^{F223L}$, we made use of a C-terminal mNeonGreen tag (Mfn1/2-mNeon), which was brighter and more photostable than Mitofusin-eGFP. These constructs were also expressed at near endogenous levels by viral transduction (Fig. S3.4) and the mitochondrial morphology was scored in cells with mitochondrial mNeon signal in three independent, blinded experiments.

Wildtype MEFs expressing Mfn1$^{F202L}$-mNeon appear unaltered, with a connected and distributed mitochondrial network (Fig. 3.3A and B). Therefore, the mutant phenotype is recessive and does not interfere with function of endogenous Mitofusin in cells. Consistent with our analysis of clonal populations above, the mitochondrial network in Mfn1-null MEFs expressing Mfn1$^{F202L}$-mNeon were highly connected and collapsed around the nucleus in about half of the cells. In contrast, in Mfn2-null cells, which possess only Mfn1 homotypic complexes, the expression of Mfn1$^{F202L}$-mNeon did not alter mitochondrial morphology, and the vast majority of cells had a fragmented network. Finally, when Mfn1$^{F202L}$-mNeon is expressed alone in Mfn1/2-null cells, we observed fragmented mitochondria that are either distributed or aggregated. In sum, these data indicate that Mfn1$^{F202L}$ does not mediate fusion alone or with Mfn1$^{WT}$, and that it requires Mfn2 for fusion activity.

In wildtype MEFs, Mfn2$^{F223L}$-mNeon expression also did not alter the mitochondrial network, which remained reticular (Fig. 3.3C and D). In Mfn1-null MEFs, the fragmented mitochondrial network did not change with expression Mfn2$^{F223L}$ -mNeon. This suggests that, similar to Mfn1$^{F202L}$, Mfn2$^{F223L}$-Mfn2$^{WT}$ complexes do not support fusion. Consistent with our analysis of clonal populations described above (see Fig. 3.2D and E), Mfn2$^{F223L}$-mNeon expression in Mfn2-null MEFs generated a reticular mitochondrial network. Expression of Mfn2$^{F223L}$-mNeon in Mfn1/2-null MEFs resulted in a similar phenotype to Mfn1$^{F202L}$ with cells having mitochondrial networks that were fragmented with some cells where the fragments were aggregated, indicating that Mfn2$^{F223L}$ homotypic complexes are not able to support mitochondrial fusion. Collectively, these data suggest that Mfn1$^{F202L}$ and Mfn2$^{F223L}$ only support molecular activities required for fusion in heterotypic fusion complexes with a wildtype paralog.

One unique property of Mfn1 is that it can functionally complement a subset of Mfn2 mutants altered at conserved positions in the GTPase domain in a heterotypic fusion complex (Detmer & Chan, 2007). Mfn2$^{W260A}$ is an Mfn2 mutant variant that is predicted to lack nucleotide binding and hydrolysis and has been shown to lack fusion activity in cells when expressed alone (in Mfn1/2-null cells) (Cao et al., 2017). We tested the function of Mfn2$^{W260A}$ in heterotypic fusion complexes with wildtype Mfn1 by expressing the mutant in Mfn2-null cells. Similar to Mfn2$^{F223L}$, we observe that Mfn2$^{W260A}$-mNeon expression in these cells supports the formation of a reticular mitochondrial network (Fig. S3.5). Therefore, Mfn2$^{W260A}$ can mediate fusion with Mfn1$^{WT}$, but not alone. In contrast to Mfn1$^{F202L}$, expression of the Mfn1$^{W239A}$-mNeon mutant variant in Mfn1-null cells failed to support the formation of a reticular mitochondrial network (Fig. S3.5). These data suggest that when both Mfn1 and Mfn2 are present, only Mfn1 needs to have GTPase activity to facilitate mitochondrial outer membrane fusion.

To further test that Mfn1$^{F202L}$ is in a unique mutant class, we tested whether Mfn1$^{F202L}$ supports fusion with Mfn2$^{W260A}$. To do this, we generated clonal populations of Mfn1/2-null MEFs stably expressing Mfn1$^{F202L}$-FLAG at near wildtype levels (Fig. S3.6). Utilizing these stable cell lines, we then transduced Mitofusins with a C-terminal mNeon and quantified mitochondrial morphology in cells expressing mNeon.

Consistent with data presented in Figure 3.3A and B, the mitochondrial network in cells expressing only Mfn1$^{F202L}$-FLAG and transduced with empty vector were fragmented, with some cells also exhibiting a change in distribution as some of the fragmented mitochondria were clustered together (Fig. 3.4A and B). As expected, expression of Mfn1$^{WT}$-mNeon did not alter the mitochondrial structure in these cells, whereas expression of Mfn2$^{WT}$-mNeon corresponded with a reticular mitochondrial network in the majority of cells. These data support our previous conclusion that Mfn1$^{F202L}$ can facilitate fusion with Mfn2$^{WT}$, but not Mfn1$^{WT}$. To our knowledge, this is the first report of a mutant variant of Mfn1 that can be functionally complemented by wildtype Mfn2. In contrast, Mfn2$^{W260A}$-mNeon did not restore fusion activity with Mfn1$^{F202L}$-FLAG as we observed fragmented mitochondria in the majority of cells. Therefore, unlike Mfn1$^{WT}$, Mfn1$^{F202L}$ uniquely requires a variant of Mfn2 with normal catalytic function. Together, this analysis reveals that Mfn1$^{F202L}$ has a molecular defect that makes Mfn1 dependent on the catalytic function of Mfn2, further supporting our conclusion that Mfn1$^{F202L}$ is a unique class of mutant.

### 3.3.4 Mfn1$^{F202L}$ and Mfn2$^{F223L}$ have impaired fusion activity in vitro

In cells, mitochondrial structure is determined by the combined activities of mitochondrial division, fusion, transport, and positioning. To directly assess the fusion activity of

Mfn1$^{F202L}$ and Mfn2$^{F223L}$ in the absence of these other factors, we utilized a quantitative in vitro mitochondrial fusion assay (Hoppins et al., 2011). Mitochondria were isolated from populations of cells expressing either a matrix targeted red or cyan fluorescent protein. Following incubation of red and cyan mitochondria with fusion buffer, fluorescence microscopy was used to score fusion events, which are indicated by overlap of the two fluorophores in three dimensions. The fusion activity of the mutants was compared to wildtype controls performed in parallel and expressed as a relative amount. We assessed protein stability in the reaction conditions and found that the level of wildtype and mutant Mitofusin proteins were not significantly altered over the course of the reaction (Fig. S3.7A).

First, we assessed fusion of mitochondria isolated from the Mfn1-null clonal populations expressing endogenous Mfn2 with either Mfn1$^{WT}$-FLAG, Mfn1$^{F202L}$-FLAG or empty vector described in Fig 3.2A and B. Mitochondria containing Mfn2 and Mfn1-FLAG had a relative rate of fusion that was comparable to wildtype controls, consistent with complete rescue of the Mfn1 null phenotype (Fig. 3.5A and Fig. S3.7B). In contrast, the mitochondria containing Mfn2 and Mfn1$^{F202L}$ possessed only 40% of the fusion activity of wildtype controls, which was comparable to mitochondria from vector control cells that only express Mfn2 (Fig. 3.5A).

Second, we assessed fusion of mitochondria isolated from the Mfn2-null clonal populations expressing endogenous Mfn1 with either Mfn2$^{WT}$-FLAG, Mfn2$^{F223L}$-FLAG or empty vector described in Fig 3.2D and E. As expected, mitochondria isolated from the Mfn2-null cells expressing endogenous Mfn1 and Mfn2-FLAG fused at rates close to wildtype controls (Fig. 3.5A and Fig. S3.7B). Similar to the defect observed with the Mfn1 variant, mitochondria with Mfn1 and Mfn2$^{F223L}$ possessed 30% of wildtype fusion activity, which was also comparable to mitochondria from vector control cells that only possess Mfn1. This indicates that the

replacement of phenylalanine with leucine at this position creates hypomorphic variants of Mfn1 and Mfn2, despite the high degree of mitochondrial connectivity observed in cells.

We considered the possibility that soluble factors in the cytosol were enhancing fusion in cells but were absent in the in vitro fusion assay. To test this, we added crude cytosol enriched fractions to the in vitro fusion reactions. Consistent with previously published data (Hoppins et al., 2011), addition of cytosol increased fusion with wildtype mitochondrial moderately (~1.2 fold) (Fig. 3.5B). For both the $Mfn1^{F202L}$ and $Mfn2^{F223L}$ mutant mitochondria, fusion was also stimulated (~2 fold) when crude cytosol was included in the reaction conditions (Fig. 3.5B). This was modestly higher than the stimulation observed with mitochondria isolated from vector control cells. Therefore, cytosolic factors may play a role in compensating for the molecular defect and increase the fusion efficiency in cells**.** Previous work has shown that recombinantly purified Bax stimulates in vitro mitochondrial fusion (Hoppins et al., 2011). Therefore, we postulated that Bax may be the stimulatory factor. Indeed, addition of recombinantly purified Bax stimulated both WT and $Mfn1^{F202L}$ mitochondria (Fig. S3.10). The level of stimulation with Bax for both WT and $Mfn1^{F202L}$ mitochondria was similar to the stimulation observed with total cytosol (compare to Fig. 3.5B).

The low fusion efficiency associated with homotypic Mfn1 or Mfn2 complexes can be significantly increased when partnered with wildtype mitochondria in trans (Fig. 3.5C) (Hoppins et al., 2011). To determine if the fusion defects observed with $Mfn1^{F202L}$ and $Mfn2^{F223L}$ are complemented in trans, we performed in vitro fusion reactions with mitochondria isolated from wildtype cells and mitochondria from Mfn-null cells expressing the mutant variant, as described in Fig 3.5A. When $Mfn1^{F202L}$ $Mfn2^{WT}$ mitochondria are combined with $Mfn1^{WT}$ $Mfn2^{WT}$ mitochondria, fusion was ~75% of wildtype controls, significantly higher than homotypic mutant

fusion reactions, but similar to heterotypic fusion reactions with wildtype and Mfn1-null mitochondria (Fig. 3.5C). Similarly, both Mfn2-null and Mfn1$^{WT}$ Mfn2$^{F223L}$ mitochondria fused more efficiently with wildtype mitochondria than with themselves (Fig. 3.5C). These data indicate that the mutant variants have little effect on fusion when wildtype Mfn1-Mfn2 heterotypic complexes can form in trans.

The analysis of mitochondrial fusion in vitro indicates that despite the connected appearance of the mitochondrial network in Mfn1-null cells expressing Mfn1$^{F202L}$ or Mfn2-null cells expressing Mfn2$^{F223L}$, the Mitofusin variants are functionally compromised. To gain insight into the molecular defect, we further characterized the fusion properties of the Mfn1$^{F202L}$ variant in vitro.

### 3.3.5 Mfn1$^{F202L}$ requires Mfn2 exclusively in trans

While our data have established that Mfn1$^{F202L}$ requires wildtype Mfn2 for fusion activity, we sought to determine if Mfn2 had to be present on the same membrane, in cis, or if Mfn2 could complement on the opposite membrane, in trans. To do this, we exploited the in vitro mitochondrial fusion assay and tested specific combinations of Mitofusins both in cis and in trans. As described above, we had generated a clonal population of Mfn1/2-null MEFs expressing Mfn1$^{F202L}$-FLAG at near wildtype levels (Fig. S3.6). Therefore, we could test mitochondrial fusion activity of Mfn1$^{F202L}$ homotypic complexes. We also constructed Mfn1/2-null cells expressing Mfn1$^{WT}$-FLAG as a control (Fig. S3.6). Consistent with previously published data (Hoppins et al., 2011), mitochondria with only Mfn1$^{WT}$-FLAG fused at low levels compared to wildtype controls (Fig. 3.5D and Fig. S3.7C). Mitochondria with only Mfn1$^{F202L}$-

FLAG fused significantly less than mitochondria with only Mfn1$^{WT}$ (2.2% and 10.4% of wildtype, respectively).

For both Mfn1$^{WT}$ and Mfn1$^{F202L}$, fusion was significantly increased in heterotypic reactions with wildtype mitochondria (Fig. 3.5D). To distinguish between complementation by Mfn1, Mfn2 or both in trans, we performed in vitro fusion reactions with mitochondria from either Mfn2-null and Mfn1-null cells in combination with the mitochondria with homotypic Mfn1$^{WT}$ or Mfn1$^{F202L}$ complexes. Mitochondrial fusion was relatively inefficient when Mfn1$^{WT}$ was on both membranes and even lower when Mfn1$^{WT}$ was paired with Mfn1$^{F202L}$ mitochondria. In contrast, mitochondria with either Mfn1$^{F202L}$ or Mfn1$^{WT}$ had significantly higher fusion efficiency when Mfn2 was present in trans, utilizing mitochondria from Mfn1-null cells (38% and 39% of wildtype controls, respectively). Together, these data indicate that Mfn1$^{F202L}$ has impaired fusion activity that is significantly improved when Mfn2$^{WT}$ is present on the opposite membrane.

### 3.3.6 Mfn1$^{F202L}$ forms tethered complexes as efficiently as wildtype Mfn1

An early step in mitochondrial outer membrane fusion is establishment of a physical interaction, or tether, between the opposing membranes. It has been proposed that the dimer interface formed by the GTPase domain is responsible for Mitofusin-dependent tethering (Cao et al., 2017; Liming Yan et al., 2018). To determine if the molecular defect of the Mfn1$^{F202L}$ variant was in formation of a membrane tether, we developed an assay to test the physical interaction of Mitofusins on opposing mitochondrial membranes using co-immunoprecipitation analysis of two epitope tags (FLAG and eGFP) (Fig. 3.6A and B). Mitochondria isolated from clonal populations of Mfn1-null MEFs expressing either Mfn1-FLAG or Mfn1-eGFP at near endogenous levels

were combined and incubated in the presence or absence of the transition state mimic, GDP $BeF_3$ to trap fusion complexes before lipid mixing. When only $BeF_3$ is present, virtually no $Mfn1^{WT}$-eGFP is co-immunoprecipitated with $Mfn1^{WT}$-FLAG, indicating that no significant interaction was observed under these control conditions. In contrast, when mixed mitochondria are incubated in the presence of the transition state mimic (GDP $BeF_3$), Mfn1-eGFP co-immunoprecipitated with $Mfn1^{WT}$-FLAG (Fig. 3.6B, left panel, arrowhead). This is consistent with mitochondria forming a tethered intermediate in trans where the differentially tagged Mitofusin proteins are physically interacting. Importantly, we observe no mitochondrial fusion under these conditions. To determine if $Mfn1^{F202L}$-FLAG can tether opposing membranes, we tested co-immunoprecipitation of $Mfn1^{F202L}$-eGFP and $Mfn1^{WT}$-eGFP proteins with $Mfn1^{F202L}$-FLAG. We detected similar amounts of $Mfn1^{F202L}$-eGFP and $Mfn1^{WT}$-eGFP following immunoprecipitation of $Mfn1^{F202L}$-FLAG, indicating that the mutant variant did not have a measurable defect in the formation of tethering complexes under these conditions (Fig. 3.6B, C and D).

### 3.3.7 Nucleotide-dependent assembly of $Mfn1^{F202L}$ and $Mfn2^{F223L}$ are reduced

A common characteristic of the members of the dynamin family is nucleotide dependent assembly into higher order structures. Given that $Mfn1^{F202L}$ effectively formed trans membrane tethering complexes, we considered that the molecular defect was in the formation of a higher-order assembly. Therefore, we probed the assembly state of $Mfn1^{F202L}$ utilizing BN-PAGE analysis of detergent solubilized mitochondria. Previously published work has shown that both Mfn1 and Mfn2 form large oligomeric complexes by BN-PAGE ranging from ~140-440 kilodaltons (kDa) without nucleotide (Ishihara et al., 2004; Karbowski et al., 2006; Steffen et al.,

2017). To determine the assembly state of the Mfn1$^{F202L}$ variant, mitochondria were isolated from the clonal populations of the Mfn1-null cells expressing either Mfn1$^{WT}$-FLAG or Mfn1$^{F202L}$-FLAG described in Figure 3.2. These were incubated with the indicated nucleotide, detergent solubilized, and analyzed by BN-PAGE and western blot analysis. The majority of both Mfn1$^{WT}$ and Mfn1$^{F202L}$ were found as a predicted dimer, which migrates slightly higher than the 146 kDa marker in untreated mitochondria (Fig. 3.7A, see arrow). In contrast, when mitochondria were incubated with either GTP or the non-hydrolyzable GTP analog GMP-PNP, we saw a significant shift in the population to two larger species (Fig. 3.7A and B, see asterisks). Mfn1$^{F202L}$ formed some of these large oligomers, but we observed significantly less of the mutant protein shifted to the higher molecular weight species as compared to Mfn1$^{WT}$ (Fig. 3.7B). Interestingly, we observed the same result when analyzing mitochondria with only Mfn1, isolated from the Mfn1/2-null cells expressing either Mfn1$^{WT}$-FLAG or Mfn1$^{F202L}$-FLAG (Fig. 3.7C and D). Therefore, the formation of these oligomeric species does not require Mfn2. Under our conditions, incubation of mitochondria with the transition state mimic, GDP $BeF_3$ also resulted in a significant shift to higher oligomeric states, which was more prominent for Mfn1$^{WT}$ as compared to Mfn1$^{F202L}$ (Fig. S3.8A and B). Together, these data suggest that nucleotide-dependent assembly of Mfn1$^{F202L}$ is reduced. To determine if Mfn2$^{F223L}$ has a similar molecular defect, we isolated mitochondria from Mfn2-null cells expressing either Mfn2$^{WT}$ or Mfn2$^{F223L}$ and analyzed assembly under the same conditions. Similar to Mfn1, we observe that most Mfn2 and Mfn2$^{F223L}$ migrate as a predicted dimer in the absence of additional nucleotide and that Mfn2$^{WT}$ forms a larger oligomer in the presence of GTP or GMPPNP. In contrast, Mfn2$^{F223L}$ has a greatly reduced capacity to form higher order assemblies under the nucleotide conditions tested here. Together, these observations indicate that this mutant variant is selectively defective in

nucleotide dependent higher order assembly. Therefore, we postulate that post-tethering nucleotide dependent assembly is required to couple GTP hydrolysis to membrane fusion.

## 3.4 Discussion

In this work, we have performed an extensive functional assessment of both Mitofusin paralogs with a mutation at a conserved position on beta strand 4G. The variant $Mfn2^{F223L}$ is associated with the neurodegenerative disease, CMT2A, which is inherited in a dominant fashion. In the structure obtained with $Mfn1_{IM}$, F202 is located in an aromatic network that also includes phenylalanine at positions 81, 112, 219, 220, 263 and 320 (Figure S3.9). The conversion to leucine at position 202 may destabilize this feature and lead to the observed fusion and assembly defects.

Our analysis indicates that basal enzyme activity is not markedly impacted. This activity was assessed utilizing a construct lacking the second helical bundle and transmembrane region, suggesting that the defect associated with the mutation is best evaluated in the context of the full-length protein. Rescue experiments utilizing established and well-characterized null cells do not suggest a complete loss of function, as each $Mfn1^{F202L}$ and $Mfn2^{F223L}$ restore the reticular mitochondrial network in Mfn1-null and Mfn2-null cells, respectively. This type of complementation has been previously demonstrated for other Mfn2 mutant variants associated with CMT2A (18), but this is the first report of a mutant variant of Mfn1 that is functionally complemented by Mfn2. In contrast to wildtype Mfn1, which can mediate fusion with several variants of Mfn2 that are non-functional on their own, $Mfn1^{F202L}$ requires Mfn2 to have catalytic function. This denotes a novel class of Mfn1 mutant and extends our understanding of the heterotypic fusion complex and indicates that, not only can Mfn1 compensate for defects in Mfn2, but the reverse is also true. Our data suggest that Mfn2 need not hydrolyze GTP when Mfn1 is present. This is similar to Mgm1, the yeast mitochondrial inner membrane fusion

machine, which only requires GTPase activity in the short isoform and not the membrane anchored long isoform (DeVay et al., 2009). From our data, we speculate that while Mfn1 must hydrolyze GTP, a defect in nucleotide dependent higher order assembly can be overcome if Mfn1 is partnered with wildtype Mfn2. In the context of vertebrate cells that express both Mfn1 and Mfn2, this provides significant protection against deleterious mutations.

The collapsed perinuclear mitochondrial distribution in Mfn1-null cells expressing $Mfn1^{F202L}$ reveals another unique property of this variant. We do not see the same coalescence in the perinuclear region in wildtype cells expressing this variant, indicating that the phenotype is not dominant. Perinuclear clusters of mitochondria have also been observed in cells overexpressing Mfn1/2 or the dominant negative variants of Drp1, the mitochondrial division machine. In the latter case, disruption of the microtubule network also releases the cluster to reveal a highly connected network (Smirnova et al., 1998). The cells analyzed here are not overexpressing the Mitofusin, making it unlikely that these clusters are equivalent to those formed by high Mitofusin protein levels. Our data indicate that $Mfn1^{F202L}$ uniquely alters mitochondrial transport to favor retrograde directed movement and it is unclear why the same phenotype is not observed with the Mfn2 mutant variant. Given the very high degree of connectivity of the mitochondrial networks in cells expressing $Mfn1^{F202L}$ and Mfn2, the perinuclear clustering may facilitate fusion by establishing proximity of mitochondria in the cell.

Significantly, our analysis of mitochondrial fusion efficiency in vitro revealed that both $Mfn1^{F202L}$ and $Mfn2^{F223L}$ variants were defective for membrane fusion. This defect was diminished upon the addition of crude cytosol extract to the reactions, suggesting that cytosolic factors contribute to fusion in cells, where mitochondrial structure was consistent with no fusion deficiency. Our analysis of $Mfn1^{F202L}$ in different Mfn-null cells indicates that Mfn2 is required

for fusion activity. Therefore, to directly test for functional complementation of the mutant variant, we generated clonal populations of Mfn1/2- double null cells expressing $Mfn1^{F202L}$ or $Mfn1^{WT}$ as a control. Mitochondria isolated from these cells fused most efficiently with a wildtype partner, but rates of fusion were also relatively high when wildtype Mfn2 homotypic complexes were paired in trans. In contrast, homotypic fusion with either $Mfn1^{WT}$ or $Mfn1^{F202L}$ was very low. These data confirm and extend our understanding of the role of Mfn1 and Mfn2 on opposite membranes and indicate that variants of Mfn1 that are non-functional alone can contribute to fusion when wildtype Mfn2 is present.

We further dissected the steps of membrane fusion and developed an assay to measure the tethering efficiency of the Mitofusins. With this assay, we find that $Mfn1^{WT}$ and $Mfn1^{F202L}$ can physically interact across two membranes with similar efficiency. These data indicate that the defect in mitochondrial fusion is not likely to be at the initial step of membrane tethering. In contrast, we report a difference in nucleotide dependent assembly of the mutant variant compared with wildtype controls. Together, these data suggest that the $Mfn1^{F202L}$ does not efficiently couple tethering to subsequent steps in membrane fusion, which includes nucleotide dependent assembly. Therefore, we postulate that following nucleotide dependent tethering, higher order assembly is required to drive membrane fusion.

## 3.5 Methods

### 3.5.1 Cell culture

All cells were grown at 37°C and 5% $CO_2$ and cultured in DMEM (Thermo Fisher Scientific) containing 1X GlutaMAX (Thermo Fisher Scientific) with 10% FBS (Seradigm) or 15% FBS for Mfn1/2-null mouse embryonic fibroblasts and 1% penicillin/streptomycin (Thermo Fisher Scientific). Mouse embryonic fibroblasts cells (Mfn wildtype, Mfn1-null, Mfn2-null and Mfn1/2-null) were purchased from ATCC.

### 3.5.2 Retroviral transduction and generation of clonal populations

Plat-E cells (Cell Biolabs) were maintained in complete media supplemented with 1 μg/mL puromycin and 10 μg/mL blasticidin and plated at approximately 80% confluency the day prior to transfection. Plat-E cells were transfected with FuGENE™ HD (Promega) and transfection regent was incubated overnight before a media change. Viral supernatants were collected at approximately 48, 56, 72, and 80 hours post transfection and incubated with MEFs in the presence of 8 mg/ml polybrene. Approximately 16 hours after the last viral transduction, MEF cells were split and selection was added if needed (1 μg/mL puromycin or 200 μg/mL hygromycin).

Clonal populations were generated by plating cells at very low density and clones were collected onto sterile filter paper dots soaked in trypsin. Following expansion, whole cell extract from clonal populations were screened by western blot analysis for Mitofusin against wildtype controls.

### 3.5.3 Transfection and microscopy

All cells were plated in No. 1.5 glass-bottomed dishes (MatTek). Mouse embryonic fibroblasts were incubated with 0.1 μg/mL Mitotracker Red CMX Ros (Invitrogen) for 15 minutes at 37°C with 5% $CO_2$, washed and incubated with complete media for at least 45 minutes prior to imaging. Cells treated with nocodazole were first incubated with 0.1 μg/mL Mitotracker Red CMX Ros for 15 minutes at 37°C with 5% $CO_2$, washed, incubated with complete media for at least 45 minutes, and then changed into complete media with 5 μM nocodazole. Cell were incubated with nocodazole for 45 minutes to 1 hour before imaging. MEFs were imaged at 37°C with 5% $CO_2$. A Z-series with a step size of 0.3 μm was collected with a Nikon Ti-E widefield microscope with a 63X NA 1.4 oil objective (Nikon), a solid-state light source (Spectra X, Lumencor), and an sCMOS camera (Zyla 5.5 Megapixel). Each cell line was imaged on at least three separate occasions (n > 100 cells per experiment).

### 3.5.4 Image analysis

Images were deconvolved using 8-15 iterations of 3D Landweber deconvolution. Deconvolved images were then analyzed using Nikon Elements software. Maximum intensity projections were created using ImageJ Software (NIH). Mitochondrial morphology was scored as follows: hyperfused indicates that the entire mitochondrial network in the cell was connected as a single structure; reticular indicates that fewer than 30% of the mitochondria in the cell were fragments (fragments defined as mitochondria less than 2 μm in length); fragmented indicates that most of the mitochondria in the cell were less than 2 μm in length; aggregated indicates fragmented mitochondria that were not distributed throughout the cytosol.

### 3.5.5 Preparation of mitochondria or cytosol-enriched fraction

For each experiment, three to five 15 cm plates each of MEFs stably expressing either mitochondria-targeted TagRFP or CFP were grown to ~90% confluency. Cells were harvested by cell scrapping, pelleted, and washed in mitochondrial isolation buffer (MIB) (0.2 M sucrose, 10 mM Tris-MOPS [pH 7.4], 1 mM EGTA). The cell pellet was resuspended in one cell pellet volume of cold MIB, and cells were homogenized by 10 to 14 strokes on ice with a Kontes Potter-Elvehjem tissue grinder set at 400 RPM. The homogenate was centrifuged (500 × *g*, 5 min, 4°C) to remove nuclei and unbroken cells, and homogenization of the pellet fraction was repeated followed by centrifugation at 500 × *g*, 5 min, 4°C. The supernatant fractions were combined and centrifuged again at 500 × *g*, 5 min, 4°C to remove remaining debris. The supernatant was transferred to a clean microfuge tube and centrifuged (7400 × *g*, 10 min, 4°C) to pellet a crude mitochondrial fraction. The post-mitochondrial supernatant fraction was saved as the cytosol-enriched fraction. The crude mitochondrial pellet was resuspended in a small volume of MIB. Protein concentration of fractions was determined by Bradford assay (Bio-Rad Laboratories).

### 3.5.6 In vitro mitochondrial fusion

An equivalent mass (10 - 12.5 μg) of TagRFP and CFP mitochondria were mixed, washed in 500uL MIB and concentrated by centrifugation (7400 × *g*, 10 min, 4°C). Following a 10 min incubation on ice, the supernatant was removed and the mitochondrial pellet was resuspended in 10 μl fusion buffer (20 mM PIPES-KOH [pH 6.8], 150 mM KOAc, 5 mM $Mg(OAc)_2$, 0.4 M sorbitol, 0.12 mg/ml creatine phosphokinase, 40 mM creatine phosphate, 1.5 mM ATP, 1.5 mM

GTP) or 10 μl cytosol-enriched buffer (2.5 μL of the cytosol-enriched fraction obtained from WT MEFs and 7.5 μL fusion buffer) or 10 μl recombinant Bax protein buffer (2.75 μL 3 μM Bax and 7.25 μL fusion buffer). Fusion reactions were incubated at 37°C for 30 or 60 minutes.

### 3.5.7 Analysis of mitochondrial fusion

Mitochondria were imaged on depression microscope slides by pipetting 4μL fusion reaction onto a 3% low-melt agarose bed, made in modified fusion buffer (20 mM PIPES-KOH [pH 6.8], 150 mM KOAc, 5 mM $Mg(OAc)_2$, 0.4 M sorbitol). A Z-series of 6 0.2 μm steps was collected with a Nikon Ti-E widefield microscope with a 100X NA 1.4 oil objective (Nikon), a solid state light source (Spectra X, Lumencor), and a sCMOS camera (Zyla 5.5 Megapixel). For each condition tested, mitochondrial fusion was assessed by counting ≥ 300 total mitochondria per condition from ≥ 4 images per condition (50 – 200 mitochondria per image collected), and fusion was scored by colocalization of the red and cyan fluorophores in three dimensions.

### 3.5.8 Photo-activatable mt-GFP

Cells transduced with mito-PAGFP (Addgene #23348) were plated in No. 1.5 glass-bottomed dishes (MatTek). Mouse embryonic fibroblasts were incubated with 0.1 μg/mL Mitotracker Red CMX Ros (Invitrogen) for 15 minutes at 37°C with 5% $CO_2$, washed and incubated with complete media for at least 45 minutes prior to imaging. MEFs were imaged at 37°C with 5% $CO_2$. A region that was approximately 1 micron square was activated using a 405 nm laser and the same cell was imaged after 50 minutes. Images were collected with a Nikon Ti-E widefield microscope with a 63X NA 1.4 oil objective (Nikon), a solid-state light source (Spectra X,

Lumencor), and an sCMOS camera (Zyla 5.5 Megapixel).

### 3.5.9 Protein expression and purification

$Mfn1_{IM}C$ pET28 plasmid was obtained from Song Gao (25). Mutations were made by Gibson assembly and confirmed by sequencing. $MFN1_{IM}$ constructs were expressed in *Escherichia coli* Rosetta (DE3) cells. Cells were cultured in Luria-Bertani medium with 150 μg/mL ampicillin and 25 μg/mL chloramphenicol at 37°C to an $OD_{600}$ of ~ 0.6 and protein expression was induced by the addition of 100 μM isopropyl-1-thio-β-d-galactopyranoside (IPTG). Induced cultures were grown overnight at approximately 17–18°C. The cells were harvested by centrifugation at 6,000 x *g* for 10 minutes. Cell pellets expressing $MFN1_{IM}$ were resuspended in 5 mL phosphate buffered saline, pelleted by centrifugation at 6,000 x *g* for 5 minutes, frozen in liquid nitrogen and stored at -80° C. Cells were thawed in a room temperature water bath and resuspended in 50 mL 50 mM HEPES-KOH [pH 7.4], 400 mM NaCl, 5 mM $MgCl_2$, 30 mM imidazole, 1 mM phenylmethanesulfonylfluoride (PMSF), 1x protease inhibitor cocktail (Thermo Scientific), 2.5 mM β-mercaptoethanol (β-ME) and lysed using a microfluidizer (Avestin). The lysate was subjected to centrifugation at 14,000 RPM for 45 minutes. The supernatant was applied to 2.5 mL HisPur™ Ni-NTA beads (Thermo Scientific) equilibrated with Binding buffer 1 (20 mM HEPES-KOH [pH 7.4], 400 mM NaCl, 5 mM $MgCl_2$, 30 mM imidazole [pH 8.0], 2.5 mM β-ME) and nutated at 4°C for 30 minutes. Ni-NTA beads bound to protein were washed with 20 column volumes of Binding buffer 1 and proteins were eluted with Elution buffer (20 mM HEPES-KOH [pH 7.4], 400 mM NaCl, 5 mM $MgCl_2$, 300 mM imidazole, 2.5 mM β-ME). $Mfn1_{IM}C$-containing elutions were incubated with 800 μg glutathione *S*-transferase (GST)-fused PreScission protease (PSP) to remove the amino-terminal $His_6$-tag. This was dialyzed overnight against Binding

buffer 2 (20 mM HEPES-KOH [pH 7.4], 400 mM NaCl, 5 mM $MgCl_2$, 2.5 mM β-ME). After dialysis, PSP was removed using a GST column. The protein was re-applied to a second Ni-NTA column equilibrated with Binding buffer 2. Binding buffer 1 was used to elute the protein, which were subsequently loaded onto a Superdex200 16/60 column (GE Healthcare) equilibrated with gel filtration buffer containing 20 mM HEPES-KOH [pH 7.4], 150 mM NaCl, 5 mM $MgCl_2$ and 1 mM dithiothreitol. The protein eluted in a discrete peak corresponding to a molecular mass of approximately 50 kDa. Protein was concentrated on an Amicon Ultra Centrifugal Filter (MWCO 30) (Millipore) to 30 mg/mL and glycerol was added to 20% before the protein was aliquoted and stored at -80°C. Protein purification was performed at 4°C. Protein concentration was determined by Bradford assay (Bio-Rad Laboratories).

### 3.5.10 BN-PAGE

Isolated mitochondria (15 – 30 µg) were incubated with or without 2 mM nucleotide and 2.5 mM $BeSO_4$, and 25 mM NaF as indicated in 0.2 M sucrose, 10 mM Tris-MOPS [pH 7.4], 1 mM EGTA, 5 mM $Mg(OAc)_2$ buffer at 37°C for 30 minutes. Mitochondria were then lysed in 1% w/v digitonin, 50 mM Bis-Tris, 50 mM NaCl, 10% w/v glycerol, 0.001% Ponceau S; pH 7.2 for 15 minutes on ice. Lysates were centrifuged at 16,000 x *g* at 4° C for 30 minutes. The cleared lysate was mixed with Invitrogen NativePAGE™ 5% G-250 Sample Additive to a final concentration of 0.25%. Samples were separated on a Novex™ NativePAGE™ 4 - 16% Bis-Tris Protein Gels (Invitrogen) at 4°C. Gels were run at 40 volts for 30 minutes then 100 volts for 30 minutes with dark cathode buffer (1X NativePAGE™ Running Buffer (Invitrogen), 0.02% (w/v) Coomassie G-250). Dark cathode buffer was replaced with light cathode buffer (1X NativePAGE™ Running Buffer (Invitrogen), 0.002% (w/v) Coomassie G-250) and the gel was run at 100 volts

for 30 minutes and subsequently at 250 volts for 60-75 minutes until the dye front ran off the gel. After electrophoresis was complete, gels were transferred to PVDF membrane (Bio-Rad Laboratories) at 30 volts for 16 hours in transfer buffer (25 mM Tris, 192 mM glycine, 20% methanol). Membranes were incubated with 8% acetic acid for 15 minutes and washed with $H_2O$ for 5 minutes. Membranes were dried at 37°C for 20 minutes and then rehydrated in 100% methanol and washed in $H_2O$. Membranes were blocked in 4% milk for 20 minutes and were probed with anti-FLAG (Sigma) for 4 hours at room temperature or overnight at 4°C. Membranes were incubated with HRP-linked secondary antibody (Cell Signaling Technology) at room temperature for 1 hour. Membranes were developed in SuperSignal Femto ECL reagent (Thermo Fisher Scientific) for 5 minutes and imaged on iBright Imaging System (Thermo Fisher Scientific). Band intensities were quantified using ImageJ software (NIH). NativeMark Unstained Protein Standard (Life Technologies) was used to estimate molecular weights of Mitofusin protein complexes.

### 3.5.11 Tethering co-immunoprecipitation

Differentially tagged isolated mitochondrial populations (50 μg each) were mixed together. Mitochondria were incubated at 37°C for 30 minutes with beryllium fluoride (2.5 mM $BeSO_4$, 25 mM NaF) with or without 2 mM GDP in fusion buffer (20 mM PIPES-KOH [pH 6.8], 150 mM KOAc, 5 mM $Mg(OAc)_2$, 0.4 M sortibal with 0.12 mg/mL creatine kinase, 40 mM creatine phosphate, 1.5 mM ATP). Mitochondria were solubilized in lysis buffer (20 mM HEPES-KOH [pH 7.4], 50 mM KCl, 5 mM $MgCl_2$) with 1.5% w/v n-Dodecyl β-D-maltoside (DDM), and 1X Halt Protease Inhibitor (Thermo Scientific) for 30 minutes on ice. Lysates were cleared at 10,000 x *g* for 15 minutes at 4°C. Supernatant was incubated with 50 μL magnetic μMACS Anti-

DYKDDDDK MicroBeads (Miltenyi Biotec) for 30 minutes on ice. The sample was applied to a MACS Column (Miltenyi Biotec) placed in the magnetic field using a μMACS Separator (Miltenyi Biotec) and washed twice with 400 μL 20 mM HEPES-KOH [pH 7.4], 50 mM KCl, 5 mM $MgCl_2$, 0.1% DDM and once with 200 μL 20 mM HEPES-KOH [pH 7.4], 50 mM KCl, 5 mM $MgCl_2$. One column volume (25 μl) SDS-PAGE loading buffer (60 mM Tris-HCl [pH 6.8], 2.5% sodium dodecyl sulfate, 5% βME, 5% sucrose, 0.1% bromophenol blue) was incubated for 15 minutes at room temperature and proteins were eluted twice with 35 μL SDS-PAGE loading buffer. The majority of the protein eluted in the first 35 μL elution. Samples were run on an SDS-PAGE gel and transferred onto nitrocellulose at 94V for 1 hour in 1X transfer buffer. Membranes were blocked in 4% Milk for at least 45 minutes and were probed with anti-Mfn1 antibody for 4 hours at room temperature or overnight at 4°C. Membranes were incubated with DyLight secondary antibody (Invitrogen) at room temperature for 1 hour. Membranes were imaged on LI-COR Imaging System (LI-COR Biosciences).

### 3.5.12 Western blot analysis

Protein lysates from MEFs were obtained by resuspending PBS washed cells in RIPA lysis buffer (150 mM NaCl, 1% Nonidet P-40, 1% Sodium deoxycholate, 0.1% SDS, 25 mM Tris [pH 7.4], 1X Halt Protease Inhibitor Cocktail, EDTA-Free [Thermo Scientific]). Samples were incubated on ice for 15 minutes and then spun at 21,000 x g for 15 minutes at 4°C. Supernatant was transferred to a clean tube and protein concentration was measured by BCA assay (Thermo Scientific). Samples were run on an SDS-PAGE gel and transferred onto nitrocellulose at 94V for 1 hour in 1X transfer buffer. Membranes were blocked in 4% Milk for at least 45 minutes and were probed with anti-Mfn1, anti-Mfn2 (Sigma), anti-VDAC (Invitrogen) or anti-alpha Tubulin

(Invitrogen) antibody for 4 hours at room temperature or overnight at 4°C. Membranes were incubated with DyLight secondary antibody (Invitrogen) at room temperature for 1 hour. Membranes were imaged on LI-COR Imaging System (LI-COR Biosciences).

### 3.5.13 GTPase assay

Frozen protein was thawed on ice and diluted to 2.5 μM in 20 mM HEPES-KOH [pH 7.4], 50 mM KCl, 5 mM $MgCl_2$, 1 mM dithiothreitol. Protein concentrations were confirmed by Bradford assay (Bio Rad Laboratories). Reactions were set up in triplicate in a 96 well plate on ice. Variable concentrations of GTP were added and reactions were incubated at 37°C for 15 minutes. Reactions were stopped by adding 200 mM EDTA on ice. Concentrations of free inorganic phosphate were measured by malachite green reagent. Malachite green reagent was added, and reactions were incubated at room temperature for 15 minutes. The optical density at 650 nM was measured and a potassium phosphate standard curve was used to determine the amount of GTP hydrolyzed.

### 3.5.14 Protein crystallization

Purified $MFN1_{IM}$ F202L at 23mg/mL in 20 mM HEPES-KOH [pH 7.4], 30 mM NaCl, 5 mM $MgCl_2$ and 1 mM dithiothreitol was incubated with tenfold concentration of GDP relative to protein for 1 h at room temperature before being crystallized at 20°C via hanging drop vapour diffusion by mixing equal volumes of protein and reservoir solution of 0.1M Tris (base); BICINE [pH 8.5], 20% v/v Glycerol; 10% w/v PEG 4000, 0.2M 1,6-Hexanediol; 0.2M 1-Butanol; 0.2M 1,2-Propanediol; 0.2M 2-Propanol; 0.2M 1,4-Butanediol; 0.2M 1,3-Propanediol.

Crystals formed within 2 days and grew to full size within 1 week. Crystals were directly frozen in $N_2$(l).

### 3.5.15 Bax protein expression and purification

pTYB1-Bax was expressed in *Escherichia coli* BL21 RIPL cells. Cells were cultured in Luria-Bertani medium with 150 μg/mL ampicillin and 25 μg/mL chloramphenicol at 37°C to an $OD_{600}$ of ~ 0.6 and protein expression was induced by the addition of 1 mM isopropyl-1-thio-β-d-galactopyranoside (IPTG). Induced cultures were grown for 3 hours at 37°C. The cells were harvested by centrifugation at 6,000 x *g* for 10 minutes. Cell pellets expressing Bax were resuspended in 5 mL phosphate buffered saline, pelleted by centrifugation at 6,000 x *g* for 5 minutes, frozen in liquid nitrogen and stored at -80°C. Cells were thawed in a room temperature water bath and resuspended in 50 mL 20 mM Tris-HCl [pH 8.0], 500 mM NaCl, 1 mM EDTA, 1 mM phenylmethanesulfonylfluoride (PMSF), 1x protease inhibitor cocktail (Thermo Scientific), and lysed using a microfluidizer (Avestin). The lysate was subjected to centrifugation at 14,000 RPM for 45 minutes and supernatant was filtered through 0.2 micron filter. The supernatant was applied to 5 mL Chitin column (NEB) equilibrated with 20 mM Tris-HCl [pH 8.0], 500 mM NaCl, 1 mM EDTA buffer. Chitin beads bound to protein were washed with 15 mL of 20 mM Tris-HCl [pH 8.0], 500 mM NaCl, 1 mM EDTA, 30 mM DTT buffer. The column was placed at 4°C for 48 hours. After 48 hours, protein was eluted with 15 mL 20 mM Tris-HCl [pH 8.0], 500 mM NaCl, 1 mM EDTA buffer. Protein containing elutions were desalted using Zeba™ Spin Desalting Columns 10 MWCO (Thermo Fisher Scientific) against 20 mM Tris-HCl [pH 8.0] buffer. Protein was loaded onto a 1 mL Q ion column (Bio-Rad) equilibrated in 20 mM Tris-HCl [pH 8.0], 10% glycerol buff. Proteins were then eluted with a linear 20 mM/min NaCl

gradient using a flow rate of 0.5 mL/min in 20 mM Tris-HCl [pH 8.0], 10% glycerol buffer. Bax protein eluted between 200-300 mM NaCl. 1 mM TCEP was added to protein containing elutions and protein was aliquoted, flash frozen in liquid nitrogen and stored at -80°C. Protein purification was performed at 4°C. Protein concentration was determined by Bradford assay (Bio-Rad Laboratories).

### 3.5.16 Plasmids & primers

The following plasmids were purchased from Addgene: pBABE-hygro (#1765), pBABE-puro (#1764), mito-PAGFP (#23348), pclbw-mito TagRFP (#58425), pclbw-mitoCFP (addgene #58426). The $Mfn1_{IM}C$ pET28 plasmid was a kind gift from Song Gao (25). The following primers were used to for site directed mutagenesis by Gibson Assembly: $Mfn1^{F202L}$ Human F (5'-CTAGATGCTGATGTCTTAGTTTTGGTCGCAAAC-3'), $Mfn1^{F202L}$ Human R (5'-GTTTGCGACCAAAACTAAGACATCAGCATCTAG-3'), $Mfn1^{F202L}$ Mouse F (5'-GCCTGGATGCTGATGTGTTGGTGCTGGTGGCCAAC-3'), $Mfn1^{F202L}$ Mouse R (5'-GTTGGCCACCAGCACCAACACATCAGCATCCAGGC-3'), $Mfn1^{W239A}$ Mouse F (5'-CTGAATAACCGTGCGGATGCTTCTGCTTCGG-3'), $Mfn1^{W239A}$ Mouse R (5'-CCGAAGCAGAAGCATCCGCACGGTTATTCAG-3'), $Mfn2^{W260A}$ Mouse F (5'-CATCCTGAACAACCGCGCGGATGCGTCTGCCTCGG-3'), $Mfn2^{W260A}$ Mouse R (5'-CCGAGGCAGACGCATCCGCGCGGTTGTTCAGGATG-3') $Mfn1^{R83W}$ Mouse F (5'-CATTTTTTGGCTGGACAAGTAGTGG-3'), $Mfn1^{R83W}$ Mouse R (5'-CCACTACTTGTCCAGCCAAAAAATG-3'), $Mfn1^{H107R}$ Mouse F (5'-AGCGGGATTGGTAGGACAACCAACTGC-3'), $Mfn1^{H107R}$ Mouse R (5'-GCAGTTGGTTGTCCTACCAATCCCGCT-3'), $Mfn1^{T109A}$ Mouse F (5'-

GATTGGTCACACAGCAAACTGCTTCCTG-3'), Mfn1$^{T109A}$ Mouse R (5'-CAGGAAGCAGTTTGCTGTGTGACCAATC-3'), Mfn1$^{A143V}$ Mouse F (5'-TGTTAATCAGCTGGTGCATGCCCTCCAT-3'), Mfn1$^{A143V}$ Mouse R (5'-ATGGAGGGCATGCACCAGCTGATTAACA-3'), Mfn1$^{H144R}$ Mouse F (5'-AATCAGCTGGCCAGGGCCCTCCATATG-3'), Mfn1$^{H144R}$ Mouse R (5'-CATATGGAGGGCCCTGGCCAGCTGATT-3'), Mfn1$^{D178A}$ Mouse F (5'-CCTGGTTTTAGTAGCAAGCCCAGGTACAGA-3'), Mfn1$^{D178A}$ Mouse R (5'-TCTGTACCTGGGCTTGCTACTAAAACCAGG-3'), Mfn1$^{P230A}$ Mouse F (5'-TGAGCGGCTCTCCAAGGCCAACA-3'), Mfn1$^{P230A}$ Mouse R (5'-TGTTGGCCTTGGAGAGCCGCTCA-3'), Mfn1$^{V252G}$ Mouse F (5'-AGTACATGGAGGATGGGCGCAGA-3'), Mfn1$^{V252G}$ Mouse R (5'-TCTGCGCCCATCCTCCATGTACT-3'), Mfn1$^{Q255R}$ Mouse F (5'-GATGTGCGCAGAAGGCACATGGAGAGA-3'), Mfn1$^{Q255R}$ Mouse R (5'-TCTCTCCATGTGCCTTCTGCGCACATC-3'), Mfn1$^{R259H}$ Mouse F (5'-CAGCACATGGAGCATTGTCTTCACTTCTTGGTAGAAG-3'), Mfn1$^{R259H}$ Mouse R (5'-CTTCTACCAAGAAGTGAAGACAATGCTCCATGTGCTG-3'), Mfn1$^{F263Y}$ Mouse F (5'-AGAGATGTCTTCACTACTTGGTAGAAGAG-3'), Mfn1$^{F263Y}$ Mouse R (5'-CTCTTCTACCAAGTAGTGAAGACATCTCT-3'), Mfn2$^{F223L}$ Mouse F (5'-GCCTGGATGCTGATGTGTTGGTGCTGGTGGCCAAC-3'), Mfn2$^{F223L}$ Mouse R (5'-GTTGGCCACCAGCACCAACACATCAGCATCCAGGC-3').

## 3.6 Acknowledgements

We would like to thank members of the Hoppins lab, Laura Lackner and Marijn Ford for scientific suggestions and critical reading of the manuscript. Jesse Hanson a graduate student in Justin Kollman's lab helped me crystalize and solve the structure of $Mfn1_{IM}^{F202L}$.

## 3.7 Figures

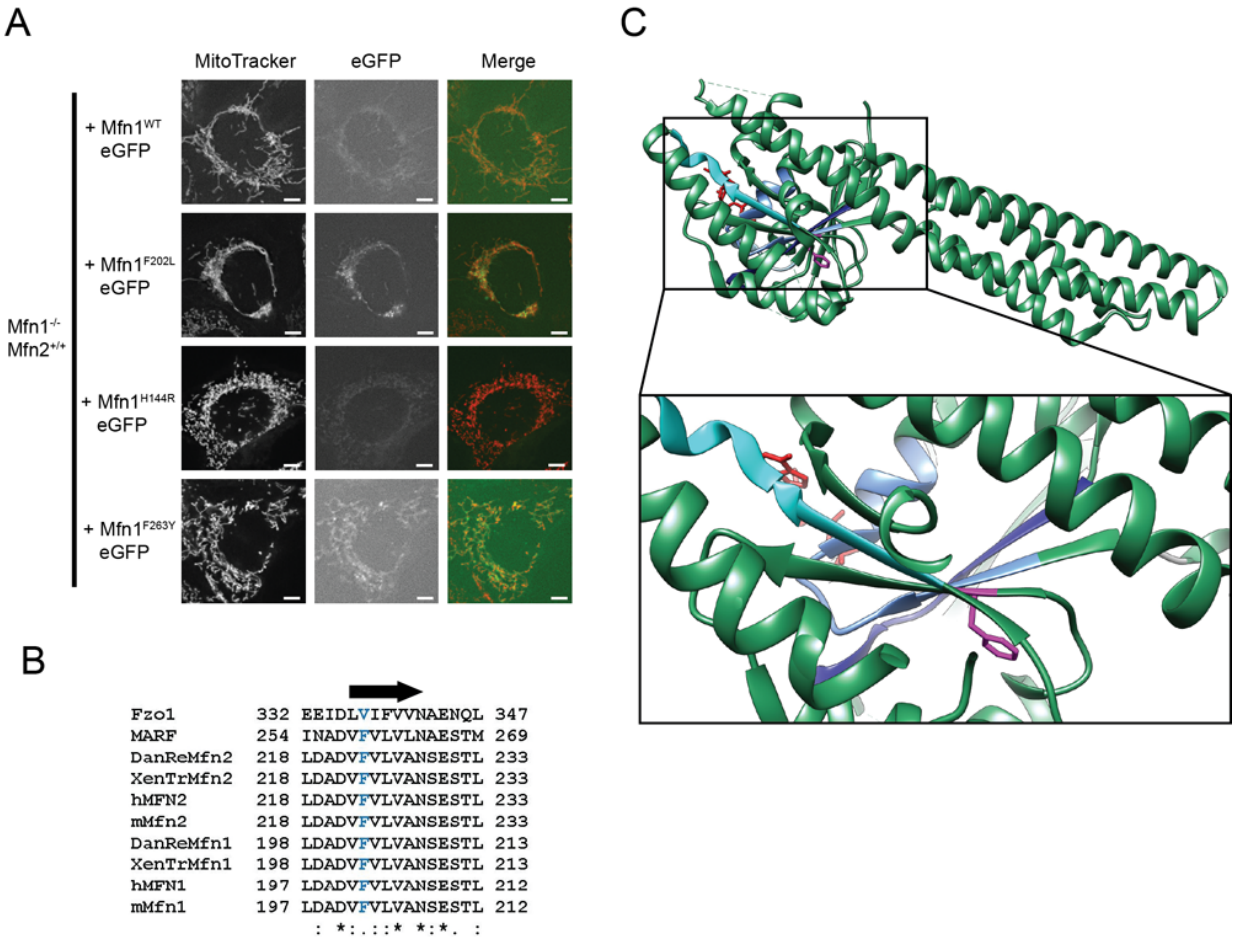


**Figure 3.1 Mfn1F202 is a highly conserved residue in a central beta strand**

**(A)** Representative images of Mfn1$^{-/-}$ Mfn2$^{+/+}$ cells stably expressing Mfn1-eGFP or Mfn1$^{F202L}$-eGFP following retroviral transduction. Mitochondria were labeled with MitoTracker Red CMXRos and visualized by fluorescence microscopy. Images represent maximum intensity projections. Scale bars are 5 μM. **(B)** Sequence alignment of Mfn1 F202 region generated using Clustal Omega. Arrow indicates position of beta strand 4G and the conserved phenylalanine (Mfn1-F202 and Mfn2-F223) is in blue text. **(C)** Mfn1$_{IM}$ crystal structure with F202 highlighted in fuchsia. Critical residues in conserved catalytic domains are highlighted: the P-loop in cornflower blue, G2/switch I in light blue, G3/switch II in dark blue and G4 in turquoise (PDB ID: 5GOE).

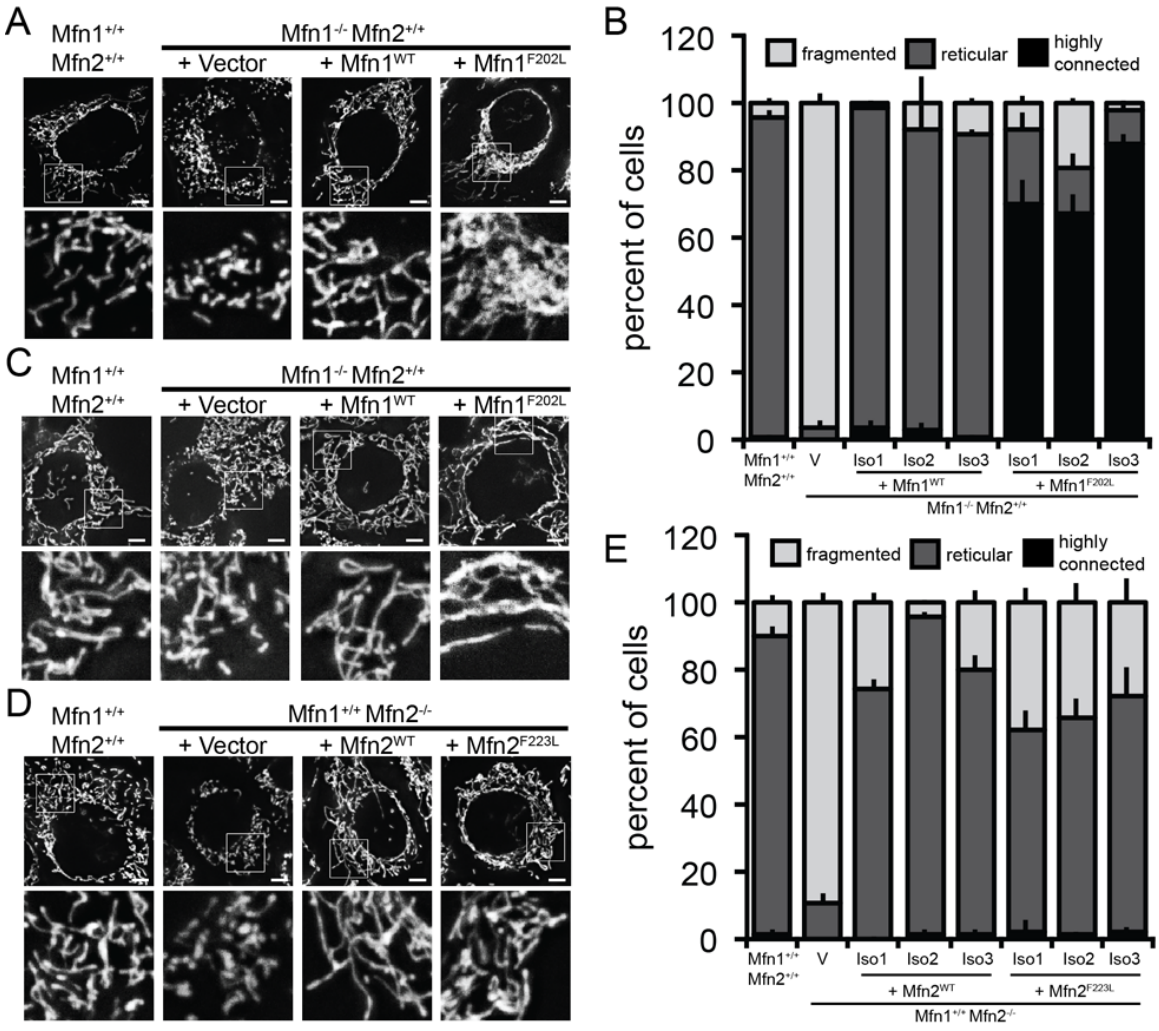


**Figure 3.2 Mfn1$^{F202L}$ and Mfn2$^{F223L}$ support mitochondrial fusion when expressed in Mfn1-null and Mfn2-null cells, respectively**

**(A)** Representative images of clonal populations of Mfn1$^{-/-}$ Mfn2$^{+/+}$ cells either transduced with empty vector (V) or stably expressing Mfn1-FLAG or Mfn1$^{F202L}$-FLAG. Mitochondria were labeled with MitoTracker Red CMXRos and visualized by fluorescence microscopy. Images represent maximum intensity projections. Scale bars are 5 μM. The vector panel is representative of a cell with a fragmented mitochondrial network; the wildtype and Mfn1-FLAG cells are representative of cells with a reticular mitochondrial network; the Mfn1-F202L cell is representative of a cell with a highly connected network. **(B)** Quantification of the mitochondrial morphology of cell lines described in (A). Error bars indicate mean + standard deviation from three blinded experiments (n > 100 cells per cell line per experiment). **(C)** Representative images of clonal populations from (A) treated with 1.5 nM nocodazole for 1 hour. Mitochondria were labeled with MitoTracker Red CMXRos and visualized by fluorescence microscopy. Images represent maximum intensity projections. Scale bars are 5 μM. **(D)** Representative images of clonal populations of Mfn1$^{+/+}$ Mfn2$^{-/-}$ cells stably either tranduced with empty vector (V) or expressing Mfn2-FLAG, Mfn2$^{F223L}$-FLAG. Mitochondria were labeled with MitoTracker Red CMXRos and

visualized by fluorescence microscopy. Images represent maximum intensity projections. Scale bars are 5 μM. **(E)** Quantification of the mitochondrial morphology of cell lines described in (D). Error bars indicate mean + standard deviation from three blinded experiments (n > 100 cells per cell line per experiment).

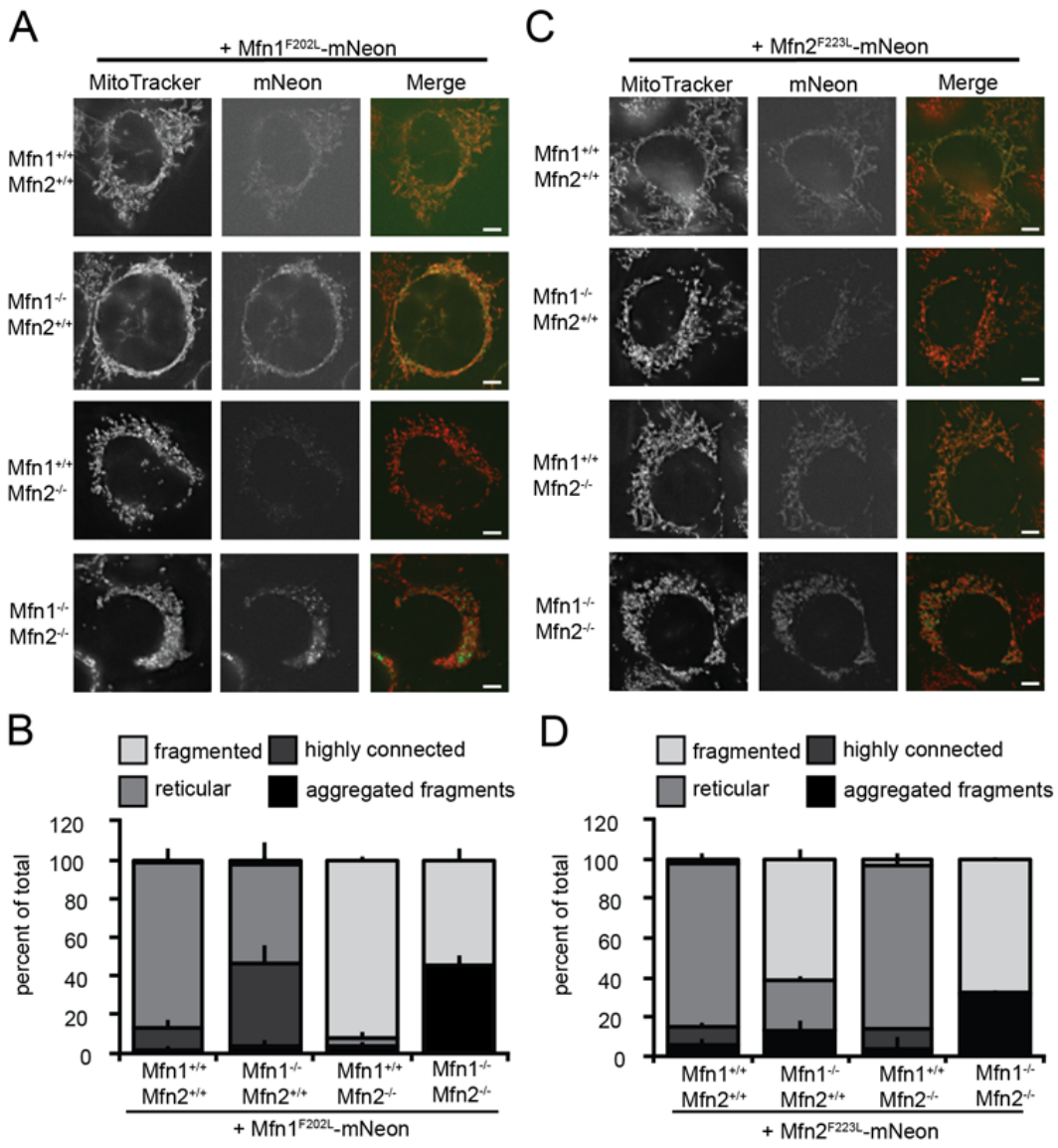


**Figure 3.3 Mfn1$^{F202L}$ and Mfn2$^{F223L}$ only support fusion in heterotypic complexes.**

**(A)** Representative images of the indicated cell lines stably expressing Mfn1$^{F202L}$-mNeon. Mitochondria were labeled with MitoTracker Red CMXRos and visualized by fluorescence microscopy. Images represent maximum intensity projections. Scale bars are 5 μM. **(B)** Quantification of the mitochondrial morphology of cell lines described in (A). Error bars indicate mean + standard deviation from three blinded experiments (n > 100 cells per cell line per experiment). **(C)** Representative images of the indicated cell lines stably expressing Mfn2$^{F223L}$-mNeon. Mitochondria were labeled with MitoTracker Red CMXRos and visualized by fluorescence microscopy. Images represent maximum intensity projections. Scale bars are 5 μM. **(D)** Quantification of the mitochondrial morphology of cell lines described in (C). Error bars indicate mean + standard deviation from three blinded experiments (n > 100 cells per cell line per experiment).

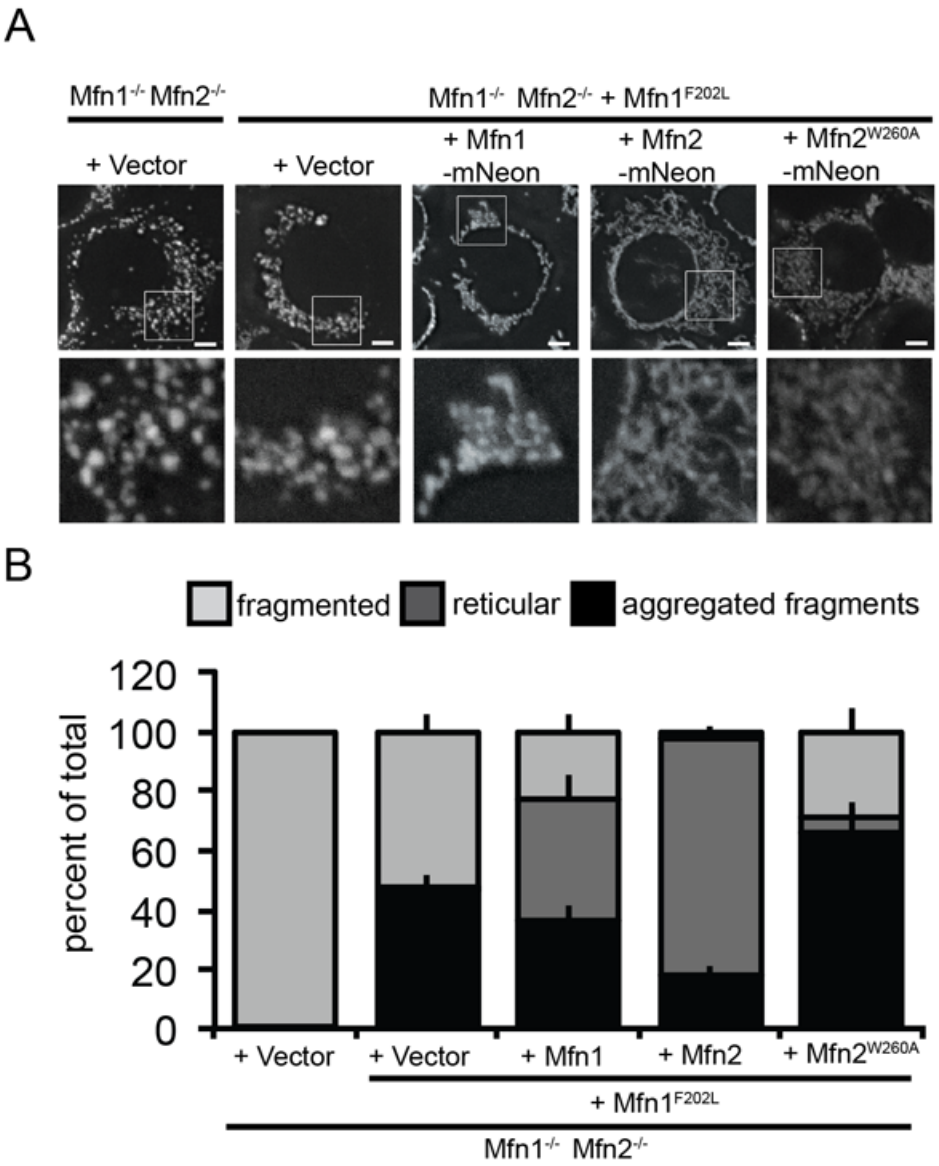


**Figure 3.4 Mfn1$^{F202L}$ requires wildtype Mfn2 to function in a heterotypic complex**

**(A)** Representative images of a clonal population of Mfn1$^{-/-}$ Mfn2$^{-/-}$ + Mfn1$^{F202L}$-FLAG stably expressing the indicated Mfn-mNeon. Mitochondria were labeled with MitoTracker Red CMXRos and visualized by fluorescence microscopy. Images represent maximum intensity projections. Scale bars are 5 μM. **(B)** Quantification of the mitochondrial morphology of cell lines described in (A). Error bars indicate mean + standard deviation from three blinded experiments (n > 100 cells per cell line per experiment).

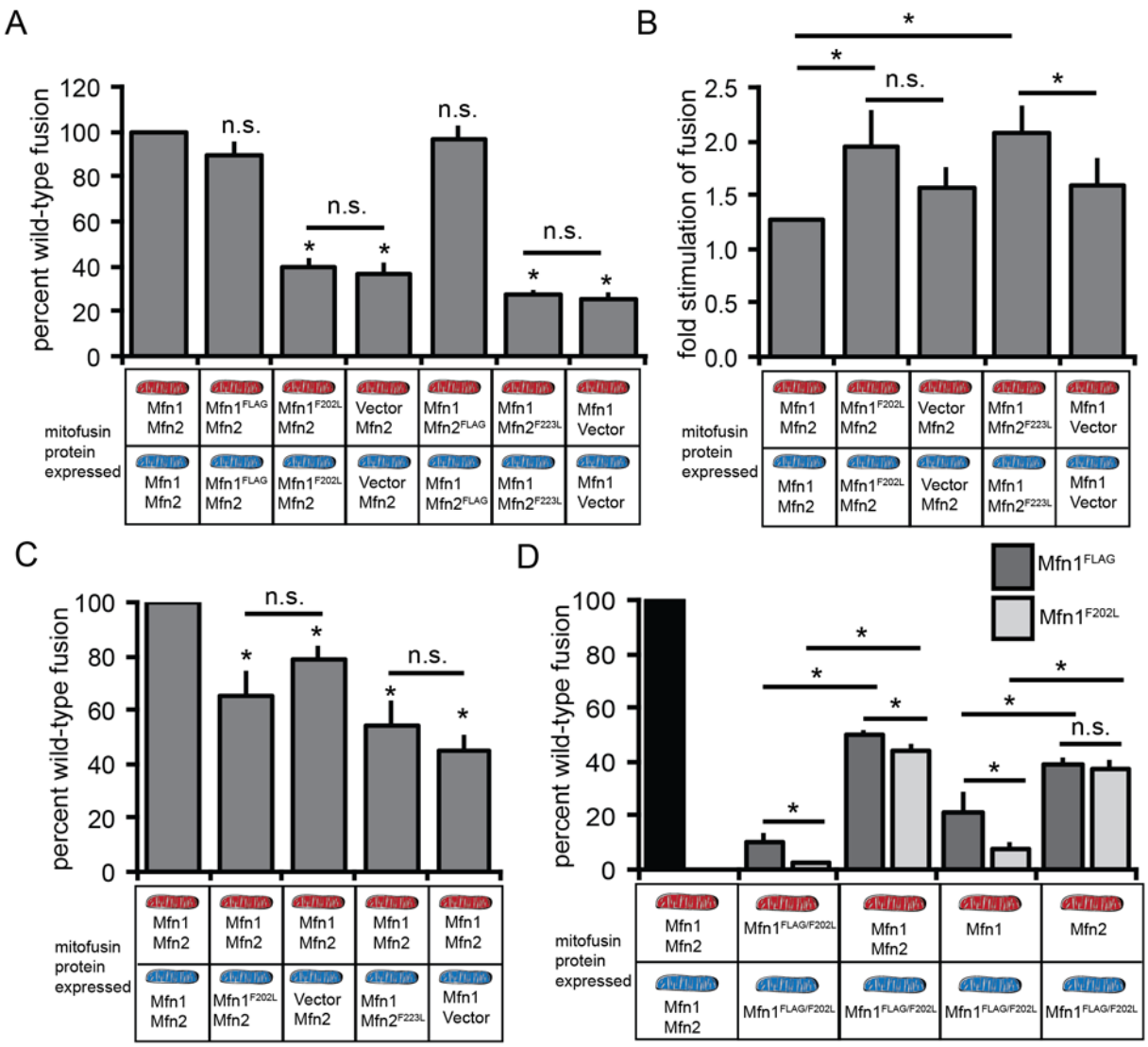


**Figure 3.5 Mitochondrial in vitro fusion assay reveals a fusion defect for Mfn1$^{F202L}$ and Mfn2$^{F223L}$**

**(A)** Mitochondria were isolated from wildtype cells (Mfn1$^{+/+}$Mfn2$^{+/+}$), a clonal population of Mfn1$^{WT}$-expressing Mfn1-null cells (Mfn1$^{WT}$Mfn2$^{+/+}$), a clonal population of Mfn1$^{F202L}$-expressing Mfn1-null cells (Mfn1$^{F202L}$Mfn2$^{+/+}$), a clonal population of Mfn1-null cells transduced with empty vector (Mfn1$^{-/-}$ Mfn2$^{+/+}$), a clonal population of Mfn2$^{WT}$-expressing Mfn2-null cells (Mfn1$^{+/+}$Mfn2$^{WT}$), a clonal population of Mfn2$^{F223L}$-expressing Mfn2-null cells (Mfn1$^{+/+}$Mfn2$^{F223L}$), and a clonal population of Mfn2-null cells transduced with empty vector (Mfn1$^{+/+}$Mfn2$^{-/-}$). The indicated mitochondrial combinations were subject to in vitro fusion conditions at 37°C for 30 minutes. **(B)** Mitochondria were isolated from wildtype cells (Mfn1$^{+/+}$Mfn2$^{+/+}$), a clonal population of Mfn1$^{F202L}$-expressing Mfn1-null cells (Mfn1$^{F202L}$Mfn2$^{+/+}$), a clonal population of Mfn1-null cells transduced with empty vector (Mfn1$^{-/-}$ Mfn2$^{+/+}$), a clonal population of Mfn2$^{F223L}$-expressing Mfn2-null cells (Mfn1$^{+/+}$Mfn2$^{F223L}$), and a clonal population of Mfn2-null cells transduced with empty vector (Mfn1$^{+/+}$Mfn2$^{-/-}$). The indicated

mitochondrial combinations were subject to in vitro fusion conditions in the presence of cytosol-enriched fraction at 37°C for 30 minutes. **(C)** Mitochondria were isolated from wildtype cells ($Mfn1^{+/+}Mfn2^{+/+}$), a clonal population of $Mfn1^{F202L}$-expressing Mfn1-null cells ($Mfn1^{F202L}Mfn2^{+/+}$), a clonal population of Mfn1-null cells transduced with empty vector ($Mfn1^{-/-}Mfn2^{+/+}$), a clonal population of $Mfn2^{F223L}$-expressing Mfn2-null cells ($Mfn1^{+/+}Mfn2^{F223L}$), and a clonal population of Mfn2-null cells transduced with empty vector ($Mfn1^{+/+}Mfn2^{-/-}$). The indicated mitochondrial combinations were subject to in vitro fusion conditions at 37°C for 30 minutes. **(D)** Mitochondria were isolated from wildtype cells ($Mfn1^{+/+}Mfn2^{+/+}$), Mfn1-null cells ($Mfn1^{-/-}Mfn2^{+/+}$), Mfn2-null cells ($Mfn1^{+/+}Mfn2^{-/-}$), a clonal population of $Mfn1^{WT}$-expressing Mfn1/2-double null cells ($Mfn1^{WT}Mfn2^{-/-}$), and a clonal population of $Mfn1^{F202L}$-expressing Mfn1/2-double null cells ($Mfn1^{F202L}Mfn2^{-/-}$). The indicated mitochondrial combinations were subject to in vitro fusion conditions at 37°C for 60 minutes. Data are expressed as a percent of wildtype control reactions performed in parallel. Error bars indicate mean + standard deviation from at least four independent experiments and paired student t-test analysis was performed to determine statistical significance *$P<0.05$.

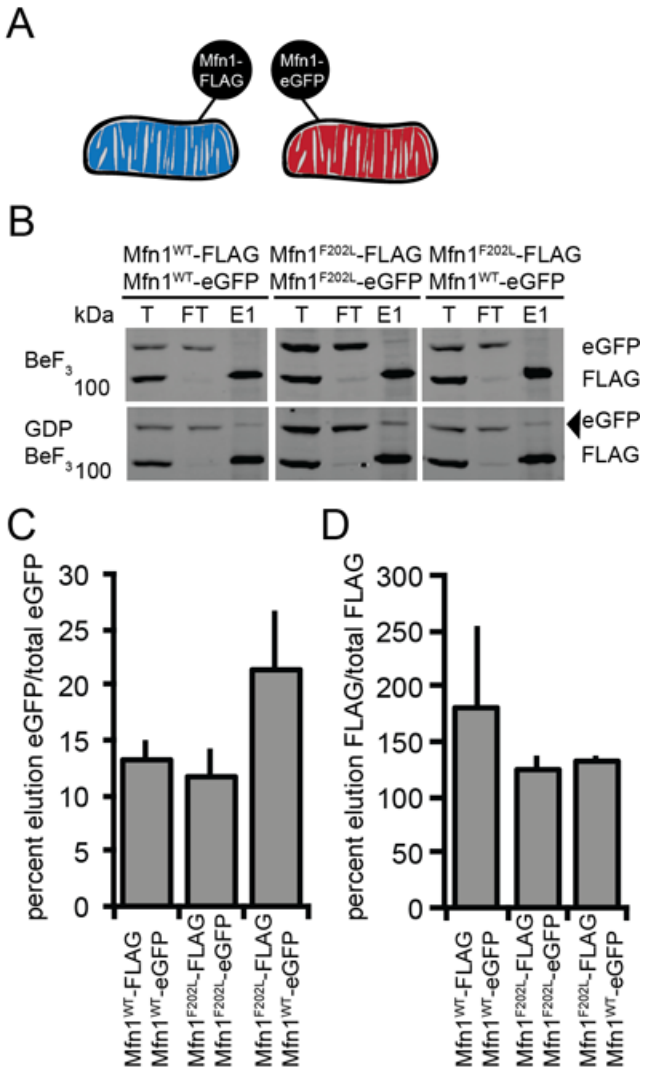


**Figure 3.6 Tethering assay to assess the physical interaction of Mitofusin proteins in trans**

**(A)** Schematic of the differential epitope labeling utilized in the tethering assay. **(B)** Mitochondria were isolated from a clonal population of Mfn1$^{WT}$-FLAG-expressing Mfn1-null cells (Mfn1$^{WT}$Mfn2$^{+/+}$), a clonal population of Mfn1$^{WT}$eGFP-expressing Mfn1-null cells (Mfn1$^{WT}$Mfn2$^{+/+}$), a clonal population of Mfn1$^{F202L}$FLAG-expressing Mfn1-null cells (Mfn1$^{F202L}$Mfn2$^{+/+}$), and a clonal population of Mfn1$^{F202L}$-eGFP-expressing Mfn1-null cells (Mfn1$^{F202L}$Mfn2$^{+/+}$) and incubated with $BeF_3$ in the absence or presence of GDP. Following lysis, immunoprecipitation was performed with α-FLAG magnetic beads. Proteins eluted from the beads were subjected to SDS-PAGE and immunoblotted with α-Mfn1. Arrowhead indicates the eGFP protein eluted from FLAG beads. Total (T) represents 3% of the input, flow through (FT) represents 3% of the unbound protein, and elution (E) represents 40% of the immunoprecipitated protein. (C) The percentage of the indicated Mitofusin-eGFP in the elution compared to the total is shown as the mean + standard deviation of three independent experiments. (D) The percentage

of the indicated Mitofusin-FLAG in the elution compared to the total is shown as the mean + standard deviation of three independent experiments.

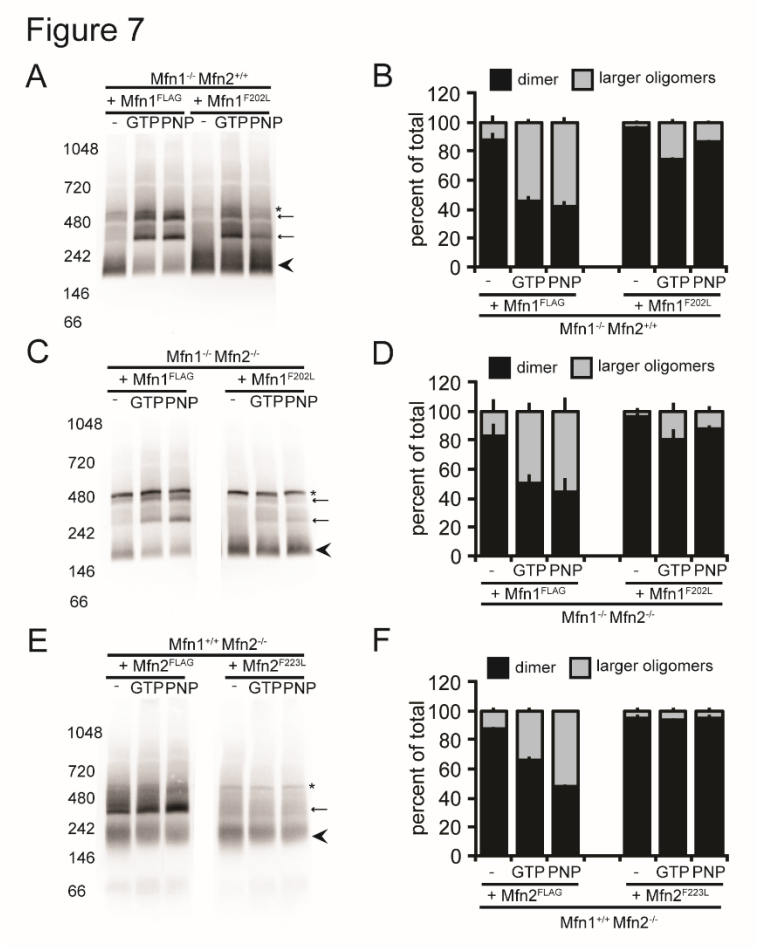


**Figure 3.7 Mfn1$^{F202L}$ has impaired nucleotide dependent assembly**

**(A)** Mitochondria were isolated from a clonal population of Mfn1$^{WT}$-expressing Mfn1-null cells (Mfn1$^{WT}$Mfn2$^{+/+}$) and a clonal population of Mfn1$^{F202L}$-expressing Mfn1-null cells (Mfn1$^{F202L}$Mfn2$^{+/+}$). Mitochondria were either not treated, or incubated with the specified nucleotide prior to lysis, and were then subjected to BN-PAGE and immunoblotted with α-FLAG. arrowhead denotes the predicted dimer state, arrows denote the larger oligomeric species, and * denotes a non-specific band. **(B)** The percentage of total protein in the smaller oligomeric state (arrowhead) (predicted dimer) and the higher oligomeric states (arrows) for each condition in (A) is represented in the bar graph as mean + standard deviation of three independent experiments. **(C)** Mitochondria were isolated from a clonal population of Mfn1$^{WT}$-expressing Mfn1/2-double null cells (Mfn1$^{WT}$Mfn2$^{-/-}$) and a clonal population of Mfn1$^{F202L}$-expressing Mfn1/2-double null cells (Mfn1$^{F202L}$Mfn2$^{-/-}$). Mitochondria were either not treated, or incubated with the specified nucleotide prior to lysis, and then were subjected to BN-PAGE and immunoblotted with α-FLAG. Arrowhead denotes the predicted dimer state, arrows denote the larger oligomeric species and * denotes a non-specific band. **(D)** The percentage of total protein in the smaller oligomeric state (arrowhead) (predicted dimer) and the higher oligomeric states (arrows) for each condition in (C) is represented in the bar graph as mean + standard deviation of

three independent experiments. **(E)** Mitochondria were isolated from a clonal population of $Mfn2^{WT}$-expressing Mfn2-null cells ($Mfn1^{+/+}Mfn2^{WT}$) and a clonal population of $Mfn2^{F223L}$-expressing Mfn2-null cells ($Mfn1^{+/+}Mfn2^{F223L}$). Mitochondria were either not treated, or incubated with the specified nucleotide prior to lysis, and then were subjected to BN-PAGE and immunoblotted with α-FLAG. Arrowhead denotes the predicted dimer state, an arrow denotes the larger oligomeric species and * denotes a non-specific band. **(F)** The percentage of total protein in the smaller oligomeric state (arrowhead) (predicted dimer) and the higher oligomeric states (arrow) for each condition in (E) is represented in the bar graph as mean + standard deviation of three independent experiments.

Table S1

| Mutation | Mitochondrial Morphology |
|---|---|
| Mfn1$^{R83W}$ | Fragmented, short tubules |
| Mfn1$^{H107R}$ | Fragmented, aggregated fragments |
| Mfn1$^{T109A}$ | Fragmented |
| Mfn1$^{A143V}$ | Short tubules |
| Mfn1$^{H144R}$ | Fragmented |
| Mfn1$^{D178A}$ | Fragmented |
| Mfn1$^{F202L}$ | Highly elongated, perinuclear collapse |
| Mfn1$^{P230A}$ | Reticular |
| Mfn1$^{V252G}$ | Fragmented, short tubules, some reticular |
| Mfn1$^{Q255R}$ | Fragmented |
| Mfn1$^{R259H}$ | Short tubules, reticular |
| Mfn1$^{F263Y}$ | Reticular |

**Table S3.1 Functional screen of Mfn1 GTPase domain mutant variants**

Description of the mitochondrial morphology of GTPase domain mutant variants generated in Mfn1-eGFP and expressed in Mfn1$^{-/-}$ Mfn2$^{+/+}$ cells by retroviral transduction.

A

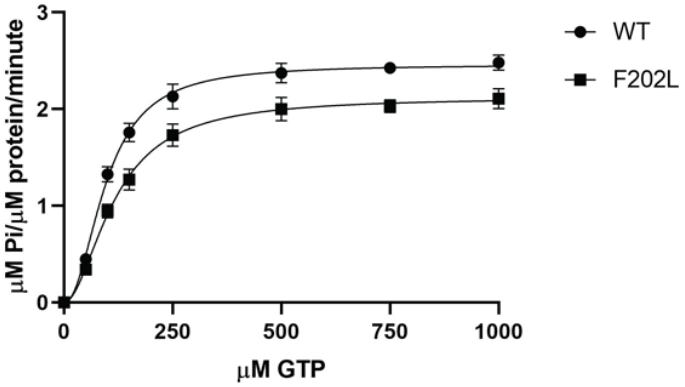


B

| | WT | F202L |
|---|---|---|
| Vmax | 2.461 | 2.123 |
| h | 2.119 | 1.884 |
| Khalf | 96.51 | 116.6 |

**Figure S3.1 Kinetic analysis of GTP hydrolysis of $Mfn1_{IM}C$ and $Mfn1^{F202L}{}_{IM}C$**

**(A)** A representative kinetic plot fit to an allosteric sigmoidal equation is shown. **(B)** Kinetic parameters for $Mfn1_{IM}C$ and $Mfn1^{F202L}{}_{IM}C$.

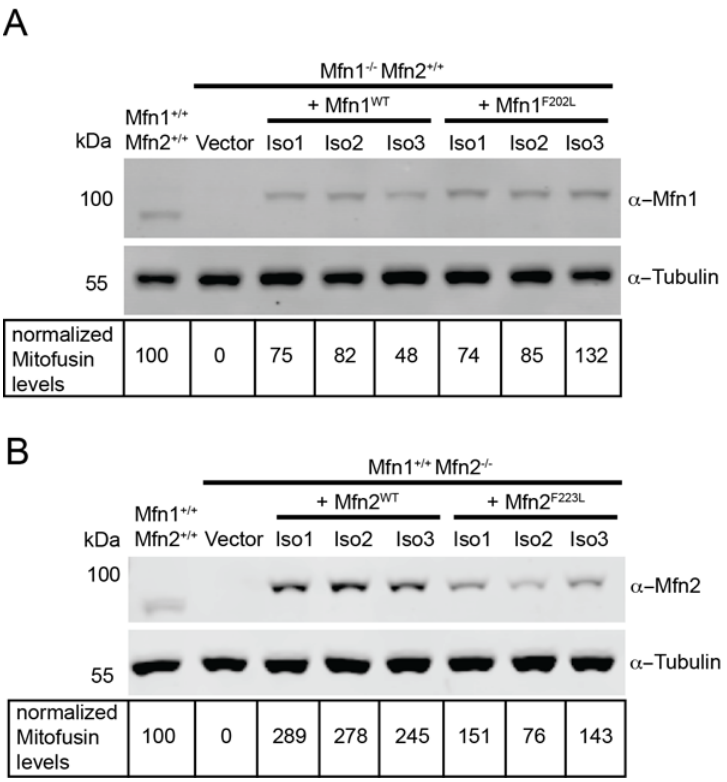


**Figure S3.2 Mitofusin-FLAG protein expression in MEF clonal populations**

**(A)** Whole-cell lysates prepared from indicated cell lines were subjected to SDS-PAGE and immunoblotting with α-Mfn1 and α-Tubulin. Protein loading was normalized to Tubulin and for each clonal population, the relative amount of Mfn1-FLAG to endogenous Mfn1 is listed below. **(B)** Whole-cell lysates prepared from indicated cell lines were subjected to SDS-PAGE and immunoblotting with α-Mfn2 and α-Tubulin. Protein loading was normalized to Tubulin and for each clonal population, the relative amount of Mfn2-FLAG to endogenous Mfn2 is listed below.

Figure S3

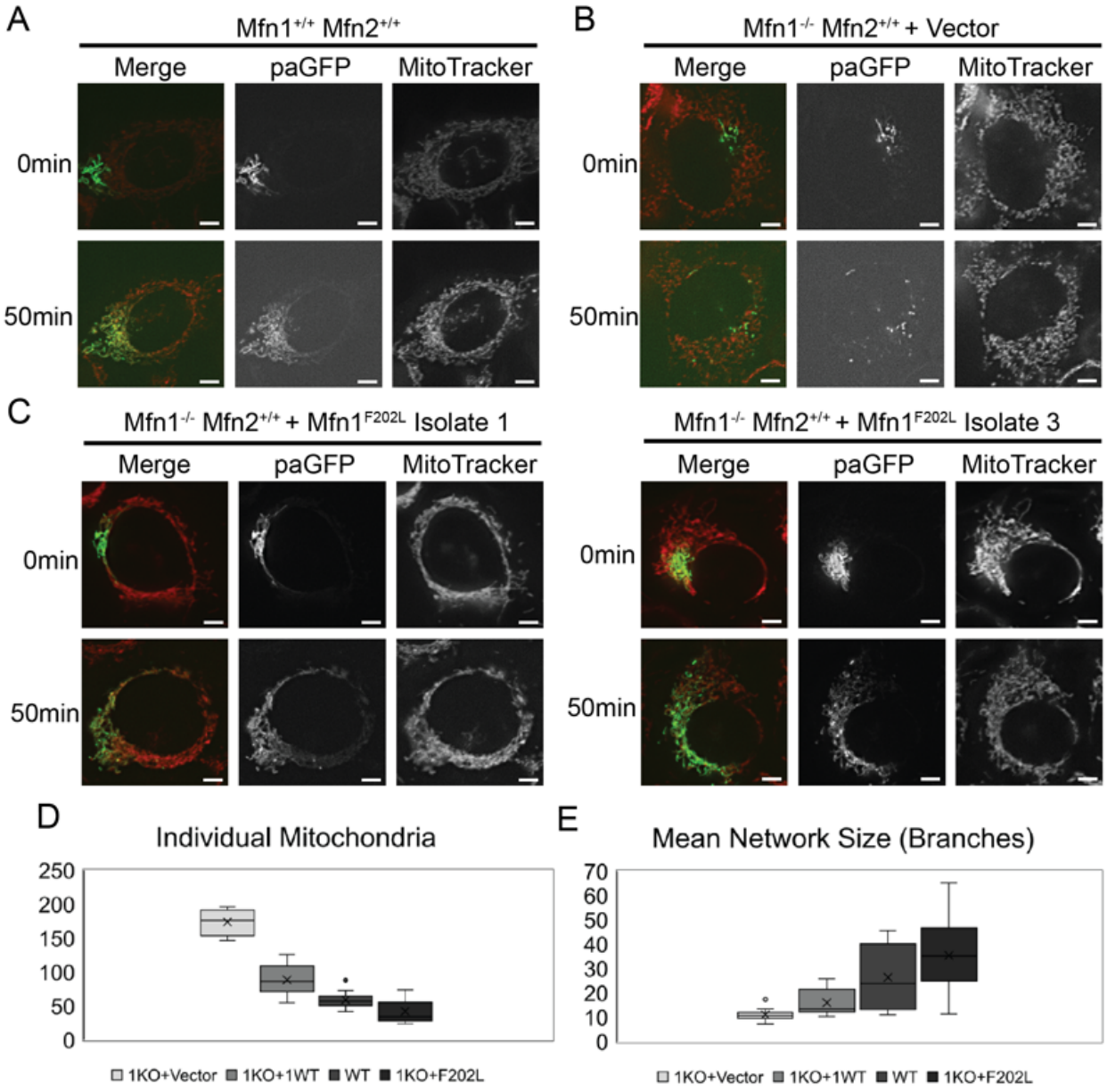


**Figure S3.3 Mitochondrial connectivity and fusion as measured by redistribution of GFP**

Wildtype **(A)** or clonal populations of Mfn1-null cells transduced with empty vector **(B)** or Mfn1$^{F202L}$ **(C)** trasduced with mitochondrial matrix-targed photoactivatible-GFP (mt-paGFP) were labeled with MitoTracker Red CMXRos and visualized by fluorescence microscopy. A small region of the cell that contained mitochondria (approximately 1 micron square) was activated using a 405 nm laser (t=0 min) and the same cell was re-imaged 50 minutes later (t-50 min). The Pearson's correlation co-efficient for red and green pixels was calculated as a measure of GFP spreading through the mitochondrial network. For wildtype controls, the co-efficient was

0.32 at t=0 and 0.627 at t=50; for empty vector, the co-efficient was 0.09 at t=0 and 0.077 at t=50; for F202L isolate 1, the co-efficient was 0.315 at t=0 and 0.603 at t=50; for F202L isolate 3, the co-efficient was 0.459 at t=0 and 0.653 at t=50. Mitochondrial network analysis was performed with the Image J MiNa plugin to assess the number of individual mitochondria **(D)** and the mean network size **(E)** in wildtype, or clonal populations of Mfn1-null cells transduced with empty vector or expressing Mfn1F202L.

Figure S4

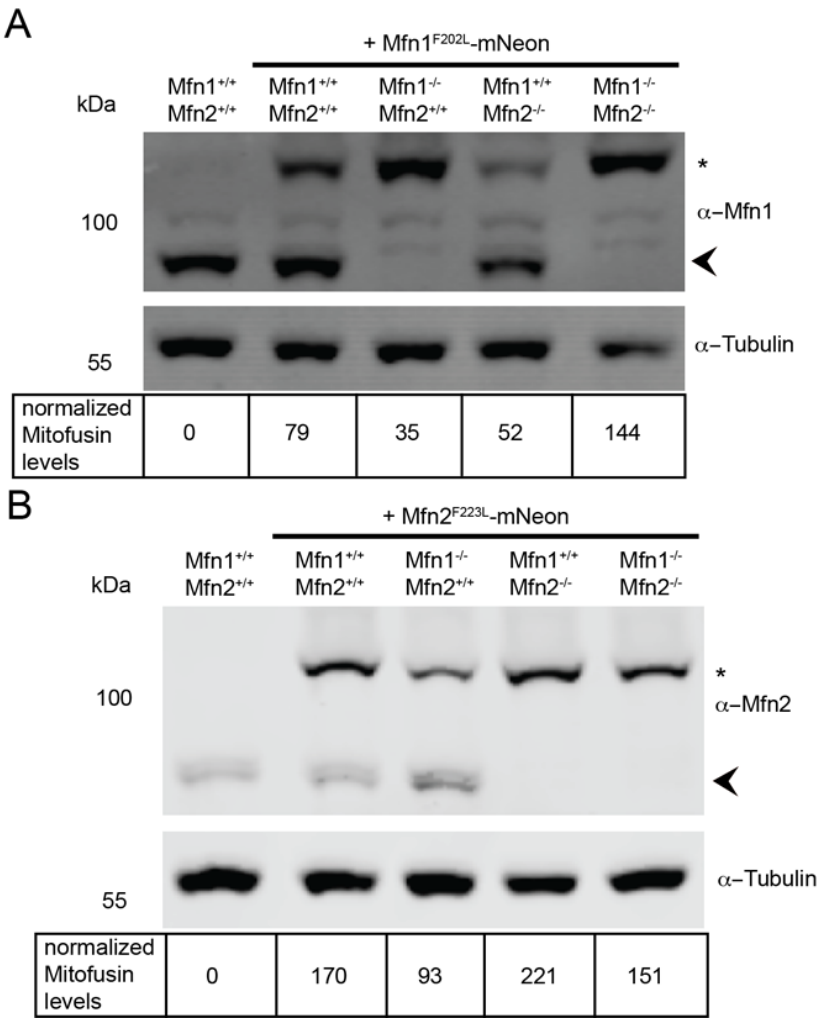


**Figure S3.4 Mitofusin-mNeon protein expression in MEFs of the indicated genotype**

**(A)** Whole-cell lysates prepared from indicated cell lines expressing Mfn1$^{F202L}$-mNeon were subjected to SDS-PAGE and immunoblotting with α-Mfn1and α-Tubulin. Protein loading was normalized to Tubulin and for each cell line, the relative amount of Mfn1-mNeon to endogenous Mfn1 is listed below. **(B)** Whole-cell lysates prepared from indicated cell lines expressing Mfn2$^{F223L}$-mNeon were subjected to SDS-PAGE and immunoblotting with α-Mfn2 and α-Tubulin. Protein loading was normalized to Tubulin and for each cell line, the relative amount of Mfn2-mNeon to endogenous Mfn2 is listed below. Arrowhead indicated endogenous Mitofusin and asterisk indicates Mitofusin with C-terminal mNeonGreen.

# Figure S5

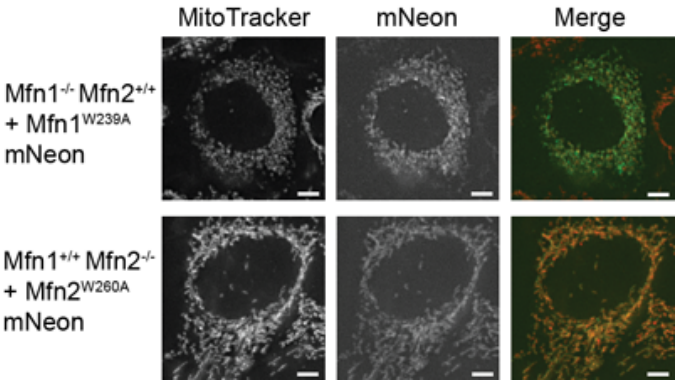


**Figure S3.5 Functional assessment of Mfn1$^{W239A}$ and Mfn2$^{W260A}$**

Representative images of Mfn1-null cells expressing Mfn1$^{W239A}$-mNeon and Mfn2-null cells expressing Mfn2$^{W260A}$-mNeon following viral transduction. Mitochondria were labeled with MitoTracker Red CMXRos and visualized by fluorescence microscopy. Images represent maximum intensity projections. Scale bars are 5 μM.

Figure S6

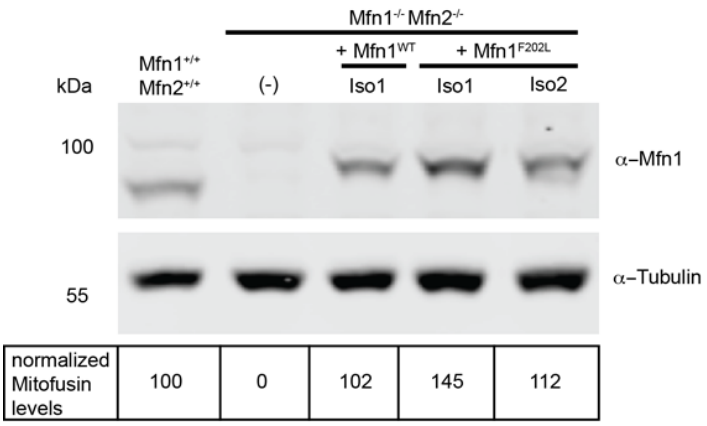


**Figure S3.6 Mfn1-FLAG and Mfn1$^{F202L}$-FLAG protein expression in Mfn1/2-null clonal populations**

Whole-cell lysates prepared from indicated cell lines were subjected to SDS-PAGE and immunoblotting with α-Mfn1 and α-Tubulin. Protein loading was normalized to Tubulin and for each clonal population, the relative amount of Mfn1-FLAG to endogenous Mfn1 is listed below.

Figure S7

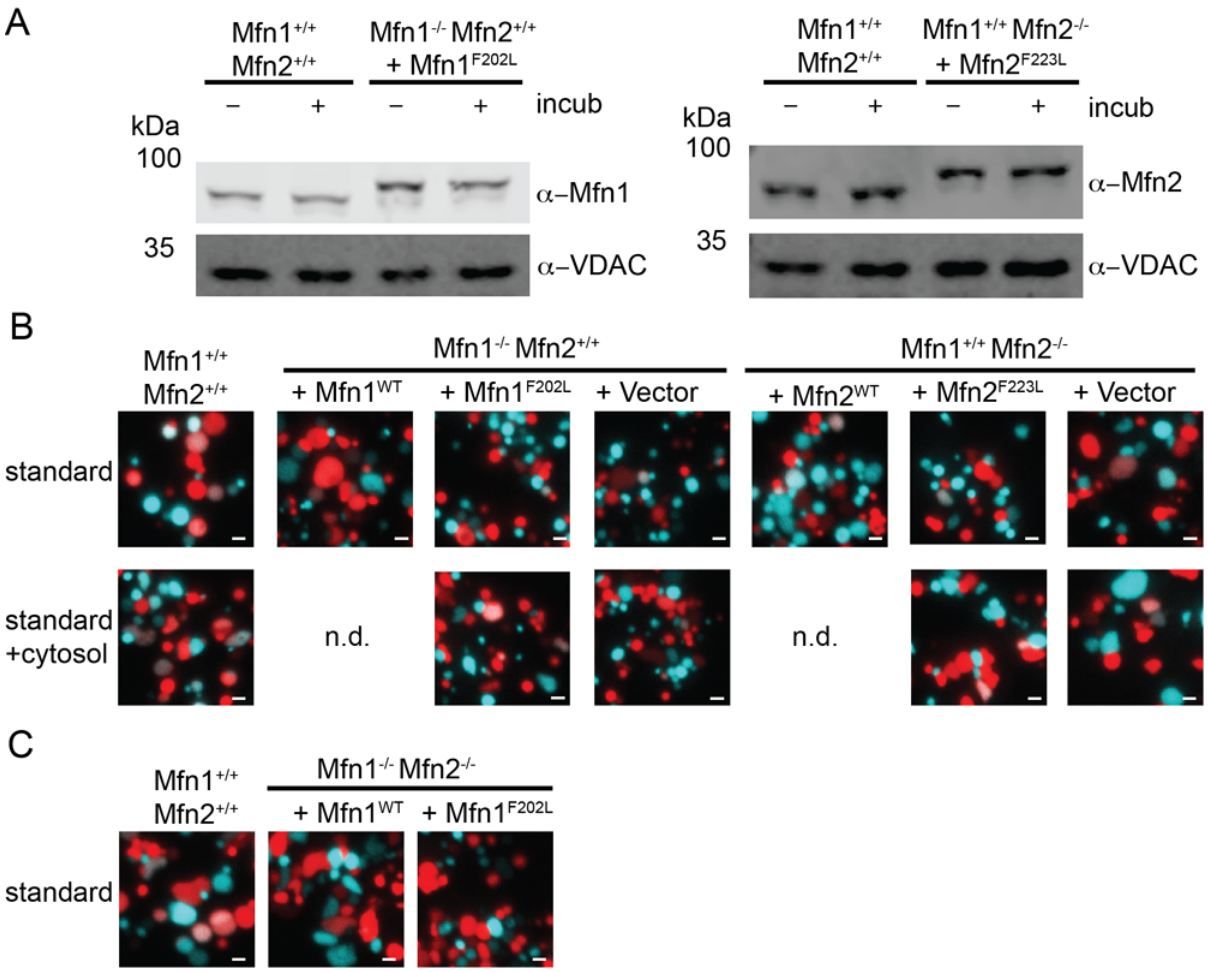


**Figure S3.7 Mitofusin protein stability and mitochondrial morphology in vitro**

**(A)** To assess the protein stability under the in vitro fusion conditions, isolated mitochondria were either left untreated (-) or were subject to in vitro fusion conditions (+) prior to analysis by SDS-PAGE and immunoblotting with α-Mfn1, α-Mfn2 and, α-VDAC. **(B)** Representative images from in vitro fusion reactions described in Figure 3.5A & B. **(C)** Representative images from in vitro fusion reactions described in Figure 3.5D.

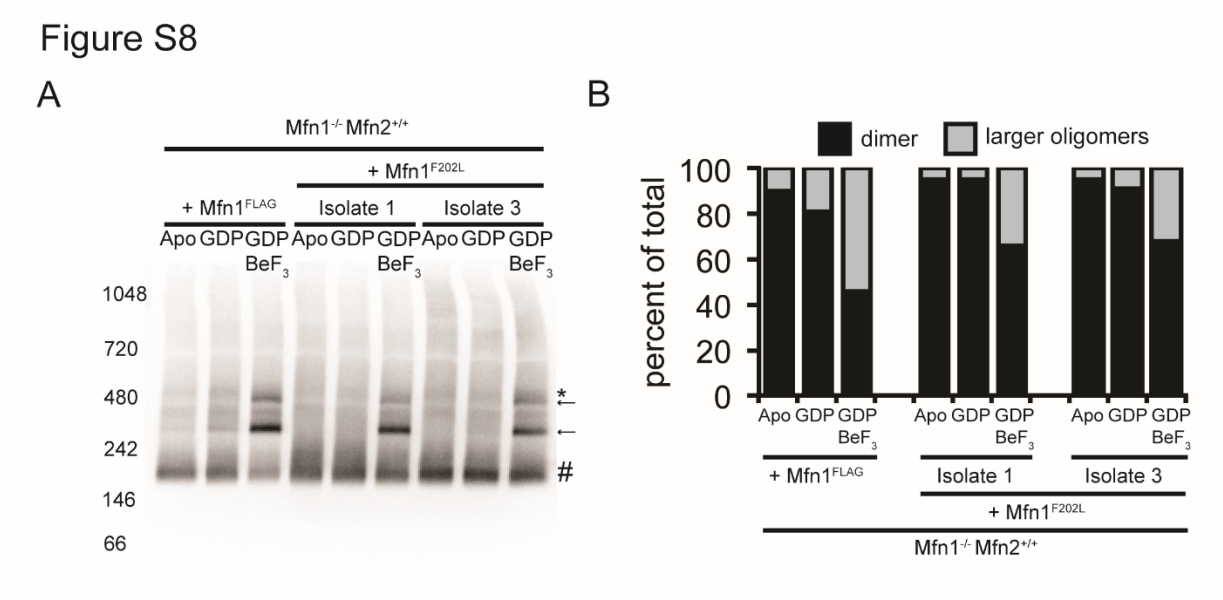


**Figure S3.8 Mfn1$^{F202L}$ has impaired nucleotide dependent assembly**

**(A)** Mitochondria were isolated from indicated cell lines, either left untreated, or were incubated with the indicated nucleotide condition prior to lysis and were then subjected to BN-PAGE and immunoblotted with α-FLAG. # denotes the predicted dimer state, arrows denote the larger oligomeric species and * denotes a non-specific band. **(B)** The percentage of total protein in the smaller oligomeric state (#)(predicted dimer) and the higher oligomeric states (arrows) for each condition in (A) is represented in the bar graph.

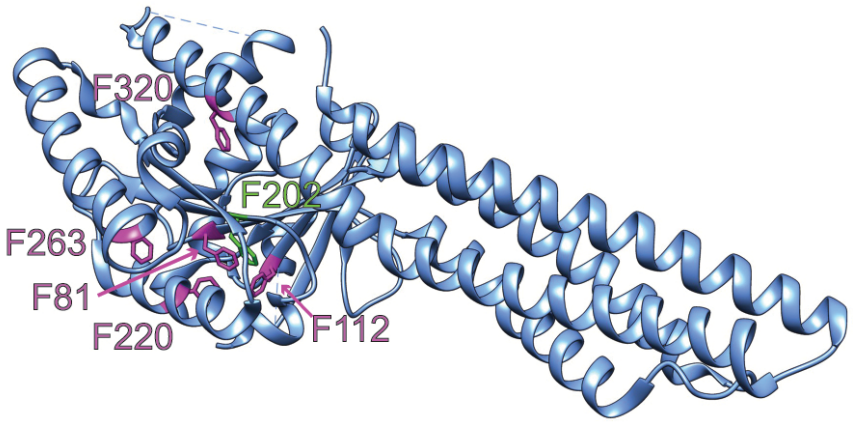


**Figure S3.9 Aromatic network that includes F202** as well as F81, F112, F219, F220, F263 and F320 (PDB 5G04).

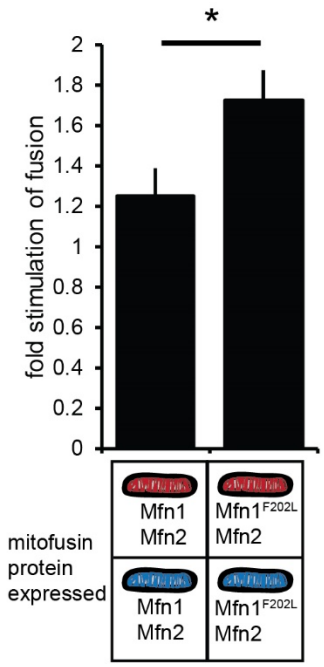


**Figure S3.10 Mitochondrial in vitro fusion assay reveals recombinantly purified Bax protein stimulates Mfn1$^{F202L}$**

Mitochondria were isolated from wildtype cells (Mfn1$^{+/+}$Mfn2$^{+/+}$) and a clonal population of Mfn1$^{F202L}$-expressing Mfn1-null cells (Mfn1$^{F202L}$Mfn2$^{+/+}$). The indicated mitochondrial combinations were subjected to in vitro fusion conditions with 750 nM recombinantly purified Bax protein at 37°C for 30 minutes. Data are expressed as a percent of wildtype control reactions performed in parallel. Error bars indicate mean + standard deviation from at least four independent experiments and paired student t-test analysis was performed to determine statistical significance *P<0.05.

A

B

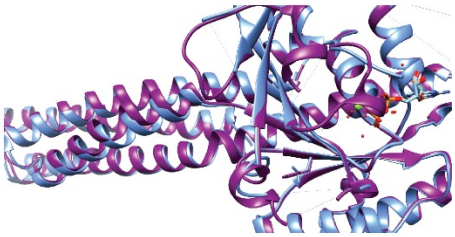

C

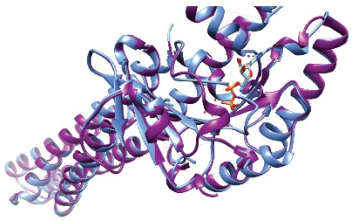

D

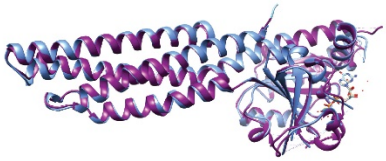

**Figure S3.11 Crystal structure of $Mfn1_{IM}^{F202L}$**

**(A)** Distance map generated in UCSF Chimera shows that Mfn1IMF202L is missing density for many loops compared to $Mfn1_{IM}^{WT}$ (PDB 5GOE) **(B)** Overlay of $Mfn1_{IM}^{WT}$ (purple) and $Mfn1_{IM}^{F202L}$ (blue) shows that the F202L mutation does not alter the residue's rotamer or the β-sheet secondary structure **(C)** Overlay of $Mfn1_{IM}^{WT}$ (purple) and $Mfn1_{IM}^{F202L}$ (blue) shows that the F202L mutation causes many loops to lose density **(D)** Overlay of $Mfn1_{IM}^{WT}$ (purple) and $Mfn1_{IM}^{F202L}$ (blue) shows that the F202L mutation does not alter structure of helical bundle 1.

# Chapter 4: Fractionation of mammalian cytosol to identity new cytosolic pro-fusion factors

## 4.1 Abstract

Mitochondrial fusion can be enhanced or inhibited by cytosolic factors including protein binding partners and post-translational modifications. Using the in vitro mitochondrial fusion assay described in Chapter 3, we can quantify the amount of mitochondrial fusion under different conditions. Our strategy was to find new pro-fusion proteins by performing cytosolic fractionation by ion exchange chromatography. We found that proteins which bound tightly to cation exchange resin stimulated mitochondrial fusion in vitro whereas proteins unable to bind cation exchange resin could not. We then performed mass spectrometry analysis and compared fractions that did and did not have stimulatory activity. We obtained a large list of proteins only present in high abundance in the stimulatory fraction with no obvious candidates. Interestingly, incubation of the stimulatory fraction with RNase, trypsin protease or heat treatment reduced its activity, which indicates that the stimulatory factor might be an RNA binding protein. Further fractionation will be required to determine the identity of this pro-fusion protein.

## 4.2 Introduction

The rate of mitochondrial fusion events in cells is difficult to quantify. A multitude of factors contribute the overall connectivity of the mitochondrial network as well as individual fusion and division events are difficult count. In addition, in cells mitochondrial fusion relies on the correct positioning of the organelles via microtubule-based transport and mitochondrial fusion is opposed by mitochondrial division. Therefore, we utilize an in vitro fusion assay to quantify the rate of mitochondrial fusion in the absence of mitochondrial transport, mitochondrial division and cytosolic regulatory factors. This assay allows us to assess changes in fusion activity under different conditions including the presence cytosol-enriched fractions, purified proteins, energy sources or small molecules. From previous work, we know that the addition of purified recombinant Bax protein stimulates mitochondrial fusion to a similar level as addition of crude cytosol-enriched fraction (Hoppins et al., 2011). A few other cytosolic proteins have been shown to interact directly with the Mitofusins to enhance mitochondrial fusion in cells including the Smad2/RIN1 complex and Gβ2 (Kumar et al., 2016; Zhang et al., 2010). In addition, post-translational modifications of the Mitofusins have been shown to both increase and decrease the proteins activity (Chen & Dorn, 2013; Ferreira et al., 2019; Glauser et al., 2011; Leboucher et al., 2012; Lee et al., 2014; Pyakurel et al., 2015; Rakovic et al., 2011; Sarraf et al., 2013; Shutt et al., 2012; Tanaka et al., 2010). The in vitro mitochondrial fusion assay can therefore directly test whether these proteins, small molecules or post-translational modifications influence mitochondrial fusion without the complexity of mitochondrial transport and division to identify new regulators of mitochondrial fusion.

## 4.3 Results

We utilized the in vitro mitochondrial fusion assay to directly test the stimulation of mitochondrial fusion in an effort to identify a novel pro-fusion factor. Crude cytosol promotes a modest 1.2-1.5 fold increase in mitochondrial fusion activity in vitro compared to buffer controls. Therefore, to determine which proteins are important for this stimulation of fusion activity, cytosol was biochemically fractionated, and the fusion-stimulating activity of the fractions was followed using the in vitro fusion assay. Using ion exchange chromatography, we have followed the pro-fusion activity through several purification steps and have identified a discrete fraction that robustly stimulates mitochondrial fusion.

### 4.3.1 Fractionation of cytosol

Cytosol was fractionated by batch binding to ion exchange resins. Cytosol was first incubated with either anion exchange resin or cation exchange resin. The unbound fraction from anion exchange stimulated in vitro mitochondrial fusion as efficiently as untreated cytosol, but the stimulatory activity was lost following incubation with cation exchange resin. This suggested that pro-fusion factors are bound to the cation exchange resin, but not the anion exchange resin. Pro-fusion factors were eluted from the cation exchange resin using a step gradient of potassium chloride, which were dialyzed overnight to reduce the salt. Additionally, dialysis would remove any small molecules present therefore eliminated a small molecule as a possible pro-fusion factor. The fractions were tested for pro-fusion activity and the 250 mM KCl fraction was the only cation elution to robustly stimulate in vitro mitochondrial fusion activity. This result has been consistent over multiple cytosol fractionation experiments.

We then tested the fraction to determine if the pro-fusion factor was protein or RNA. The sample was treated with either heat or trypsin to denature or degrade proteins respectively. Additionally, the sample was treated with RNase to degrade RNA polymers. Under all three conditions tested we observed a decrease in the ability of this fraction to stimulate in vitro mitochondrial fusion activity (Figure 4.1). These results are particularly intriguing as they suggest that the stimulatory factor may be an RNA binding protein.

### 4.3.2 Mass spectroscopy

To determine the identity of the proteins in the cation 250 mM KCl fraction we performed mass spectroscopy. These proteins were then compared the proteins, in the fraction unable to stimulate mitochondrial fusion as we could remove any proteins that were in both fractions. The number of proteins in the cation 250 mM KCl fraction was very high (>1000) and the number of unique proteins in the 250 mM KCl fraction was more than 300. This included many DNA binding proteins, RNA binding proteins, actin binding proteins, kinases and cytoskeletal components. While the fractionation was robust, we cannot generate a reasonable list of candidates from these 300 proteins.

### 4.3.3 Size exclusion chromatography

Given the very large number of proteins in the mass spectrometry analysis, we sought to further fractionate the cation 250 mM KCl fraction by size exclusion chromatography (SEC). Fractions from a Superose 6 increase 10/300 SEC column were collected and some were tested for their ability to stimulate in vitro mitochondrial fusion (Figure 4.2 A). An extremely late eluting fraction, fraction 29, which represents molecules of approximately 1,000 daltons in size greatly stimulated in vitro mitochondrial fusion activity of wildtype mitochondria (~3 fold)

compared to ~1.5 fold stimulation observed with the crude cytosol (Figure 4.2 B). When this fraction was incubated with RNase, only a ~1.4 fold stimulation was observed. To determine if the fraction contained RNA, Qubit fluorescence RNA analysis was performed. Unfortunately, both the cation 250 mM KCl fraction and fraction 29 did not contain more than 20 ng/µL of RNA. Therefore, it is unlikely that RNA is stimulating in vitro mitochondrial fusion.

### 4.3.4 Fluorescence microscopy

To test the effect of some potential proteins of interest from the mass spectrometry analysis on mitochondrial morphology in cells, candidate proteins were cloned from a cDNA library into an expression vector with a C-terminal eGFP tag. These constructs were transiently transfected into HeLa or MEF cells and the mitochondrial network was visualized by fluorescence microscopy. Two different proteins were successfully transfected into cells: Filamin A and Programmed Cell Death Protein 4 (PDCD4). Filamin A is an actin binding protein, involved in crosslinking of actin filaments (Weihing, 1985). Filamin A-eGFP localized to the cytoplasm and had a clear actin localization pattern. The mitochondrial morphology in cells expressing Filamin-A-eGFP was indistinguishable from control cells. The second protein, PDCD4 is an RNA binding protein that inhibits translation and may play a role in apoptosis (Böhm et al., 2003; Göke et al., 2002; Shibahara et al., 1995; Takaki & Eto, 2018). PDCD4-eGFP had two different cellular localization patterns in the mixed population of transfected cells: exclusively nuclear or both nuclear and cytoplasmic. In HeLa cells with cytoplasmic PDCD4-eGFP, the mitochondria were collapsed around the perinuclear space in more than 80% of cells compared to less than 15% of cells with nuclear PDCD4-eGFP (Figure 4.3). This suggests that cytoplasmic PDCD4 may be influencing mitochondrial morphology or position.

## 4.4 Discussion

The goal of this project was to identify novel pro-fusion cytosolic factors. Thus far, we have developed a robust initial purification protocol and we are confident that further fractionation will narrow the candidates identified by mass spectrometry. Given that both protease and RNAse treatment reduced the ability of the fraction to increase mitochondrial fusion, we will prioritize candidates that are predicted RNA binding proteins.

Although the mass spectroscopy analysis contained more than 300 proteins enriched in the stimulatory fraction, which is too many to provide confidence in a short list of candidates, we have generated a list of proteins that are of potential interest for future investigation (Table 5.1). Future directions include cloning these genes from a cDNA library into a mammalian expression vector, transiently transfecting this construct into cells and determining if the mitochondrial morphology is affected.

In addition, further cytosolic fractionation should be performed. This could include a multitude of different changes including: (1) eluting proteins from the cation resin using an elution gradient of potassium chloride which might result in a cleaner elution profile, (2) eluting proteins from the cation resin using a step or gradient elution of increasing pH buffer which would give a different pattern of elution than potassium chloride step gradient, (3) binding cytosol to cation resin under different pH conditions which would cause differential protein binding, and (4) isolation of cytosol from a different cell type or tissue, for example mouse heart or Xenopus tropicalis egg extracts would significantly increase the amount of starting material which could allow for further fractionation. In addition, we could determine if this pro-fusion factor is conserved between cell types and species.

Size exclusion chromatography of the stimulatory fraction suggests that a small molecule, RNA or peptide is the stimulatory factor. This fraction corresponds to molecules of approximately 1,000 daltons. Although addition of RNase to this fraction reduced the stimulatory activity further analysis of the fraction for RNA by Qubit analysis failed to indicate that RNA is present in the fraction in high abundance (>20 ng/μL). A future direction would be to try adding RNA directly to the in vitro mitochondrial fusion assay to we see if any RNA is capable of stimulatory mitochondrial fusion. In conclusion, further fractionation of the cation 250 mM KCl fraction will be required to identity the stimulatory factor.

## 4.5 Methods

### 4.5.1 Cell culture

All cells were grown at 37°C and 5% $CO_2$ and cultured in DMEM (Thermo Fisher Scientific) containing 1X GlutaMAX (Thermo Fisher Scientific) with 10% FBS (Seradigm) or 15% FBS for Mfn1/2-null mouse embryonic fibroblasts and 1% penicillin/streptomycin (Thermo Fisher Scientific). Mouse embryonic fibroblasts cells (Mfn wild-type, Mfn1-null, Mfn2-null and Mfn1/2-null) and HeLa cells were purchased from ATCC.

### 4.5.2 Transient transfection

Cells were plated in No. 1.5 glass-bottomed dishes (MatTek) the day before transfection. Transfection was performed using JetPrime transfection reagent following manufacture instructions. Briefly, 200 μL JetPrime buffer and 2 μg DNA were vortexed for 10 seconds then 4 μL JetPrime reagent was added and vortexed for 10 seconds. This mixture was incubated at room temperature for 10 minutes and then dropped onto cells and incubated for 4 hours before media change. Cells were imaged 24-48 hours later.

### 4.5.3 Fluorescence microscopy

All cells were plated in No. 1.5 glass-bottomed dishes (MatTek). Cells were incubated with 0.1 μg/mL Mitotracker Red CMX Ros (Invitrogen) for 15 minutes at 37°C with 5% $CO_2$, washed and incubated with complete media for at least 45 minutes prior to imaging. All cells were imaged at 37°C with 5% $CO_2$. A Z-series with a step size of 0.3 μm was collected with a Nikon Ti-E widefield microscope with a 63X NA 1.4 oil objective (Nikon), a solid-state light source

(Spectra X, Lumencor), and an sCMOS camera (Zyla 5.5 Megapixel).

### 4.5.4 Image analysis

Images were deconvolved using 15 iterations of 3D Landweber deconvolution. Deconvolved images were then analyzed using Nikon Elements software. Maximum intensity projections were created using ImageJ Software (NIH).

### 4.5.5 Preparation of mitochondria or cytosol-enriched fraction

For in vitro mitochondrial fusion, three to five 15 cm plates each of MEFs stably expressing either mitochondria-targeted TagRFP or CFP were grown to ~90% confluency. For cytosol preparation, ten 15 cm plates each of MEFs (twenty plates total) stably expressing either mitochondria-targeted TagRFP or CFP were grown to ~90% confluency. Cells were harvested by cell scrapping, pelleted, and washed in mitochondrial isolation buffer (MIB) (0.2 M sucrose, 10 mM Tris-MOPS [pH 7.4], 1 mM EGTA). The cell pellet was resuspended in one cell pellet volume of cold MIB, and cells were homogenized by 10 to 14 strokes on ice with a Kontes Potter-Elvehjem tissue grinder set at 400 RPM. The homogenate was centrifuged (500 × *g*, 5 min, 4°C) to remove nuclei and unbroken cells, and homogenization of the pellet fraction was repeated followed by centrifugation at 500 × *g*, 5 min, 4°C. The supernatant fractions were combined and centrifuged again at 500 × *g*, 5 min, 4°C to remove remaining debris. The supernatant was transferred to a clean microfuge tube and centrifuged (7400 × *g*, 10 min, 4°C) to pellet a crude mitochondrial fraction. The post-mitochondrial supernatant fraction was centrifuged at 21,000 x g, 1 min, 4°C and saved as the cytosol-enriched fraction. The crude

mitochondrial pellet was resuspended in a small volume of MIB. Protein concentration of fractions was determined by Bradford assay (Bio-Rad Laboratories).

### 4.5.6 In vitro mitochondrial fusion

An equivalent mass (10 - 12.5 μg) of TagRFP and CFP mitochondria were mixed, washed in 500 μL MIB and concentrated by centrifugation (7400 × *g*, 10 min, 4°C). Following a 10 minute incubation on ice, the supernatant was removed and the mitochondrial pellet was resuspended in 10 μl fusion buffer (20 mM PIPES-KOH [pH 6.8], 150 mM KOAc, 5 mM $Mg(OAc)_2$, 0.4 M sorbitol, 0.12 mg/ml creatine phosphokinase, 40 mM creatine phosphate, 1.5 mM ATP, 1.5 mM GTP) or 10 μl cytosol-enriched buffer (2.5 μL of the cytosol-enriched fraction obtained from WT MEFs or 2.5 μL of fractionated fraction and 7.5 μL fusion buffer). Fusion reactions were incubated at 37°C for 30 minutes.

### 4.5.7 Analysis of mitochondrial fusion

Mitochondria were imaged on depression microscope slides by pipetting 4μL fusion reaction onto a 3% low-melt agarose bed, made in modified fusion buffer (20 mM PIPES-KOH [pH 6.8], 150 mM KOAc, 5 mM $Mg(OAc)_2$, 0.4 M sorbitol). A Z-series of 6 0.2 μm steps was collected with a Nikon Ti-E widefield microscope with a 100X NA 1.4 oil objective (Nikon), a solid-state light source (Spectra X, Lumencor), and a sCMOS camera (Zyla 5.5 Megapixel). For each condition tested, mitochondrial fusion was assessed by counting ≥ 300 total mitochondria per condition from ≥ 4 images per condition (50 – 200 mitochondria per image collected), and fusion was scored by colocalization of the red and cyan fluorophores in three dimensions.

### 4.5.8 Fractionation of cytosol-enriched fraction

Approximately 1 mL of cytosolic-enriched fraction was nutated with 250 µL of Q sepharose fast flow beads (GE Healthcare) for 1 hour at 4°C. Beads were pelleted by centrifugation at 500 x g for 2 minutes at 4°C. Supernatant (anion fraction) was transferred to 250 µL SP sepharose fast flow beads (GE Healthcare) and nutated at 4°C for 1 hour. Beads were pelleted by centrifugation at 500 x g for 2 minutes at 4°C and supernatant was removed (cation fraction). Beads were washed in 500 µL of sequentially increasing concentrations of KCl in MIB buffer (50 mM, 100 mM, 150 mM, 200 mM, 250 mM KCl) for 10 minutes at 4°C. Beads were pelleted by centrifugation at 500 x g for 2 minutes at 4°C and supernatant was removed for each wash (cation 50, cation 100, cation 150, cation 200, cation 250 fractions). Cation fractions were dialyzed overnight against MIB buffer using Slide-A-Lyzer MINI Dialysis Device, 7K MWCO, 0.1 mL (Thermo Scientific), aliquoted, frozen and stored at -80°C.

### 4.5.9 Size exclusion chromatography of cation 250 fraction

Cation 250 fraction was centrifuged at 100,000 x g for 1 hour at 4°C. 450 µL of supernatant was loaded onto a Superose 6 Increase 10/300 GL column equilibrated with MIB buffer. 500 µL fractions were collected between 8 and 24 mL, aliquoted, frozen and stored at -80°C.

### 4.5.10 Mass spectroscopy

Cytosolic fractions were analyzed at the Fred Hutchinson Research Center at the Proteomics Core using OptiTrap Fusion Mass Spectrometer.

### 4.5.11 Generating and cloning cDNA from crude RNA

Crude RNA was isolated from HeLa cells. cDNA was generated using QuantiTect Reverse Transcription Kit (Qiagen) following manufacturer's instructions.

## 4.6 Acknowledgments

I would like to thank Carly Horn for performing the cDNA cloning and Anneke Kakebeen for helping with the Qubit RNA analysis. The mass spectrometry was performed at the Fred Hutchinson Research Center Proteomics Core.

## 4.7 Figures

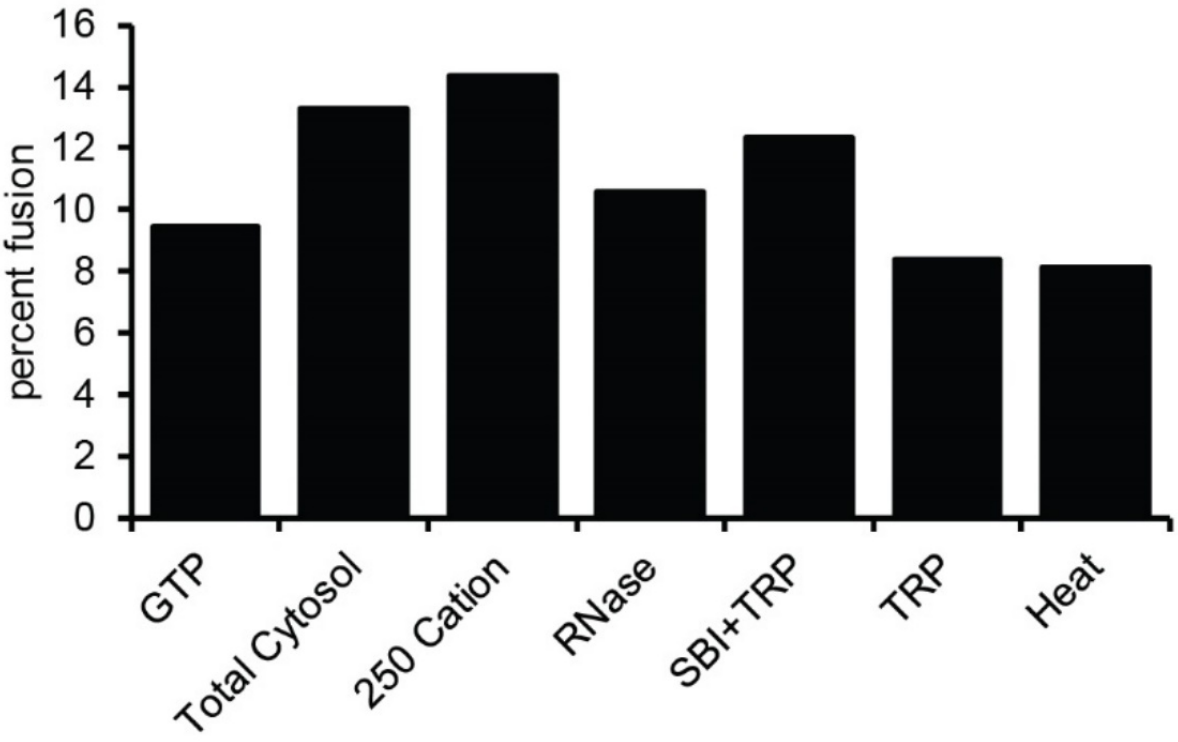


**Figure 4.1 In vitro fusion assay of fractionated cytosol**

In vitro mitochondrial fusion activity suggests that the cation 250 mM KCl fraction is sensitive to RNase, trypsin protease and heat treatment. Percent in vitro mitochondrial fusion of a clonal population of $Mfn1^{F202L}$-expressing Mfn1-null cells ($Mfn1^{F202L}Mfn2^{+/+}$) of mitochondria incubated at 37°C for 30 minutes. SBI stands for soybean inhibitor and TRP stands for trypsin protease.

A

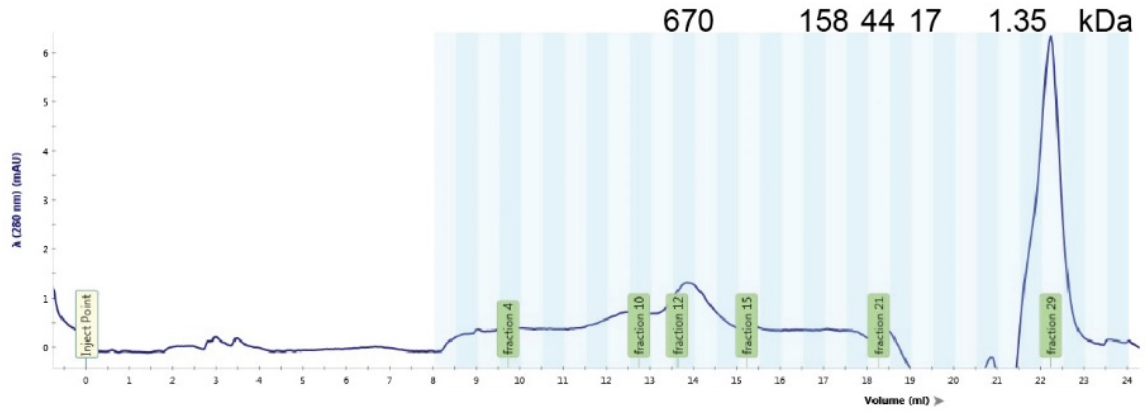


B

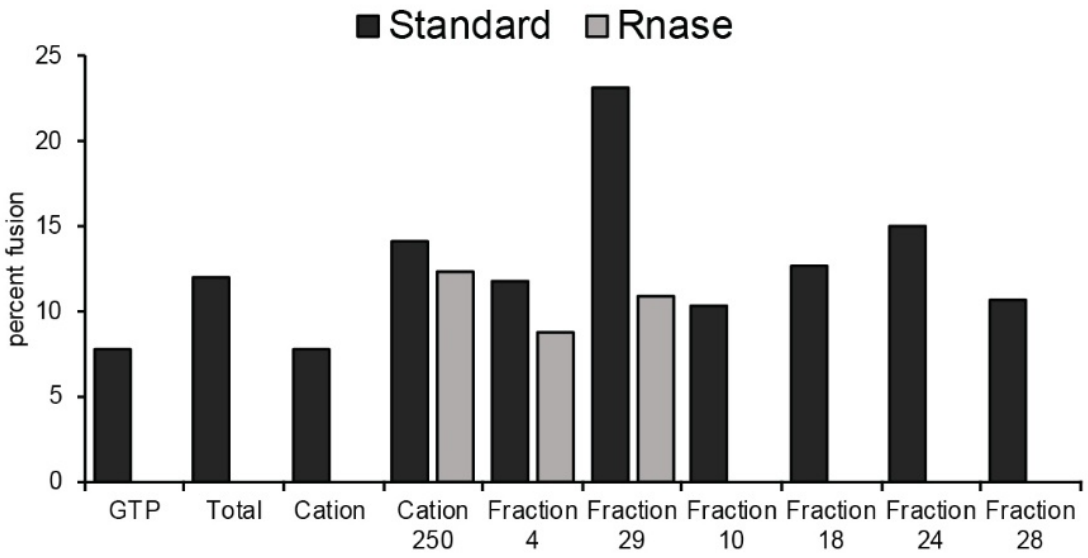


**Figure 4.2 Size exclusion chromatography of cation 250 mM KCl fraction**

**(A)** Size exclusion chromatography trace of cation 250 mM KCl fraction **(B)** Percent in vitro mitochondrial fusion of wild-type mitochondria incubated at 37°C for 30 minutes.

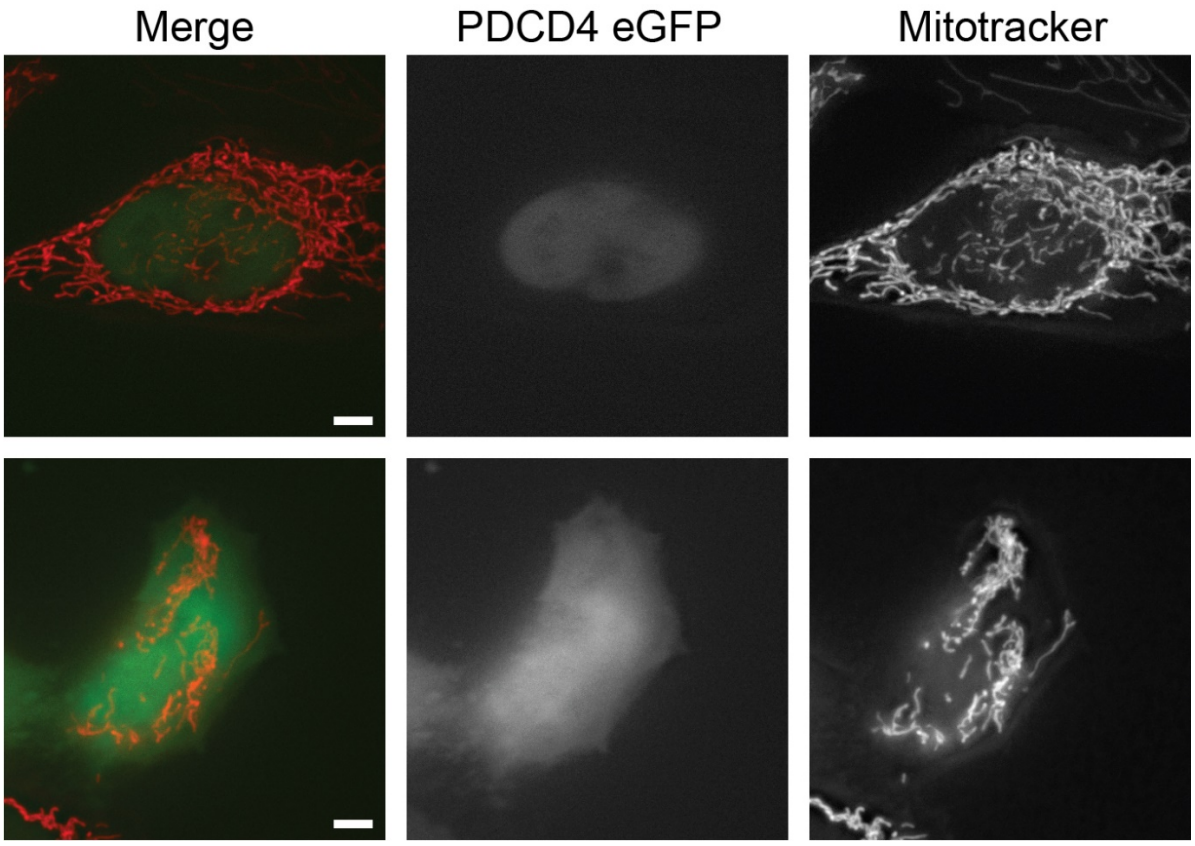


**Figure 4.3 Cytoplasmic localization of PDCD4 in HeLa results in mitochondrial perinuclear aggregation**

HeLa cells were transiently transfected with PDCD4 eGFP. Mitochondria were labeled with MitoTracker Red CMXRos and visualized by fluorescence microscopy. Images represent maximum intensity projections. Scale bars are 5 μM.

| Gene Name | Protein Name | Functions | Reference |
|---|---|---|---|
| FLNC | Filamin C | Identified in a high throughput mass spectrometry screen for protein interactors which was found to interact with Mfn1. Actin crosslinking protein that has ~70% sequence identity to Filamin A which was described in Chapter 4.3.4 | (Huttlin et al., 2017) |
| EHBP1L1 | EH Domain Binding 1-Like Protein | Rab effector protein and play a role in vesicle trafficking | (Nakajo et al., 2016) |
| Gapvd1 | GTPase Activating Protein and VPS9 Domains 1 | GAP and GEF in endocytosis | (Hunker et al., 2006) |
| GHITM | Growth Hormone Inducible Transmembrane Protein | Required for a tubular mitochondrial network, plays a role in cristae organization and is involved in apoptotic release of cytochrome C | (Oka et al., 2008) |
| ROCK1 | Rho Associated Coiled-coil Containing Protein Kinase 1 | Serine/threonine kinase involved in phosphorylation of actin to regulate skeleton organization, cell adhesion and motility, proliferation and apoptosis. ROCK1 also phosphorylates Drp1 inducing mitochondrial fission | (S. Hartmann, Ridley, & Lutz, 2015; W. Wang et al., 2012) |
| SRGAP2 | SLIT-ROBO GTPase Activating Protein 2 | GAP for Rac1 and regulates actin dynamics for cell migration and differentiation | (Coutinho-Budd, Ghukasyan, Zylka, & Polleux, 2012; Wong et al., 2001). |
| Afadin | Adherens Junction Formation Factor | F-actin binding protein. Afadin has been shown to protect against mitochondrial dysfunction in flies by interacting with Parkin and modulating its ubiquitination activity. | (Basil et al., 2017; Haskin et al., 2013; Takai & Nakanishi, 2003) |

**Table 4.1 Table of potential candidate proteins identified in mass spectrometry analysis**

# Chapter 5: General Conclusions

## 5.1 Conclusions and significance

The molecular mechanisms of mitochondrial outer membrane tethering and fusion are largely unknown. To gain insight into these processes, I developed three related but separate projects for my thesis work: (1) purification and characterization of recombinant Mitofusin protein from *Escherichia coli*, (2) identification and characterization of a mutant variant of the Mitofusins that uncouples mitochondrial tethering and fusion, and (3) fractionation of mammalian cytosol to identify new factors that stimulate mitochondrial fusion.

### 5.1.1 Recombinant Mitofusin protein purification

I developed a recombinant protein purification protocol for mouse Mitofusin from *E. coli*. I determined that this recombinantly purified Mitofusin protein possessed some nucleotide binding activity but had limited enzymatic activity. Furthermore, it had a high propensity to form soluble aggregates, which may be due to the propensity of these proteins to self-assemble into large structures. Recombinant Mitofusin inserted into liposomes mimicking the lipid composition of the mitochondrial outer membrane with the correct orientation, but these proteoliposomes lacked tethering and fusion activity. The purification of full length recombinant Mfn1 and Mfn2 would be a significant advance for the field and my work has built a critical foundation of knowledge to continue to this work. Recombinant Mitofusin protein would allow for the direct comparison of enzymatic activities between Mfn1 and Mfn2 including nucleotide binding, GTPase activity, conformational changes and would also be utilized in proteoliposomes

for tethering and fusion assays. By using a reconstituted system, we can manipulate the system in ways that are unfeasible in cells, for example by changing the lipid composition or the ratio of Mfn1 to Mfn2 to determine how these changes directly affect the enzymatic activities like GTP hydrolysis, oligomerization, and membrane tethering and fusion.

### 5.1.2 Mutant variant of Mitofusin uncouples mitochondrial tethering and fusion

By performing a screen of the GTPase domain of Mfn1 using disease-associated mutant variants, I identified a mutant variant Mfn1$^{F202L}$ that possessed unique characteristics including having a highly connected mitochondrial network that was collapsed around the nucleus. I determined that Mfn1$^{F202L}$ required enzymatically active Mfn2 to maintain a reticular network. It has been observed that mutant variants of Mfn2 can be complemented by wildtype Mfn1 (Detmer & Chan, 2007), but this is the first example of a mutant variant of Mfn1 that can be complement by wildtype Mfn2. This suggests that the enzymatic activity of Mfn2 is also important for mitochondrial fusion. Using a cell-free mitochondrial fusion assay, I determined that Mfn1$^{F202L}$ lacked fusion activity despite the overall connectivity observed in cells. The differences we observed between cells and our cell-free system underscore the importance of testing mitochondrial fusion activity independent from other activities including mitochondrial division and transport. These differences also led us to develop the cytosol fractionation project described in Chapter 4. To determine if Mfn1$^{F202L}$ was deficient in membrane tethering, I developed a co-immunoprecipitation assay which exclusively measures Mitofusin interactions on opposing membranes. In addition, this assay specifically measures nucleotide dependent assembly and is the first report of such an assay. Using this assay, I found the Mfn1$^{F202L}$

surprisingly had wildtype tethering activity. We therefore hypothesized that Mfn1$^{F202L}$ was impairing nucleotide dependent self-assembly. To measure nucleotide dependent self-assembly, I was involved in developing conditions required to measure this assembly by BN-PAGE. I found that Mfn1$^{F202L}$ had impaired higher order assembly in the presence of either GTP or GMPPNP. This was the first report of a Mitofusin mutant variant that alters self-assembly. This work suggests that after the initial membrane tethering event, higher order assembly is stimulated and required for membrane fusion. This is a significant advance for the field as it places higher order assembly after mitochondrial tethering. Furthermore, both the tethering co-immunoprecipitation assay and BN-PAGE assay are novel techniques that will become a workhorse in our lab for driving the field forward.

### 5.1.3 Cytosol fractionation

To identify novel pro-fusion factors from cells, I took a classic biochemical fractionation approach to follow the fusion-stimulating activity in our reconstituted system. I have developed a robust protocol that generates a fraction of cytosol from mouse embryonic fibroblasts of molecules that bound tightly to cation exchange resin and stimulated mitochondrial fusion activity in vitro. Further analysis of this fraction was consistent with the exciting hypothesis that an RNA binding protein may be the stimulatory factor. This approach allows us to find pro-fusion factors that directly modulate Mitofusin activity levels without the complicating factors of changes in mitochondrial division or mitochondrial transport.

## 5.2 Future Directions

### 5.2.1 Recombinant Mitofusin protein purification

Mitofusin protein purification from *E. coli* was largely unsuccessful as purifications generally resulted in the formation of large soluble aggregates as assessed by sucrose gradient centrifugation (Figure 2.5) and visualized by negative stain electron microscopy (Figure 2.7). Although expression of the protein was rarely limiting, the fraction of insoluble protein suggests that a discrete domain of Mitofusin may be misfolded. Therefore, future work should involve finding a different host expression system, such as HEK-293 cells. Purification from HEK-293 cells would allow for proper targeting of the Mitofusin to the mitochondrial outer membrane, which may be required to ensure proper folding. In this approach, mitochondria could be isolated and detergent solubilized acting as a concentration and purification step. In addition, purification from mammalian cells would allow for any post-translational modifications that might be required for proper enzymatic activity.

**How to determine if recombinant Mitofusin protein is functional?**

The biggest problem in the purification of recombinant Mitofusin from *E. coli* was obtaining soluble protein. Therefore, for initial functional tests from a new system, I would test all protein preparations by sucrose gradient centrifugation and/or by negative stain electron microscopy. Ideally, the protein would be monodispersed. Once soluble protein was obtained, I would determine if the protein self-assembles in the presence of nucleotide by either sucrose gradient ultracentrifugation, size exclusion chromatography or BN-PAGE. My data has shown that Mitofusin assembly state is dictated by nucleotide and that this activity is almost certainly

required for membrane fusion. The quantification of GTP hydrolysis activity is also critical but may be difficult if recombinant protein yields are low. Furthermore, DRP family members generally have low basal GTP hydrolysis activity, which is stimulated upon self-assembly or in the presence of lipids (Jimah & Hinshaw, 2019). Therefore, it might be necessary to insert recombinant Mitofusin protein into liposomes in order to measure GTP hydrolysis. Another consideration is that Mfn1 and Mfn2 promote fusion most efficiently together (Chen et al., 2003; Detmer & Chan, 2007; Hoppins et al., 2011). Interestingly, recent biochemical analysis of a bacterial dynamin like protein pair from *Campylobacter jejuni* (DLP1 and DLP2) revealed the DLP1 and DLP2 lack GTP hydrolysis activity alone but have activity when mixed together (Liu et al., 2018). Given this information, Mfn1 and Mfn2 may only have robust GTP hydrolysis activity when together.

### 5.2.2 Mutant variant of Mitofusin uncouples mitochondrial tethering and fusion

The mutant variant, $Mfn1^{F202L}$, is unique as it causes mitochondrial hyperfusion and perinuclear collapse when expressed in Mfn1-null cells. It also requires wildtype Mfn2 for function, which is not the case for wildtype Mfn1, indicating that this variant has impaired activity. Indeed, my analysis revealed that the variant uncoupled mitochondrial tethering from fusion through impaired higher order assembly.

**What causes mitochondrial perinuclear collapse?**

Mitochondria in cells are transported in both the anterograde and retrograde direction on microtubules. It is striking that several mutant variants of the Mitofusins that have been characterized in the Hoppins lab cause perinuclear collapse of the mitochondrial network, similar

to Mfn1$^{F202L}$. There is evidence that mitochondrial fusion and transport are connected as cells lacking Mfn1 or Mfn2 display reduced microtubule-based directional movement (H. Chen et al., 2003), but the relationship between mitochondrial transport and fusion is not well characterized. Therefore, an outstanding question in the lab is, what causes the altered distribution of the mitochondrial network? Do Mitofusin proteins with altered enzymatic activities elicit cellular signals to favor retrograde trafficking? For example, does prolonged mitochondrial tethering without mitochondrial fusion promote retrograde transport? To determine if the hyperconnected network could be converted to a completely fragmented network, CCCP was added to dissipate membrane potential and stimulate mitochondrial division. Indeed, Mfn1$^{F202L}$ cells treated with CCCP were completely fragmented after 3 hours. If the cells were allowed to recover in media without CCCP for 24 hours, the network becomes highly connected again and is collapsed around the perinuclear space. To determine if known components of the mitochondrial transport machinery are required for the change in mitochondrial distribution, the same experiment could be performed with molecules to inhibit either kinesin or dynein mediated transport or by blocking the formation of either microtubules or actin filaments. This type of experiment would give us insights into the proteins required for perinuclear mitochondria aggregation.

**Do the Mitofusins undergo large conformational changes?**

BDLP makes a large conformational change from an open extended conformation to a closed clamped conformation (Figure 1.3). The Mfn1$_{IM}$ and BDLP crystal structures overlay exceptionally well (~4Å) (Liming Yan et al., 2018). Therefore, it has been proposed that the Mitofusins might also undergo a large conformational change from a pre-fusion extended conformation to a closed post-fusion conformation. Mfn1$^{F202L}$ can bind and hydrolysis nucleotide and I hypothesize that this mutant variant fails to effectively couple GTP hydrolysis to this large

conformational change. Therefore, to test this hypothesis, I propose to develop a FRET based assay to measure these conformational changes by dual labeling either the N-terminus or C-terminus and a region predicted near the transmembrane domain. If the Mitofusin protein does indeed make these large conformational changes, we would expect to observe low FRET in the open extended conformation and observe high FRET in the closed clamp conformational when the GTPase domain is predicted to be near the membrane.

**Does Mfn2 require GTP binding and GTP hydrolysis activity?**

Several lines of evidence indicate that Mfn2 does not require GTP binding or hydrolysis activity when Mfn1 is present (Detmer & Chan, 2007; Engelhart & Hoppins, 2019; Sloat et al., 2019). Specifically, cells only expressing Mfn1 have a fragmented mitochondrial morphology but when enzymatically dead mutant variants of Mfn2 are expressed a significant number of cells have a reticular mitochondrial morphology. The reverse is not true, where wildtype Mfn2 cannot complement the same enzymatically dead mutant variants of Mfn1. My work with the $Mfn1^{F202L}$ variant shows that even though a mitochondrial network in cells can look reticular this does not mean that the mitochondrial have wildtype fusion activity in vitro. Therefore, I propose to determine if Mfn2 mutant variants that lack enzymatic activities ($Mfn2^{K109A}$, $Mfn2^{T130A}$, $Mfn2^{E230A}$, $Mfn2^{W260A}$) have wildtype activities including in vitro mitochondrial activity, tethering activity and high order assembly. Using these mutant variants of Mfn2 we may be able to determine at which steps in the fusion process nucleotide binding and GTP hydrolysis are required.

### 5.2.3 Cytosol fractionation

**Possible RNA binding proteins identified in mass spectrometry screen**

As described above, my data indicate that the pro-fusion factor in the cytosol could be an RNA binding protein. The mass spectrometry analysis identified several RNA binding proteins. One protein of interest was Programmed Cell Death Protein 4 (PDCD4). PDCD4 is an RNA binding protein which plays roles in translation and apoptotic cell death. Its role in apoptosis is not well understood, but PDCD4 could play a similar pro-fusion role to the pro-apoptotic protein, Bax (Hoppins et al., 2011; Karbowski et al, 2006). Preliminary data indicate that PDCD4 impacts mitochondrial structure, making this an interesting candidate to investigate further. To further probe the role of PDCD4 in mitochondrial fusion, the protein could be recombinantly purified and added to the in vitro mitochondrial fusion assay to determine if it has stimulatory activity. Protein purification would be initially performed in *E. coli*, but because a specific RNA may be required for its function, purification using a mammalian expression system could be required. Using recombinant PDCD4, we could determine if the Mitofusins directly interact with PDCD4 by co-immunoprecipitation or if PDCD4 alters Mitofusin assembly state by BN-PAGE. If these experiments give promising results, PDCD4 knockout cells could be generated by CRISPR to determine if PDCD4 has effects on mitochondrial morphology in cells. In addition, cytosol isolated from these knockout cells could be tested for a lack of stimulatory activity using the in vitro fusion assay.

A number of other proteins with an RNA binding molecular function GO terms were exclusively found in the stimulatory fraction (summarized in Table 5.1). These proteins could be tested by screening them by either overexpression or RNAi in MEF or HeLa cells looking for

changes in mitochondrial morphology. Additionally, proteins that have already been successfully purified from *E. coli,* could be recombinantly purified and tested using the in vitro mitochondrial fusion assay. Proteins of particular interest are Nosip a E3 ubiquitin ligase, Diaph1 an actin elongation factor, and Myo18a which may play a role in golgi trafficking.

## 5.3 Figures

| Protein Name | Gene |
|---|---|
| Programmed cell death protein 4 | Pdcd4 |
| PHD finger-like domain-containing protein 5A | Phf5a |
| Nitric oxide synthase-interacting protein | Nosip |
| Polyadenylate-binding protein 2 | Pabpn1 |
| Apoptotic chromatin condensation inducer in the nucleus | Acin1 |
| U1 small nuclear ribonucleoprotein A | Snrpa |
| HIV Tat-specific factor 1 homolog | Htatsf1 |
| Ubiquitin associated protein 2-like | Ubap2l |
| Eukaryotic translation initiation factor 5A-1 | Eif5a |
| RIKEN cDNA 5830416A07, isoform CRA_c | Zc3h18 |
| Zinc finger protein 622 | Znf622 |
| Basic leucine zipper and W2 domain-containing protein 1 | Bzw1 |
| Protein diaphanous homolog 1 | Diaph1 |
| Eukaryotic translation initiation factor 5 | Eif5 |
| Probable ATP-dependent RNA helicase DDX46 | Ddx46 |
| N-alpha-acetyltransferase 15, NatA auxiliary subunit | Naa15 |
| Nuclear speckle splicing regulatory protein 1 | Nsrp1 |
| Unconventional myosin-XVIIIa | Myo18a |
| Eukaryotic translation initiation factor 1 | Eif1 |
| Eukaryotic peptide chain release factor GTP-binding subunit ERF3A | Gspt1 |

**Table 5.1 RNA binding proteins**

Summary of proteins with an RNA binding molecular function GO term identified in mass spectrometry analysis.

# Bibliography


Alexander, C., Votruba, M., Pesch, U. E., Thiselton, D. L., Mayer, S., Moore, a, … Wissinger, B. (2000). OPA1, encoding a dynamin-related GTPase, is mutated in autosomal dominant optic atrophy linked to chromosome 3q28. *Nature Genetics*, *26*(2), 211–215. https://doi.org/10.1038/79944

Anand, R., Wai, T., Baker, M. J., Kladt, N., Schauss, A. C., Rugarli, E., & Langer, T. (2014). The i-AAA protease YME1L and OMA1 cleave OPA1 to balance mitochondrial fusion and fission. *The Journal of Cell Biology*, *204*(6), 919–929. https://doi.org/10.1083/jcb.201308006

Antonny, B., Burd, C., De Camilli, P., Chen, E., Daumke, O., Faelber, K., … Schmid, S. (2016). Membrane fission by dynamin: what we know and what we need to know. *The EMBO Journal*, *35*(21), 2270–2284. https://doi.org/10.15252/embj.201694613

Atsuko Kasahara, Sara Cipolat, Yun Chen, Gerald W. Dorn II, L. S. (2013). Mitochondrial fusion directs cardiomyocyte differentiation via calcineurin and notch signaling. *Science*, *342*(November), 734–738.

Babic, M., Russo, G. J., Wellington, A. J., Sangston, R. M., Gonzalez, M., & Zinsmaier, K. E. (2015). Miro's N-terminal GTPase domain is required for transport of mitochondria into axons and dendrites. *The Journal of Neuroscience : The Official Journal of the Society for Neuroscience*, *35*(14), 5754–5771. https://doi.org/10.1523/JNEUROSCI.1035-14.2015

Ban, T., Ishihara, T., Kohno, H., Saita, S., Ichimura, A., Maenaka, K., … Ishihara, N. (2017). Molecular basis of selective mitochondrial fusion by heterotypic action between OPA1 and cardiolipin. *Nature Cell Biology*, *19*(7), 856–863. https://doi.org/10.1038/ncb3560

Baricault, L., Ségui, B., Guégand, L., Olichon, A., Valette, A., Larminat, F., & Lenaers, G. (2007). OPA1 cleavage depends on decreased mitochondrial ATP level and bivalent metals. *Experimental Cell Research*, *313*, 3800–3808. https://doi.org/10.1016/j.yexcr.2007.08.008

Bartsakoulia, M., Pyle, A., Troncoso-Chandía, D., Vial-Brizzi, J., Paz-Fiblas, M. V, Duff, J., … Horvath, R. (2018). A novel mechanism causing imbalance of mitochondrial fusion and fission in human myopathies. *Human Molecular Genetics*, *27*(7), 1186–1195. https://doi.org/10.1093/hmg/ddy033

Basil, A. H., Sim, J. P. L., Lim, G. G. Y., Lin, S., Chan, H. Y., Engelender, S., & Lim, K.-L. (2017). AF-6 Protects Against Dopaminergic Dysfunction and Mitochondrial Abnormalities in Drosophila Models of Parkinson's Disease. *Frontiers in Cellular Neuroscience*, *11*, 241. https://doi.org/10.3389/fncel.2017.00241

Bian, X., Klemm, R. W., Liu, T. Y., Zhang, M., Sun, S., Sui, X., … Hu, J. (2011). Structures of the atlastin GTPase provide insight into homotypic fusion of endoplasmic reticulum membranes. *Proceedings of the National Academy of Sciences*, *108*(10), 3976–3981. https://doi.org/10.1073/pnas.1101643108

Böhm, M., Sawicka, K., Siebrasse, J. P., Brehmer-Fastnacht, A., Peters, R., & Klempnauer, K.-

H. (2003). The transformation suppressor protein Pdcd4 shuttles between nucleus and cytoplasm and binds RNA. *Oncogene*, *22*(31), 4905–4910. https://doi.org/10.1038/sj.onc.1206710

Bohuszewicz, O., & Low, H. H. (2018). Structure of a mitochondrial fission dynamin in the closed conformation. *Nature Structural & Molecular Biology*, *25*(8), 722–731. https://doi.org/10.1038/s41594-018-0097-6

Bramkamp, M. (2012). Structure and function of bacterial dynamin-like proteins. *Biological Chemistry*, *393*(11), 1203–1214. https://doi.org/10.1515/hsz-2012-0185

Brandt, T., Cavellini, L., Kühlbrandt, W., & Cohen, M. M. (2016). A mitofusin-dependent docking ring complex triggers mitochondrial fusion in vitro. *ELife*, *5*. https://doi.org/10.7554/eLife.14618

Byrnes, L. J., Singh, A., Szeto, K., Benvin, N. M., O'Donnell, J. P., Zipfel, W. R., & Sondermann, H. (2013). Structural basis for conformational switching and GTP loading of the large G protein atlastin. *The EMBO Journal*, *32*(3), 369–384. https://doi.org/10.1038/emboj.2012.353

Byrnes, L. J., & Sondermann, H. (2011). Structural basis for the nucleotide-dependent dimerization of the large G protein atlastin-1/SPG3A. *Proceedings of the National Academy of Sciences of the United States of America*, *108*(6), 2216–2221. https://doi.org/10.1073/pnas.1012792108

Cao, Y.-L., Meng, S., Chen, Y., Feng, J.-X., Gu, D.-D., Yu, B., … Gao, S. (2017). MFN1 structures reveal nucleotide-triggered dimerization critical for mitochondrial fusion. *Nature*, *542*(7641), 372–376. https://doi.org/10.1038/nature21077

Cereghetti, G. M., Stangherlin, A., Martins de Brito, O., Chang, C. R., Blackstone, C., Bernardi, P., & Scorrano, L. (2008). Dephosphorylation by calcineurin regulates translocation of Drp1 to mitochondria. *Proceedings of the National Academy of Sciences of the United States of America*, *105*(41), 15803–15808. https://doi.org/10.1073/pnas.0808249105

Chan, D. C. (2012). Fusion and fission: interlinked processes critical for mitochondrial health. *Annual Review of Genetics*, *46*, 265–287. https://doi.org/10.1146/annurev-genet-110410-132529

Chang, C.-R., & Blackstone, C. (2007). Cyclic AMP-dependent protein kinase phosphorylation of Drp1 regulates its GTPase activity and mitochondrial morphology. *The Journal of Biological Chemistry*, *282*(30), 21583–21587. https://doi.org/10.1074/jbc.C700083200

Chang, C.-R., Manlandro, C. M., Arnoult, D., Stadler, J., Posey, A. E., Hill, R. B., & Blackstone, C. (2010). A lethal de novo mutation in the middle domain of the dynamin-related GTPase Drp1 impairs higher order assembly and mitochondrial division. *The Journal of Biological Chemistry*, *285*(42), 32494–32503. https://doi.org/10.1074/jbc.M110.142430

Chao, Y.-H., Robak, L. A., Xia, F., Koenig, M. K., Adesina, A., Bacino, C. A., … Wangler, M. F. (2016). Missense variants in the middle domain of DNM1L in cases of infantile encephalopathy alter peroxisomes and mitochondria when assayed in Drosophila. *Human*

*Molecular Genetics*, *25*(9), 1846–1856. https://doi.org/10.1093/hmg/ddw059

Chen, H., Chomyn, A., & Chan, D. C. (2005). Disruption of fusion results in mitochondrial heterogeneity and dysfunction. *The Journal of Biological Chemistry*, *280*(28), 26185–26192. https://doi.org/10.1074/jbc.M503062200

Chen, H., Detmer, S. A., Ewald, A. J., Griffin, E. E., Fraser, S. E., & Chan, D. C. (2003). Mitofusins Mfn1 and Mfn2 coordinately regulate mitochondrial fusion and are essential for embryonic development. *The Journal of Cell Biology*, *160*(2), 189–200. https://doi.org/10.1083/jcb.200211046

Chen, H., McCaffery, J. M., & Chan, D. C. (2007). Mitochondrial fusion protects against neurodegeneration in the cerebellum. *Cell*, *130*(3), 548–562. https://doi.org/10.1016/j.cell.2007.06.026

Chen, Y., & Dorn, G. W. (2013). PINK1-phosphorylated mitofusin 2 is a Parkin receptor for culling damaged mitochondria. *Science (New York, N.Y.)*, *340*(6131), 471–475. https://doi.org/10.1126/science.1231031

Choi, S.-Y., Huang, P., Jenkins, G. M., Chan, D. C., Schiller, J., & Frohman, M. a. (2006). A common lipid links Mfn-mediated mitochondrial fusion and SNARE-regulated exocytosis. *Nature Cell Biology*, *8*(11), 1255–1262. https://doi.org/10.1038/ncb1487

Cipolat, S., Martins de Brito, O., Dal Zilio, B., & Scorrano, L. (2004). OPA1 requires mitofusin 1 to promote mitochondrial fusion. *Proceedings of the National Academy of Sciences of the United States of America*, *101*(45), 15927–15932. https://doi.org/10.1073/pnas.0407043101

Coutinho-Budd, J., Ghukasyan, V., Zylka, M. J., & Polleux, F. (2012). The F-BAR domains from srGAP1, srGAP2 and srGAP3 regulate membrane deformation differently. *Journal of Cell Science*, *125*(Pt 14), 3390–3401. https://doi.org/10.1242/jcs.098962

Cribbs, J. T., & Strack, S. (2007). Reversible phosphorylation of Drp1 by cyclic AMP-dependent protein kinase and calcineurin regulates mitochondrial fission and cell death. *EMBO Reports*, *8*(10), 939–944. https://doi.org/10.1038/sj.embor.7401062

Daste, F., Sauvanet, C., Bavdek, A., Baye, J., Pierre, F., Le Borgne, R., … Tareste, D. (2018). The heptad repeat domain 1 of Mitofusin has membrane destabilization function in mitochondrial fusion. *EMBO Reports*, *19*(6). https://doi.org/10.15252/embr.201643637

Daumke, O., & Roux, A. (2017). Mitochondrial Homeostasis: How Do Dimers of Mitofusins Mediate Mitochondrial Fusion? *Current Biology : CB*, *27*(9), R353–R356. https://doi.org/10.1016/j.cub.2017.03.024

Davies, V. J., Hollins, A. J., Piechota, M. J., Yip, W., Davies, J. R., White, K. E., … Votruba, M. (2007). Opa1 deficiency in a mouse model of autosomal dominant optic atrophy impairs mitochondrial morphology, optic nerve structure and visual function. *Human Molecular Genetics*, *16*(11), 1307–1318. https://doi.org/10.1093/hmg/ddm079

de Brito, O. M., & Scorrano, L. (2009). Mitofusin-2 regulates mitochondrial and endoplasmic reticulum morphology and tethering: The role of Ras. *Mitochondrion*, *9*(3), 222–226. https://doi.org/10.1016/j.mito.2009.02.005

Detmer, S. a., & Chan, D. C. (2007). Complementation between mouse Mfn1 and Mfn2 protects mitochondrial fusion defects caused by CMT2A disease mutations. *Journal of Cell Biology*, *176*(4), 405–414. https://doi.org/10.1083/jcb.200611080

DeVay, R. M., Dominguez-Ramirez, L., Lackner, L. L., Hoppins, S., Stahlberg, H., & Nunnari, J. (2009). Coassembly of Mgm1 isoforms requires cardiolipin and mediates mitochondrial inner membrane fusion. *Journal of Cell Biology*, *186*(6), 793–803. https://doi.org/10.1083/jcb.200906098

Dorn, G. W. (2019). Evolving Concepts of Mitochondrial Dynamics. *Annual Review of Physiology*, *81*, 1–17. https://doi.org/10.1146/annurev-physiol-020518-114358

Ehses, S., Raschke, I., Mancuso, G., Bernacchia, A., Geimer, S., Tondera, D., … Langer, T. (2009). Regulation of OPA1 processing and mitochondrial fusion by m-AAA protease isoenzymes and OMA1. *The Journal of Cell Biology*, *187*(7), 1023–1036. https://doi.org/10.1083/jcb.200906084

Engelhart, E. A., & Hoppins, S. (2019). A catalytic domain variant of Mitofusin requiring a wildtype paralog for function uncouples mitochondrial outer-membrane tethering and fusion. *The Journal of Biological Chemistry*. https://doi.org/10.1074/jbc.RA118.006347

Eura, Y., Ishihara, N., Yokota, S., & Mihara, K. (2003). Two Mitofusin Proteins, Mammalian Homologues of FZO, with Distinct Functions Are Both Required for Mitochondrial Fusion. *Journal of Biochemistry*, *134*(3), 333–344. https://doi.org/10.1093/jb/mvg150

Fahrner, J. A., Liu, R., Perry, M. S., Klein, J., & Chan, D. C. (2016). A novel de novo dominant negative mutation in DNM1L impairs mitochondrial fission and presents as childhood epileptic encephalopathy. *American Journal of Medical Genetics. Part A*, *170*(8), 2002–2011. https://doi.org/10.1002/ajmg.a.37721

Fang, D., Yan, S., Yu, Q., Chen, D., & Yan, S. S. (2016). Mfn2 is Required for Mitochondrial Development and Synapse Formation in Human Induced Pluripotent Stem Cells/hiPSC Derived Cortical Neurons. *Scientific Reports*, *6*, 31462. https://doi.org/10.1038/srep31462

Ferreira, J. C. B., Campos, J. C., Qvit, N., Qi, X., Bozi, L. H. M., Bechara, L. R. G., … Mochly-Rosen, D. (2019). A selective inhibitor of mitofusin 1-βIIPKC association improves heart failure outcome in rats. *Nature Communications*, *10*(1), 329. https://doi.org/10.1038/s41467-018-08276-6

Ford, M. G. J., Jenni, S., & Nunnari, J. (2011). The crystal structure of dynamin. *Nature*, *477*(7366), 561–566. https://doi.org/10.1038/nature10441

Franco, A., Kitsis, R. N., Fleischer, J. A., Gavathiotis, E., Kornfeld, O. S., Gong, G., … Dorn, G. W. (2016). Correcting mitochondrial fusion by manipulating mitofusin conformations. *Nature*, *540*(7631), 74–79. https://doi.org/10.1038/nature20156

Francy, C. A., Alvarez, F. J. D., Zhou, L., Ramachandran, R., & Mears, J. A. (2015). The mechanoenzymatic core of dynamin-related protein 1 comprises the minimal machinery required for membrane constriction. *The Journal of Biological Chemistry*, *290*(18), 11692–11703. https://doi.org/10.1074/jbc.M114.610881

Francy, C. A., Clinton, R. W., Fröhlich, C., Murphy, C., & Mears, J. A. (2017). Cryo-EM Studies of Drp1 Reveal Cardiolipin Interactions that Activate the Helical Oligomer. *Scientific Reports*, *7*(1), 10744. https://doi.org/10.1038/s41598-017-11008-3

Fransson, Å., Ruusala, A., & Aspenström, P. (2006). The atypical Rho GTPases Miro-1 and Miro-2 have essential roles in mitochondrial trafficking. *Biochemical and Biophysical Research Communications*, *344*(2), 500–510. https://doi.org/10.1016/j.bbrc.2006.03.163

Frezza, C., Cipolat, S., Martins de Brito, O., Micaroni, M., Beznoussenko, G. V, Rudka, T., … Scorrano, L. (2006). OPA1 controls apoptotic cristae remodeling independently from mitochondrial fusion. *Cell*, *126*(1), 177–189. https://doi.org/10.1016/j.cell.2006.06.025

Friedman, J. R., & Nunnari, J. (2014). Mitochondrial form and function. *Nature*, *505*(7483), 335–343. https://doi.org/10.1038/nature12985

Fröhlich, C., Grabiger, S., Schwefel, D., Faelber, K., Rosenbaum, E., Mears, J., … Daumke, O. (2013). Structural insights into oligomerization and mitochondrial remodelling of dynamin 1-like protein. *The EMBO Journal*, *32*(9), 1280–1292. https://doi.org/10.1038/emboj.2013.74

Glauser, L., Sonnay, S., Stafa, K., & Moore, D. J. (2011). Parkin promotes the ubiquitination and degradation of the mitochondrial fusion factor mitofusin 1. *Journal of Neurochemistry*, *118*(4), 636–645. https://doi.org/10.1111/j.1471-4159.2011.07318.x

Göke, A., Göke, R., Knolle, A., Trusheim, H., Schmidt, H., Wilmen, A., … Chen, Y. H. (2002). DUG is a novel homologue of translation initiation factor 4G that binds eIF4A. *Biochemical and Biophysical Research Communications*, *297*(1), 78–82. Retrieved from http://www.ncbi.nlm.nih.gov/pubmed/12220511

Hartmann, B., Wai, T., Hu, H., MacVicar, T., Musante, L., Fischer-Zirnsak, B., … Kaindl, A. M. (2016). Homozygous YME1L1 mutation causes mitochondriopathy with optic atrophy and mitochondrial network fragmentation. *ELife*, *5*. https://doi.org/10.7554/eLife.16078

Hartmann, S., Ridley, A. J., & Lutz, S. (2015). The Function of Rho-Associated Kinases ROCK1 and ROCK2 in the Pathogenesis of Cardiovascular Disease. *Frontiers in Pharmacology*, *6*, 276. https://doi.org/10.3389/fphar.2015.00276

Haskin, J., Szargel, R., Shani, V., Mekies, L. N., Rott, R., Lim, G. G. Y., … Engelender, S. (2013). AF-6 is a positive modulator of the PINK1/parkin pathway and is deficient in Parkinson's disease. *Human Molecular Genetics*, *22*(10), 2083–2096. https://doi.org/10.1093/hmg/ddt058

Hatch, A. L., Gurel, P. S., & Higgs, H. N. (2014). Novel roles for actin in mitochondrial fission. *Journal of Cell Science*, *127*(21), 4549–4560. https://doi.org/10.1242/jcs.153791

Head, B., Griparic, L., Amiri, M., Gandre-Babbe, S., & van der Bliek, A. M. (2009). Inducible proteolytic inactivation of OPA1 mediated by the OMA1 protease in mammalian cells. *The Journal of Cell Biology*, *187*(7), 959–966. https://doi.org/10.1083/jcb.200906083

Heymann, J. a W., & Hinshaw, J. E. (2009). Dynamins at a glance. *Journal of Cell Science*, *122*(Pt 19), 3427–3431. https://doi.org/10.1242/jcs.051714

Hinshaw, J. E., & Schmid, S. L. (1995). Dynamin self-assembles into rings suggesting a mechanism for coated vesicle budding. *Nature*, *374*(6518), 190–192. https://doi.org/10.1038/374190a0

Hollenbeck, P. J., & Saxton, W. M. (2005). The axonal transport of mitochondria. *Journal of Cell Science*, *118*(Pt 23), 5411–5419. https://doi.org/10.1242/jcs.02745

Hoppins, S., Edlich, F., Cleland, M. M., Banerjee, S., McCaffery, J. M., Youle, R. J., & Nunnari, J. (2011). The Soluble Form of Bax Regulates Mitochondrial Fusion via MFN2 Homotypic Complexes. *Molecular Cell*, *41*(2), 150–160. https://doi.org/10.1016/j.molcel.2010.11.030

Hu, J., & Rapoport, T. A. (2016). Fusion of the endoplasmic reticulum by membrane-bound GTPases. *Seminars in Cell & Developmental Biology*, *60*, 105–111. https://doi.org/10.1016/j.semcdb.2016.06.001

Hunker, C. M., Galvis, A., Kruk, I., Giambini, H., Veisaga, M. L., & Barbieri, M. A. (2006). Rab5-activating protein 6, a novel endosomal protein with a role in endocytosis. *Biochemical and Biophysical Research Communications*, *340*(3), 967–975. https://doi.org/10.1016/j.bbrc.2005.12.099

Huttlin, E. L., Bruckner, R. J., Paulo, J. A., Cannon, J. R., Ting, L., Baltier, K., … Harper, J. W. (2017). Architecture of the human interactome defines protein communities and disease networks. *Nature*, *545*(7655), 505–509. https://doi.org/10.1038/nature22366

Ingerman, E., Perkins, E. M., Marino, M., Mears, J. a., McCaffery, J. M., Hinshaw, J. E., & Nunnari, J. (2005). Dnm1 forms spirals that are structurally tailored to fit mitochondria. *Journal of Cell Biology*, *170*(7), 1021–1027. https://doi.org/10.1083/jcb.200506078

Ishihara, N., Eura, Y., & Mihara, K. (2004). Mitofusin 1 and 2 play distinct roles in mitochondrial fusion reactions via GTPase activity. *Journal of Cell Science*, *117*(Pt 26), 6535–6546. https://doi.org/10.1242/jcs.01565

Ishihara, N., Fujita, Y., Oka, T., & Mihara, K. (2006). Regulation of mitochondrial morphology through proteolytic cleavage of OPA1. *The EMBO Journal*, *25*(13), 2966–2977. https://doi.org/10.1038/sj.emboj.7601184

Ishihara, N., Nomura, M., Jofuku, A., Kato, H., Suzuki, S. O., Masuda, K., … Mihara, K. (2009). Mitochondrial fission factor Drp1 is essential for embryonic development and synapse formation in mice. *Nature Cell Biology*, *11*(8), 958–966. https://doi.org/10.1038/ncb1907

Itoh, K., Nakamura, K., Iijima, M., & Sesaki, H. (2013). Mitochondrial dynamics in neurodegeneration. *Trends in Cell Biology*, *23*(2), 64–71. https://doi.org/10.1016/j.tcb.2012.10.006

Jimah, J. R., & Hinshaw, J. E. (2019). Structural Insights into the Mechanism of Dynamin Superfamily Proteins. *Trends in Cell Biology*, *29*(3), 257–273. https://doi.org/10.1016/j.tcb.2018.11.003

Jin, S. M., Lazarou, M., Wang, C., Kane, L. A., Narendra, D. P., & Youle, R. J. (2010). Mitochondrial membrane potential regulates PINK1 import and proteolytic destabilization by PARL. *The Journal of Cell Biology*, *191*(5), 933–942.

https://doi.org/10.1083/jcb.201008084

Kane, L. A., Lazarou, M., Fogel, A. I., Li, Y., Yamano, K., Sarraf, S. A., … Youle, R. J. (2014). PINK1 phosphorylates ubiquitin to activate Parkin E3 ubiquitin ligase activity. *The Journal of Cell Biology*, *205*(2), 143–153. https://doi.org/10.1083/jcb.201402104

Karbowski, M., Norris, K. L., Cleland, M. M., Jeong, S.-Y., & Youle, R. J. (2006). Role of Bax and Bak in mitochondrial morphogenesis. *Nature*, *443*(7112), 658–662. https://doi.org/10.1038/nature05111

Kazlauskaite, A., Kondapalli, C., Gourlay, R., Campbell, D. G., Ritorto, M. S., Hofmann, K., … Muqit, M. M. K. (2014). Parkin is activated by PINK1-dependent phosphorylation of ubiquitin at Ser65. *The Biochemical Journal*, *460*(1), 127–139. https://doi.org/10.1042/BJ20140334

Kijima, K., Numakura, C., Izumino, H., Umetsu, K., Nezu, A., Shiiki, T., … Hayasaka, K. (2005). Mitochondrial GTPase mitofusin 2 mutation in Charcot-Marie-Tooth neuropathy type 2A. *Human Genetics*, *116*(1–2), 23–27. https://doi.org/10.1007/s00439-004-1199-2

Koch, J., Feichtinger, R. G., Freisinger, P., Pies, M., Schrödl, F., Iuso, A., … Haack, T. B. (2016). Disturbed mitochondrial and peroxisomal dynamics due to loss of MFF causes Leigh-like encephalopathy, optic atrophy and peripheral neuropathy. *Journal of Medical Genetics*, *53*(4), 270–278. https://doi.org/10.1136/jmedgenet-2015-103500

Kondapalli, C., Kazlauskaite, A., Zhang, N., Woodroof, H. I., Campbell, D. G., Gourlay, R., … Muqit, M. M. K. (2012). PINK1 is activated by mitochondrial membrane potential depolarization and stimulates Parkin E3 ligase activity by phosphorylating Serine 65. *Open Biology*, *2*(5), 120080. https://doi.org/10.1098/rsob.120080

Koshiba, T., Detmer, S. a, Kaiser, J. T., Chen, H., McCaffery, J. M., & Chan, D. C. (2004). Structural basis of mitochondrial tethering by mitofusin complexes. *Science (New York, N.Y.)*, *305*(5685), 858–862. https://doi.org/10.1126/science.1099793

Koyano, F., Okatsu, K., Kosako, H., Tamura, Y., Go, E., Kimura, M., … Matsuda, N. (2014). Ubiquitin is phosphorylated by PINK1 to activate parkin. *Nature*, *510*(7503), 162–166. https://doi.org/10.1038/nature13392

Kumar, S., Pan, C. C., Shah, N., Wheeler, S. E., Hoyt, K. R., Hempel, N., … Lee, N. Y. (2016). Activation of Mitofusin2 by Smad2-RIN1 Complex during Mitochondrial Fusion. *Molecular Cell*, *62*(4), 520–531. https://doi.org/10.1016/j.molcel.2016.04.010

Labbé, K., Murley, A., & Nunnari, J. (2014). Determinants and functions of mitochondrial behavior. *Annual Review of Cell and Developmental Biology*, *30*, 357–391. https://doi.org/10.1146/annurev-cellbio-101011-155756

Lazarou, M., Sliter, D. A., Kane, L. A., Sarraf, S. A., Wang, C., Burman, J. L., … Youle, R. J. (2015). The ubiquitin kinase PINK1 recruits autophagy receptors to induce mitophagy. *Nature*, Accepted. https://doi.org/10.1038/nature14893

Leboucher, G. P., Tsai, Y. C., Yang, M., Shaw, K. C., Zhou, M., Veenstra, T. D., … Weissman, A. M. (2012). Stress-induced phosphorylation and proteasomal degradation of mitofusin 2

facilitates mitochondrial fragmentation and apoptosis. *Molecular Cell*, *47*(4), 547–557. https://doi.org/10.1016/j.molcel.2012.05.041

Lee, J.-Y., Kapur, M., Li, M., Choi, M.-C., Choi, S., Kim, H.-J., … Yao, T.-P. (2014). MFN1 deacetylation activates adaptive mitochondrial fusion and protects metabolically challenged mitochondria. *Journal of Cell Science*, *127*(22), 4954–4963. https://doi.org/10.1242/jcs.157321

Legros, F., Malka, F., Frachon, P., Lombès, A., & Rojo, M. (2004). Organization and dynamics of human mitochondrial DNA. *Journal of Cell Science*, *117*(Pt 13), 2653–2662. https://doi.org/10.1242/jcs.01134

Lemasters, J. J. (2005). Selective mitochondrial autophagy, or mitophagy, as a targeted defense against oxidative stress, mitochondrial dysfunction, and aging. *Rejuvenation Research*, *8*(1), 3–5. https://doi.org/10.1089/rej.2005.8.3

Lewis, M. R., & Lewis, W. H. (1914). MITOCHONDRIA IN TISSUE CULTURE. *Science (New York, N.Y.)*, *39*(1000), 330–333. https://doi.org/10.1126/science.39.1000.330

Ligon, L. A., & Steward, O. (2000). Role of microtubules and actin filaments in the movement of mitochondria in the axons and dendrites of cultured hippocampal neurons. *The Journal of Comparative Neurology*, *427*(3), 351–361. Retrieved from http://www.ncbi.nlm.nih.gov/pubmed/11054698

Liu, J., Noel, J. K., & Low, H. H. (2018). Structural basis for membrane tethering by a bacterial dynamin-like pair. *Nature Communications*, *9*(1), 3345. https://doi.org/10.1038/s41467-018-05523-8

Liu, X., Weaver, D., Shirihai, O., & Hajnóczky, G. (2009). Mitochondrial 'kiss-and-run': interplay between mitochondrial motility and fusion–fission dynamics. *The EMBO Journal*, *28*(20), 3074–3089. https://doi.org/10.1038/emboj.2009.255

Loson, O. C., Song, Z., Chen, H., & Chan, D. C. (2013). Fis1, Mff, MiD49, and MiD51 mediate Drp1 recruitment in mitochondrial fission. *Molecular Biology of the Cell*, *24*(5), 659–667. https://doi.org/10.1091/mbc.E12-10-0721

Low, H. H., & Löwe, J. (2006). A bacterial dynamin-like protein. *Nature*, *444*(7120), 766–769. https://doi.org/10.1038/nature05312

Low, H. H., Sachse, C., Amos, L. a., & Löwe, J. (2009). Structure of a Bacterial Dynamin-like Protein Lipid Tube Provides a Mechanism For Assembly and Membrane Curving. *Cell*, *139*(7), 1342–1352. https://doi.org/10.1016/j.cell.2009.11.003

Luchsinger, L. L., de Almeida, M. J., Corrigan, D. J., Mumau, M., & Snoeck, H.-W. (2016). Mitofusin 2 maintains haematopoietic stem cells with extensive lymphoid potential. *Nature*, *529*(7587), 528–531. https://doi.org/10.1038/nature16500

MacAskill, A. F., Rinholm, J. E., Twelvetrees, A. E., Arancibia-Carcamo, I. L., Muir, J., Fransson, A., … Kittler, J. T. (2009). Miro1 Is a Calcium Sensor for Glutamate Receptor-Dependent Localization of Mitochondria at Synapses. *Neuron*, *61*(4), 541–555. https://doi.org/10.1016/j.neuron.2009.01.030

Malka, F., Guillery, O., Cifuentes-Diaz, C., Guillou, E., Belenguer, P., Lombès, A., & Rojo, M. (2005). Separate fusion of outer and inner mitochondrial membranes. *EMBO Reports*, *6*(9), 853–859. https://doi.org/10.1038/sj.embor.7400488

Mattie, S., Riemer, J., Wideman, J. G., & McBride, H. M. (2018). A new mitofusin topology places the redox-regulated C terminus in the mitochondrial intermembrane space. *The Journal of Cell Biology*, *217*(2), 507–515. https://doi.org/10.1083/jcb.201611194

Mears, J. A., & Hinshaw, J. E. (2008). Visualization of dynamins. *Methods in Cell Biology*, *88*, 237–256. https://doi.org/10.1016/S0091-679X(08)00413-5

Mears, J. a, Lackner, L. L., Fang, S., Ingerman, E., Nunnari, J., & Hinshaw, J. E. (2011). Conformational changes in Dnm1 support a contractile mechanism for mitochondrial fission. *Nature Structural & Molecular Biology*, *18*(1), 20–26. https://doi.org/10.1038/nsmb.1949

Meeusen, S., DeVay, R., Block, J., Cassidy-Stone, A., Wayson, S., McCaffery, J. M., & Nunnari, J. (2006). Mitochondrial Inner-Membrane Fusion and Crista Maintenance Requires the Dynamin-Related GTPase Mgm1. *Cell*, *127*(2), 383–395. https://doi.org/10.1016/j.cell.2006.09.021

Meeusen, S., McCaffery, J. M., & Nunnari, J. (2004). Mitochondrial Fusion Intermediates Revealed in Vitro. *Science*, *305*(5691), 1747–1752. https://doi.org/10.1126/science.1100612

Mishra, P., & Chan, D. C. (2014). Mitochondrial dynamics and inheritance during cell division, development and disease. *Nature Reviews Molecular Cell Biology*, *15*(10), 634–646. https://doi.org/10.1038/nrm3877

Misko, A., Jiang, S., Wegorzewska, I., Milbrandt, J., & Baloh, R. H. (2010). Mitofusin 2 is necessary for transport of axonal mitochondria and interacts with the Miro/Milton complex. *The Journal of Neuroscience : The Official Journal of the Society for Neuroscience*, *30*(12), 4232–4240. https://doi.org/10.1523/JNEUROSCI.6248-09.2010

Mitra, K., Wunder, C., Roysam, B., Lin, G., & Lippincott-Schwartz, J. (2009). A hyperfused mitochondrial state achieved at G1-S regulates cyclin E buildup and entry into S phase. *Proceedings of the National Academy of Sciences of the United States of America*, *106*(29), 11960–11965. https://doi.org/10.1073/pnas.0904875106

Morin-Leisk, J., Saini, S. G., Meng, X., Makhov, A. M., Zhang, P., & Lee, T. H. (2011). An intramolecular salt bridge drives the soluble domain of GTP-bound atlastin into the postfusion conformation. *The Journal of Cell Biology*, *195*(4), 605–615. https://doi.org/10.1083/jcb.201105006

Moss, T. J., Andreazza, C., Verma, A., Daga, A., & McNew, J. a. (2011). Membrane fusion by the GTPase atlastin requires a conserved C-terminal cytoplasmic tail and dimerization through the middle domain. *Proceedings of the National Academy of Sciences of the United States of America*, *108*(27), 11133–11138. https://doi.org/10.1073/pnas.1105056108

Murley, A., Lackner, L. L., Osman, C., West, M., Voeltz, G. K., Walter, P., & Nunnari, J. (2013). ER-associated mitochondrial division links the distribution of mitochondria and

mitochondrial DNA in yeast. *ELife*, *2*, 1–16. https://doi.org/10.7554/eLife.00422

Nakajo, A., Yoshimura, S., Togawa, H., Kunii, M., Iwano, T., Izumi, A., … Harada, A. (2016). EHBP1L1 coordinates Rab8 and Bin1 to regulate apical-directed transport in polarized epithelial cells. *The Journal of Cell Biology*, *212*(3), 297–306. https://doi.org/10.1083/jcb.201508086

Narendra, D., Tanaka, A., Suen, D.-F., & Youle, R. J. (2008). Parkin is recruited selectively to impaired mitochondria and promotes their autophagy. *The Journal of Cell Biology*, *183*(5), 795–803. https://doi.org/10.1083/jcb.200809125

Nasca, A., Nardecchia, F., Commone, A., Semeraro, M., Legati, A., Garavaglia, B., … Leuzzi, V. (2018). Clinical and Biochemical Features in a Patient With Mitochondrial Fission Factor Gene Alteration. *Frontiers in Genetics*, *9*, 625. https://doi.org/10.3389/fgene.2018.00625

Nasrallah, C. M., & Horvath, T. L. (2014). Mitochondrial dynamics in the central regulation of metabolism. *Nature Reviews. Endocrinology*, *10*(11), 650–658. https://doi.org/10.1038/nrendo.2014.160

Nemani, N., Carvalho, E., Tomar, D., Dong, Z., Ketschek, A., Breves, S. L., … Madesh, M. (2018). MIRO-1 Determines Mitochondrial Shape Transition upon GPCR Activation and Ca2+ Stress. *Cell Reports*, *23*(4), 1005–1019. https://doi.org/10.1016/j.celrep.2018.03.098

O'Donnell, J. P., Cooley, R. B., Kelly, C. M., Miller, K., Andersen, O. S., Rusinova, R., & Sondermann, H. (2017). Timing and Reset Mechanism of GTP Hydrolysis-Driven Conformational Changes of Atlastin. *Structure (London, England : 1993)*, *25*(7), 997-1010.e4. https://doi.org/10.1016/j.str.2017.05.007

Oka, T., Sayano, T., Tamai, S., Yokota, S., Kato, H., Fujii, G., & Mihara, K. (2008). Identification of a novel protein MICS1 that is involved in maintenance of mitochondrial morphology and apoptotic release of cytochrome c. *Molecular Biology of the Cell*, *19*(6), 2597–2608. https://doi.org/10.1091/mbc.e07-12-1205

Olichon, A., Baricault, L., Gas, N., Guillou, E., Valette, A., Belenguer, P., & Lenaers, G. (2003). Loss of OPA1 perturbates the mitochondrial inner membrane structure and integrity, leading to cytochrome c release and apoptosis. *The Journal of Biological Chemistry*, *278*(10), 7743–7746. https://doi.org/10.1074/jbc.C200677200

Olichon, A., Emorine, L. J., Descoins, E., Pelloquin, L., Brichese, L., Gas, N., … Belenguer, P. (2002). The human dynamin-related protein OPA1 is anchored to the mitochondrial inner membrane facing the inter-membrane space. *FEBS Letters*, *523*(1–3), 171–176. https://doi.org/10.1016/S0014-5793(02)02985-X

Orso, G., Pendin, D., Liu, S., Tosetto, J., Moss, T. J., Faust, J. E., … Daga, A. (2009). Homotypic fusion of ER membranes requires the dynamin-like GTPase atlastin. *Nature*, *460*(7258), 978–983. https://doi.org/10.1038/nature08280

Otera, H., Ishihara, N., & Mihara, K. (2013). New insights into the function and regulation of mitochondrial fission. *Biochimica et Biophysica Acta*, *1833*(5), 1256–1268.

https://doi.org/10.1016/j.bbamcr.2013.02.002

Pareyson, D., Saveri, P., Sagnelli, A., & Piscosquito, G. (2015). Mitochondrial dynamics and inherited peripheral nerve diseases. *Neuroscience Letters*, *596*, 66–77. https://doi.org/10.1016/j.neulet.2015.04.001

Pendin, D., Tosetto, J., Moss, T. J., Andreazza, C., Moro, S., McNew, J. A., & Daga, A. (2011). GTP-dependent packing of a three-helix bundle is required for atlastin-mediated fusion. *Proceedings of the National Academy of Sciences*, *108*(39), 16283–16288. https://doi.org/10.1073/pnas.1106421108

Pernas, L., & Scorrano, L. (2016). Mito-Morphosis: Mitochondrial Fusion, Fission, and Cristae Remodeling as Key Mediators of Cellular Function. *Annual Review of Physiology*, *78*, 505–531. https://doi.org/10.1146/annurev-physiol-021115-105011

Pyakurel, A., Savoia, C., Hess, D., & Scorrano, L. (2015). Extracellular Regulated Kinase Phosphorylates Mitofusin 1 to Control Mitochondrial Morphology and Apoptosis. *Molecular Cell*, *58*(2), 244–254. https://doi.org/10.1016/j.molcel.2015.02.021

Qi, Y., Yan, L., Yu, C., Guo, X., Zhou, X., Hu, X., … Hu, J. (2016). Structures of human mitofusin 1 provide insight into mitochondrial tethering. *The Journal of Cell Biology*, *215*(5), 621–629. https://doi.org/10.1083/jcb.201609019

Rakovic, A., Grünewald, A., Kottwitz, J., Brüggemann, N., Pramstaller, P. P., Lohmann, K., & Klein, C. (2011). Mutations in PINK1 and Parkin impair ubiquitination of Mitofusins in human fibroblasts. *PloS One*, *6*(3), e16746. https://doi.org/10.1371/journal.pone.0016746

Rocha, A. G., Franco, A., Krezel, A. M., Rumsey, J. M., Alberti, J. M., Knight, W. C., … Dorn, G. W. (2018). MFN2 agonists reverse mitochondrial defects in preclinical models of Charcot-Marie-Tooth disease type 2A. *Science (New York, N.Y.)*, *360*(6386), 336–341. https://doi.org/10.1126/science.aao1785

Santel, a, & Fuller, M. T. (2001). Control of mitochondrial morphology by a human mitofusin. *Journal of Cell Science*, *114*(Pt 5), 867–874.

Sarraf, S. A., Raman, M., Guarani-Pereira, V., Sowa, M. E., Huttlin, E. L., Gygi, S. P., & Harper, J. W. (2013). Landscape of the PARKIN-dependent ubiquitylome in response to mitochondrial depolarization. *Nature*, *496*(7445), 372–376. https://doi.org/10.1038/nature12043

Shamseldin, H. E., Alshammari, M., Al-Sheddi, T., Salih, M. A., Alkhalidi, H., Kentab, A., … Alkuraya, F. S. (2012). Genomic analysis of mitochondrial diseases in a consanguineous population reveals novel candidate disease genes. *Journal of Medical Genetics*, *49*(4), 234–241. https://doi.org/10.1136/jmedgenet-2012-100836

Sheffer, R., Douiev, L., Edvardson, S., Shaag, A., Tamimi, K., Soiferman, D., … Saada, A. (2016). Postnatal microcephaly and pain insensitivity due to a de novo heterozygous DNM1L mutation causing impaired mitochondrial fission and function. *American Journal of Medical Genetics. Part A*, *170*(6), 1603–1607. https://doi.org/10.1002/ajmg.a.37624

Shiba-Fukushima, K., Imai, Y., Yoshida, S., Ishihama, Y., Kanao, T., Sato, S., & Hattori, N.

(2012). PINK1-mediated phosphorylation of the Parkin ubiquitin-like domain primes mitochondrial translocation of Parkin and regulates mitophagy. *Scientific Reports*, *2*, 1002. https://doi.org/10.1038/srep01002

Shibahara, K., Asano, M., Ishida, Y., Aoki, T., Koike, T., & Honjo, T. (1995). Isolation of a novel mouse gene MA-3 that is induced upon programmed cell death. *Gene*, *166*(2), 297–301. Retrieved from http://www.ncbi.nlm.nih.gov/pubmed/8543179

Shutt, T., Geoffrion, M., Milne, R., & McBride, H. M. (2012). The intracellular redox state is a core determinant of mitochondrial fusion. *EMBO Reports*, *13*(10), 909–915. https://doi.org/10.1038/embor.2012.128

Smirnova, E., Shurland, D.-L., Ryazantsev, S. N., & Van der Bliek, a M. (1998). A human dynamin-related protein controls the distribuition of mitochondria. *J. Cell Biol.*, *143*(2), 351–358. https://doi.org/10.1083/jcb.143.2.351

Song, B. D., Leonard, M., & Schmid, S. L. (2004). Dynamin GTPase Domain Mutants That Differentially Affect GTP Binding, GTP Hydrolysis, and Clathrin-mediated Endocytosis. *Journal of Biological Chemistry*, *279*(39), 40431–40436. https://doi.org/10.1074/jbc.M407007200

Song, B. D., Yarar, D., & Schmid, S. L. (2004). An Assembly-incompetent Mutant Establishes a Requirement for Dynamin Self-assembly in Clathrin-mediated Endocytosis In Vivo. *Molecular Biology of the Cell*, *15*(5), 2243–2252. https://doi.org/10.1091/mbc.e04-01-0015

Song, Z., Chen, H., Fiket, M., Alexander, C., & Chan, D. C. (2007). OPA1 processing controls mitochondrial fusion and is regulated by mRNA splicing, membrane potential, and Yme1L. *Journal of Cell Biology*, *178*(5), 749–755. https://doi.org/10.1083/jcb.200704110

Song, Z., Ghochani, M., McCaffery, J. M., Frey, T. G., & Chan, D. C. (2009). Mitofusins and OPA1 mediate sequential steps in mitochondrial membrane fusion. *Molecular Biology of the Cell*, *20*(15), 3525–3532. https://doi.org/10.1091/mbc.e09-03-0252

Steffen, J., Vashisht, A. A., Wan, J., Jen, J. C., Claypool, S. M., Wohlschlegel, J. A., & Koehler, C. M. (2017). Rapid degradation of mutant SLC25A46 by the ubiquitin-proteasome system results in MFN1/2-mediated hyperfusion of mitochondria. *Molecular Biology of the Cell*, *28*(5), 600–612. https://doi.org/10.1091/mbc.E16-07-0545

Stolz, A., Ernst, A., & Dikic, I. (2014). Cargo recognition and trafficking in selective autophagy. *Nature Cell Biology*, *16*(6), 495–501. https://doi.org/10.1038/ncb2979

Strack, S., & Cribbs, J. T. (2012). Allosteric modulation of Drp1 mechanoenzyme assembly and mitochondrial fission by the variable domain. *Journal of Biological Chemistry*, *287*(14), 10990–11001. https://doi.org/10.1074/jbc.M112.342105

Stuppia, G., Rizzo, F., Riboldi, G., Del Bo, R., Nizzardo, M., Simone, C., … Corti, S. (2015). MFN2-related neuropathies: Clinical features, molecular pathogenesis and therapeutic perspectives. *Journal of the Neurological Sciences*, *356*(1), 7–18. https://doi.org/10.1016/j.jns.2015.05.033

Sundborger, A. C., Fang, S., Heymann, J. A., Ray, P., Chappie, J. S., & Hinshaw, J. E. (2014). A

dynamin mutant defines a superconstricted prefission state. *Cell Reports*, *8*(3), 734–742. https://doi.org/10.1016/j.celrep.2014.06.054

Takai, Y., & Nakanishi, H. (2003). Nectin and afadin: novel organizers of intercellular junctions. *Journal of Cell Science*, *116*(Pt 1), 17–27. Retrieved from http://www.ncbi.nlm.nih.gov/pubmed/12456712

Takaki, S., & Eto, K. (2018). Cytoplasmic localization of programmed cell death 4 contributes to its anti-apoptotic function. *Molecular and Cellular Biochemistry*, *448*(1–2), 155–164. https://doi.org/10.1007/s11010-018-3322-z

Tanaka, A., Cleland, M. M., Xu, S., Narendra, D. P., Suen, D. F., Karbowski, M., & Youle, R. J. (2010). Proteasome and p97 mediate mitophagy and degradation of mitofusins induced by Parkin. *Journal of Cell Biology*, *191*(7), 1367–1380. https://doi.org/10.1083/jcb.201007013

Tondera, D., Grandemange, S., Jourdain, A., Karbowski, M., Mattenberger, Y., Herzig, S., … Martinou, J.-C. (2009). SLP-2 is required for stress-induced mitochondrial hyperfusion. *The EMBO Journal*, *28*(11), 1589–1600. https://doi.org/10.1038/emboj.2009.89

Valente, A. J., Maddalena, L. A., Robb, E. L., Moradi, F., & Stuart, J. A. (2017). A simple ImageJ macro tool for analyzing mitochondrial network morphology in mammalian cell culture. *Acta Histochemica*, *119*(3), 315–326. https://doi.org/10.1016/j.acthis.2017.03.001

van Spronsen, M., Mikhaylova, M., Lipka, J., Schlager, M. A., van den Heuvel, D. J., Kuijpers, M., … Hoogenraad, C. C. (2013). TRAK/Milton motor-adaptor proteins steer mitochondrial trafficking to axons and dendrites. *Neuron*, *77*(3), 485–502. https://doi.org/10.1016/j.neuron.2012.11.027

Vanstone, J. R., Smith, A. M., McBride, S., Naas, T., Holcik, M., Antoun, G., … Lines, M. A. (2016). DNM1L-related mitochondrial fission defect presenting as refractory epilepsy. *European Journal of Human Genetics : EJHG*, *24*(7), 1084–1088. https://doi.org/10.1038/ejhg.2015.243

Varlakhanova, N. V, Alvarez, F. J. D., Brady, T. M., Tornabene, B. A., Hosford, C. J., Chappie, J. S., … Ford, M. G. J. (2018). Structures of the fungal dynamin-related protein Vps1 reveal a unique, open helical architecture. *The Journal of Cell Biology*, *217*(10), 3608–3624. https://doi.org/10.1083/jcb.201712021

Wakabayashi, J., Zhang, Z., Wakabayashi, N., Tamura, Y., Fukaya, M., Kensler, T. W., … Sesaki, H. (2009). The dynamin-related GTPase Drp1 is required for embryonic and brain development in mice. *The Journal of Cell Biology*, *186*(6), 805–816. https://doi.org/10.1083/jcb.200903065

Wang, W., Wang, Y., Long, J., Wang, J., Haudek, S. B., Overbeek, P., … Danesh, F. R. (2012). Mitochondrial fission triggered by hyperglycemia is mediated by ROCK1 activation in podocytes and endothelial cells. *Cell Metabolism*, *15*(2), 186–200. https://doi.org/10.1016/j.cmet.2012.01.009

Wang, X., & Schwarz, T. L. (2009). The mechanism of Ca2+ -dependent regulation of kinesin-mediated mitochondrial motility. *Cell*, *136*(1), 163–174.

https://doi.org/10.1016/j.cell.2008.11.046

Waterham, H. R., Koster, J., van Roermund, C. W. T., Mooyer, P. A. W., Wanders, R. J. A., & Leonard, J. V. (2007). A lethal defect of mitochondrial and peroxisomal fission. *The New England Journal of Medicine*, *356*(17), 1736–1741. https://doi.org/10.1056/NEJMoa064436

Weihing, R. R. (1985). The filamins: properties and functions. *Canadian Journal of Biochemistry and Cell Biology = Revue Canadienne de Biochimie et Biologie Cellulaire*, *63*(6), 397–413. https://doi.org/10.1139/o85-059

Whitley, B. N., Lam, C., Cui, H., Haude, K., Bai, R., Escobar, L., … Hoppins, S. (2018). Aberrant Drp1-mediated mitochondrial division presents in humans with variable outcomes. *Human Molecular Genetics*, *27*(21), 3710–3719. https://doi.org/10.1093/hmg/ddy287

Winsor, J., Hackney, D. D., & Lee, T. H. (2017). The crossover conformational shift of the GTPase atlastin provides the energy driving ER fusion. *The Journal of Cell Biology*, *216*(5), 1321–1335. https://doi.org/10.1083/jcb.201609071

Winsor, J., Machi, U., Han, Q., Hackney, D. D., & Lee, T. H. (2018). GTP hydrolysis promotes disassembly of the atlastin crossover dimer during ER fusion. *Journal of Cell Biology*, *217*(12), 4184–4198. https://doi.org/10.1083/jcb.201805039

Wong, K., Ren, X. R., Huang, Y. Z., Xie, Y., Liu, G., Saito, H., … Rao, Y. (2001). Signal transduction in neuronal migration: roles of GTPase activating proteins and the small GTPase Cdc42 in the Slit-Robo pathway. *Cell*, *107*(2), 209–221. Retrieved from http://www.ncbi.nlm.nih.gov/pubmed/11672528

Yan, L., Sun, S., Wang, W., Shi, J., Hu, X., Wang, S., … Lou, Z. (2015). Structures of the yeast dynamin-like GTPase Sey1p provide insight into homotypic ER fusion. *The Journal of Cell Biology*, *210*(6), 961–972. https://doi.org/10.1083/jcb.201502078

Yan, Liming, Qi, Y., Huang, X., Yu, C., Lan, L., Guo, X., … Lou, Z. (2018). Structural basis for GTP hydrolysis and conformational change of MFN1 in mediating membrane fusion. *Nature Structural & Molecular Biology*, *25*(3), 233–243. https://doi.org/10.1038/s41594-018-0034-8

Yang, L., Long, Q., Liu, J., Tang, H., Li, Y., Bao, F., … Liu, X. (2015). Mitochondrial fusion provides an 'initial metabolic complementation' controlled by mtDNA. *Cellular and Molecular Life Sciences*, *72*(13), 2585–2598. https://doi.org/10.1007/s00018-015-1863-9

Zaha, K., Matsumoto, H., Itoh, M., Saitsu, H., Kato, K., Kato, M., … Nonoyama, S. (2016). DNM1L-related encephalopathy in infancy with Leigh syndrome-like phenotype and suppression-burst. *Clinical Genetics*, *90*(5), 472–474. https://doi.org/10.1111/cge.12805

Zhang, J., Liu, W., Liu, J., Xiao, W., Liu, L., Jiang, C., … Chen, Q. (2010). G-protein β2 subunit interacts with mitofusin 1 to regulate mitochondrial fusion. *Nature Communications*, *1*(7), 101. https://doi.org/10.1038/ncomms1099

Züchner, S., Mersiyanova, I. V, Muglia, M., Bissar-Tadmouri, N., Rochelle, J., Dadali, E. L., … Vance, J. M. (2004). Mutations in the mitochondrial GTPase mitofusin 2 cause Charcot-Marie-Tooth neuropathy type 2A. *Nature Genetics*, *36*(5), 449–451.

https://doi.org/10.1038/ng1341